

Mechanical behaviour of composite sandwich panels in bending after impact

Wouter Weijermars
MSc. Industrial Design Engineering

30-11-2016

UNIVERSITY OF TWENTE.

Mechanical behaviour of composite sandwich panels in bending after impact

MSc. Student

Wouter Weijermars

Studentnumber

0208329

Supervisor, University of Twente

Dr. Ir. I. Baran

Examination Committee, University of Twente

Dr. Ir. T. Bor	Chairman
Dr. Ir. I. Baran	Supervisor
Dr. Ir. J. Hazrati Marangalou	External member

30-11-2016

Master thesis final report

Document number: CTW-PT 16/1413

UNIVERSITY OF TWENTE.

MSc. Industrial Design Engineering

Emerging Technology Design - Advanced Materials Engineering

Acknowledgement

During my thesis I was supervised by Dr. Ir. Ismet Baran. I would like to thank him for his support, excellent guidance, his constant encouragements and his good advice. Without him, I would never have been able to succeed finishing this thesis. Furthermore, I would like Dr. Ir. Bor and Dr. Ir. J. Hazrati Marangalou for being part of my committee.

I would also like to thank Dr. Ir. L. Warnet, B. Vos and I. Vrooijink of the University of Twente, for helping me with my experimental tests. Without them I would not be able to perform the practical tests.

Finally, I would like to thank my parents who stood by me the entire duration of my graduation period. I also want to thank my girlfriend for her extended support during my entire career (especially the last heavy months).

Summary

This master thesis is about the mechanical behaviour of composite sandwich panels in bending after impact. The goals were to identify the influence of an impact loading on the residual bending stiffness, to determine the failure modes after impact and during bending, to illustrate the influence of core material type on the mechanical behaviour in bending after impact and to demonstrate the effect of impact energy on the mechanical response in bending after impact.

In literature, several articles describe the mechanical behavior in compression after impact, but bending after impact is not yet investigated before. In sandwich composites, four different failure types are described; Core Shearing, Microbuckling, Indentation and Face Wrinkling.

In order to answer the research questions, use is made of an experimental analysis and a Finite Element Method analysis. For the sandwich panels use is made of an epoxy/glass facesheet with three different core materials; SAN foam, PET foam and Balsa. A three-point bending test is performed according standard *ASTM C393/C393M* in order to determine the reference stiffness of the different panels. Then a reference impact test is performed according standard *ASTM D7136/D7136M*. Finally, an impact test is performed on specimens with the dimensions of the bending test and thereafter a three-point bending test is performed with the same specimens in order to determine the stiffness in bending after impact. The same tests are also performed in the ABAQUS FEM simulation software.

It is shown that the impact tests cause a skin-core delamination at the bottom of the Balsa cored panels, while the SAN foam and the PET foam cores do not show signs of this delamination. Furthermore, it is shown that an impact has a significant influence on the bending stiffness of composite sandwich panels, dependent on the core material. The SAN foam cored specimens lose 46.1% stiffness, the PET foam cored specimens lose 25.7% stiffness and the Balsa cored specimens lose 19.1% stiffness after impact compared to bending-only tests. The SAN foam and PET foam cored specimens also show miniature cracks in the bending-after-impact tests, which do not occur in the bending-only tests.

The FEM simulations show that the impact energy has an influence on the mechanical behaviour of the composite sandwich panels. The simulations show that the higher the impact energy, the lower the bending stiffness for the PET foam core and the Balsa core, but for the SAN foam there is no significant influence. The impact energy also has a significant influence on the shear stress distribution of the Balsa core and on the PEEQ distribution of the PET foam core.

Samenvatting

Deze afstudeeropdracht gaat over het mechanische gedrag van composiet sandwichpanelen in een buiging na impact situatie. De doelen van deze opdracht zijn; de invloed bepalen van een impact op de overgebleven stijfheid van een composiet sandwichpaneel, de faalmechanismen bepalen van composiet sandwichpanelen na een impact en tijdens buiging, de invloed bepalen van verschillende kernmaterialen op het mechanische gedrag in een buiging na impact situatie en het effect van verschillende impact energieën bepalen op het mechanische gedrag in buiging na impact.

De literatuur beschrijft in verscheidene artikelen het mechanische gedrag van composiet sandwichpanelen in een compressie-na-impact test, maar geen enkel artikel beschrijft het gedrag van een composiet sandwichpaneel gedurende een buigtest na een impact. De literatuur toont aan dat er in een sandwichpaneel vier verschillende soorten faalmechanismen zijn; afschuiving van de kern, microknikken, indeuking en het rimpelen van de huid.

Om de onderzoeksvragen te kunnen beantwoorden is er gebruik gemaakt van zowel een experimentele analyse als van een eindige elementenmethode analyse. Er is gebruik gemaakt van epoxy/glas huiden met drie verschillende kernmaterialen; SAN-schuim, PET-schuim en Balsahout. Op deze drie verschillende sandwichpanelen zijn drie soorten tests uitgevoerd. Allereerst een drie-punt buigproef volgens teststandaard *ASTM C393/C393M* om de referentiestijfheid te bepalen. Vervolgens is er een impactproef uitgevoerd volgens teststandaard *ASTM D7136/D7136M* als referentiekader voor de laatste proef. In de laatste proef is eerst een impact test gedaan op de proefstukken met de afmetingen van de drie-punt buigproef (niet volgens een standaard, vandaar de referentie impactproef) en vervolgens een drie-punt buigproef op deze beschadigde proefstukken om zo de verloren stijfheid te bepalen. Al deze tests zijn ook in de eindige elementensoftware gesimuleerd.

De impactproeven tonen aan dat de proefstukken met de balsa kern een delaminatie hebben tussen de huid en de kern aan de onderzijde van het paneel, terwijl dit niet aantoonbaar is in de proefstukken met de SAN-schuim kern en de PET-schuim kern. Verder is laten zien dat een impact een significante invloed heeft op de stijfheid van de sandwichpanelen. De proefstukken met de SAN-schuim kern verliezen 46.1% stijfheid, de proefstukken met de PET-schuim kern verliezen 25.7% stijfheid en de proefstukken met de Balsahout kern verliezen 19.1% stijfheid vergeleken met de referentie buigproeven. Verder is aangetoond dat de het SAN-schuim en het PET-schuim minischeurtjes vertonen tijdens de buigproef na een impact, wat deze proefstukken bij de referentie buigproef niet hadden.

De eindige elementenanalyse heeft aangetoond dat de impactenergie ook invloed heeft op het mechanische gedrag van de composiet sandwichpanelen. In de simulatie is aantoonbaar dat een hogere impactenergie een lagere stijfheid tot gevolg heeft voor de proefstukken met de PET-schuim en Balsahout kernen, maar er is geen correlatie gevonden tussen de stijfheid en de impactenergie voor de proefstukken met de SAN-schuim kern. Verder heeft de impactenergie een significante invloed op de verdeling van de afschuifspanning in de proefstukken met een Balsahout kern en heeft de impactenergie ook een significante invloed op de beschadigde zone in de proefstukken met een PET-schuim kern.

Abbreviations

2D	Two-dimensional
3D	Three-dimensional
ASTM	American Society for Testing Materials
BAI	Bending after Impact
BO	Bending Only
DC	Damage Criteria
FEM	Finite Element Method
FRP	Fibre Reinforced Polymer
IBB	Impact before Bending
IO	Impact Only
LVI	Low Velocity Impact
PEEQ	Plastic Strain Equivalent
PES	Polyether Sulfone
PET	Polyethylene terephthalate
PVC	Polyvinyl chloride
SAN	Styrene-acrylonitrile
RTM	Resin Transfer Moulding
VARTM	Vacuum Assisted Resin Transfer Moulding

Table of Contents

Acknowledgement.....	1
Summary	2
Samenvatting.....	3
Abbreviations	4
Table of Contents	5
1. Introduction	7
1.1 Sandwich Composites.....	8
1.2 Previous work	12
1.3 Research goal and objectives	13
1.4 Outline of the thesis	14
2. Materials and experiments	15
2.1 Experimental testing	15
2.2 Analytical calculation of maximum stresses and shear stresses.....	20
3. Finite Element Method analysis.....	21
3.1 Bending-Only (BO) model.....	22
3.2 Impact-Only (IO) model	28
3.3 Bending-after-Impact (BAI) model	31
4. Results & Discussion.....	33
4.1 Bending-Only (BO).....	33
4.2 Impact-Only (IO)	41
4.3 Bending after impact.....	52
4.4 Effect of impact energy	65
5. Conclusions & Future recommendations.....	70
5.1 Conclusions.....	70
5.2 Recommendations.....	71
6. References.....	72
Appendix A: Composites background information	75
Appendix B: Literature table	89
Appendix C: Materials	92
Appendix D: Datasheets	95
Appendix E: Microscopic analysis.....	98
Appendix F: Stress table	109

1. Introduction

Nowadays composites, mostly referring to fibre reinforced polymers (FRP), are increasingly used in several products such as wind turbine blades, aerospace structures and automobile part components. By using the specific characteristics of both the fibres and the polymer, lightweight structures can be produced, with high strength to weight ratios. When the right knowledge is available about producing these products, the performance can outstand competing conventional materials such as steel and wood.

Sandwich composites consisting of thin FRP skins and a thick low density core have been becoming increasingly popular in structural design due to their low weight and high strength to weight ratio. Some of the examples of sandwich composites are wind turbine blades (Figure 1.1-a) and trailers of trucks (Figure 1.1-b). In practical use, such products can suffer some impact loadings during their lifetimes. These impacts have negative influence on the bending stiffness of these products, from which the stiffness should remain sufficient in order to maintain their functions. It is of importance to know what influence an impact has on the bending stiffness of a product.

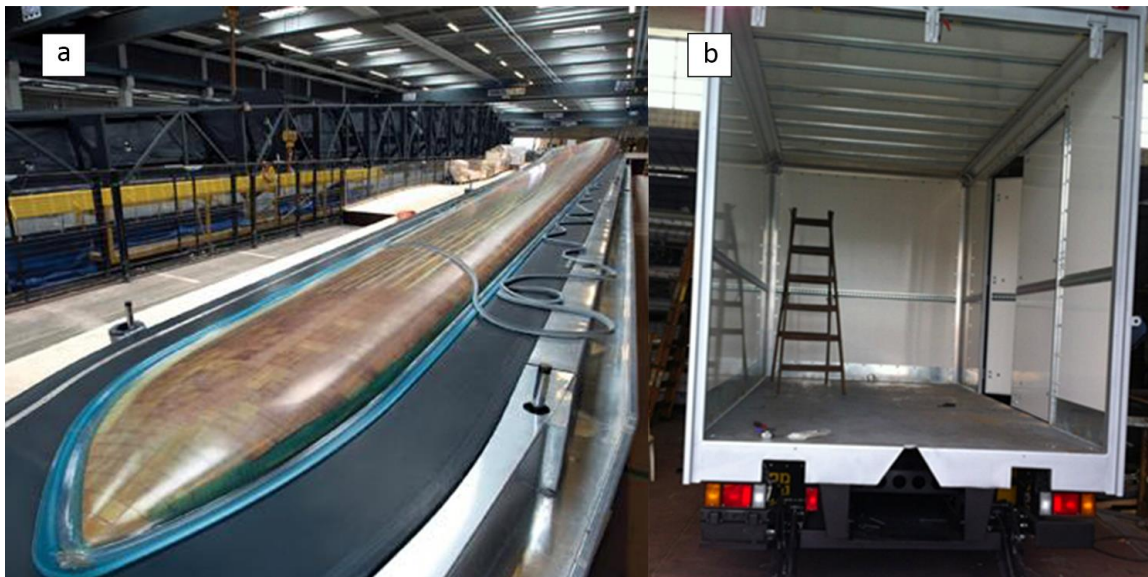


Figure 1.1: Examples of products which make use of composite sandwich panels in a) a wind turbine blades and in b) a trailer of a truck..

1.1 Sandwich Composites

A composite material can be described as a combination of two or more constituents. Generally, the characteristics of the components are combined to obtain certain properties, which can't be acquired with the individual constituents. In this report, composites will be referring to continuous fibre reinforced plastics. The fibres are used for their high strength and stiffness, whilst the matrix (resin) is used to protect the fibres, binds them together and transfers the load between the fibres. The combinations of fibres and matrices are nearly unlimited. Every composite is attuned to a certain application.

The full description of composite materials and their production techniques can be found in *Appendix A: Composites background information*.

1.1.1 Sandwich Constructions

Sandwich structures are used extensively in aerospace, automotive and commercial industries, as sandwich constructions are extremely light in weight and at the same time very strong and stiff, which means a very high strength-to-weight ratio. The American Society for Testing and Materials (ASTM) describes sandwich constructions as follows:

“A Structural Sandwich is a special form of composite comprising of a combination of different materials that are bonded to each other so as to utilize the properties of each separate component to the structural advantage of the whole assembly.”

Sandwich constructions basically are constructions consisting of two facings with a core in between. The facings of the sandwich panel, also called skins, are made of fibre reinforced polymer and have the ability to carry the bending loads on the panel while the core, usually made of a honeycomb construction or a wood or foam type, carries the shear loads and maintains the distance between the two face sheets. Typically, sandwich constructions have thin skins with a thicker core. The sandwich construction can be considered as the concept of an I-beam. The main advantage of sandwich constructions, is that they are extremely structural sufficient, explicitly in stiffness-critical applications. It can be seen in Figure 1.2, that the stiffness as well as flexural strength increase with an increasing thickness, while the weight only increases slightly which can be considered as negligible. In addition to the structural applications, the sandwich constructions are also used for their insulation properties (thermal and electrical).

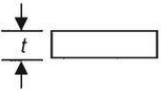
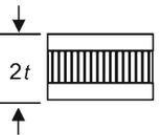
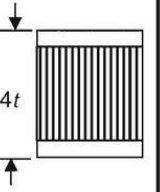
	Solid Material	Sandwich Construction	Thicker Sandwich
			
Stiffness	1.0	7.0	37.0
Flexural Strength	1.0	3.5	9.2
Weight	1.0	1.03	1.06

Figure 1.2: Sandwich principle, by increasing the thickness, the stiffness has a large increases while the weight has a small increase. (Campbell, 2010)

In Figure 1.3 overall (mechanical) performance is plotted as a function of price of several sandwich cores (Campbell, 2010). It can be seen that the highest (mechanical) performance can be achieved with honeycomb cores, since they are very light and very strong.

In order to bond the faces together with the skin, several bonding methods can be used. It is possible to adhesively bond the two skins on the core (gluing); the skins and the core are produced and prepared separately and bonded together afterwards. A different option is in-situ bonding, like in pultrusion; the skins are impregnated and, with a core in between, pressed together in a die to form a solid sandwich panel. Another way to ensure the bonding between skins and core is by placing the dry laminates, with the core in between, in a mould and infuse resin through it by RTM or vacuum infusion. In this way the skins and the core bond together very well (Campbell, 2010).

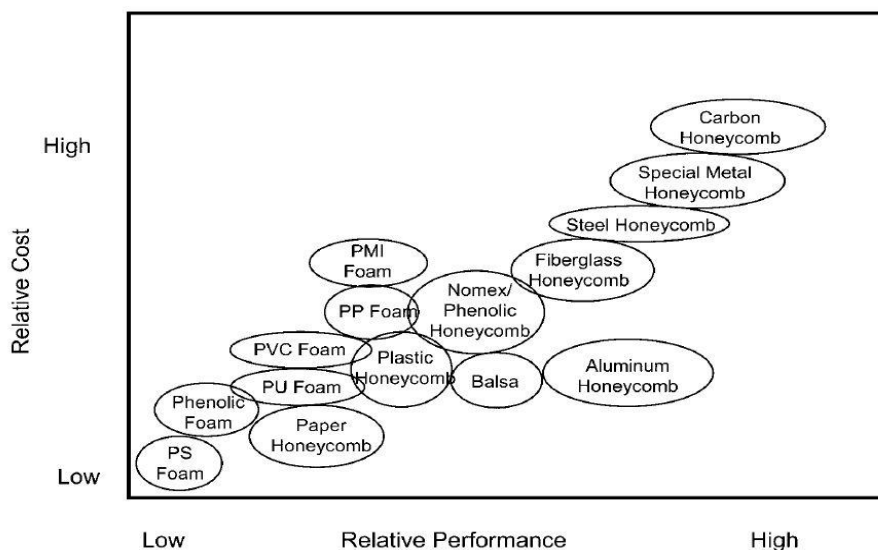


Figure 1.3: The overall relative performance of sandwich cores verses the relative costs. (Campbell, 2010)

1.1.2 Cores

As mentioned in section 0, the core of a sandwich construction is of main importance to absorb the shear stresses and maintain the distance between the two skins. Many different cores are available for commercial use; some common used examples are (Figure 1.4):

- Balsa
- Cork
- Synthetic polymer foams
- Honeycombs
- Fibre reinforced foams

The different core materials have all different characteristics and therefore different advantages. Most honeycomb constructions are very light and very strong, but are not convenient in a continuous or closed mould process. Polymer foams are usually very light and have many different sorts and therefore many diverse properties. Balsa and cork are natural products and therefore compostable after use.

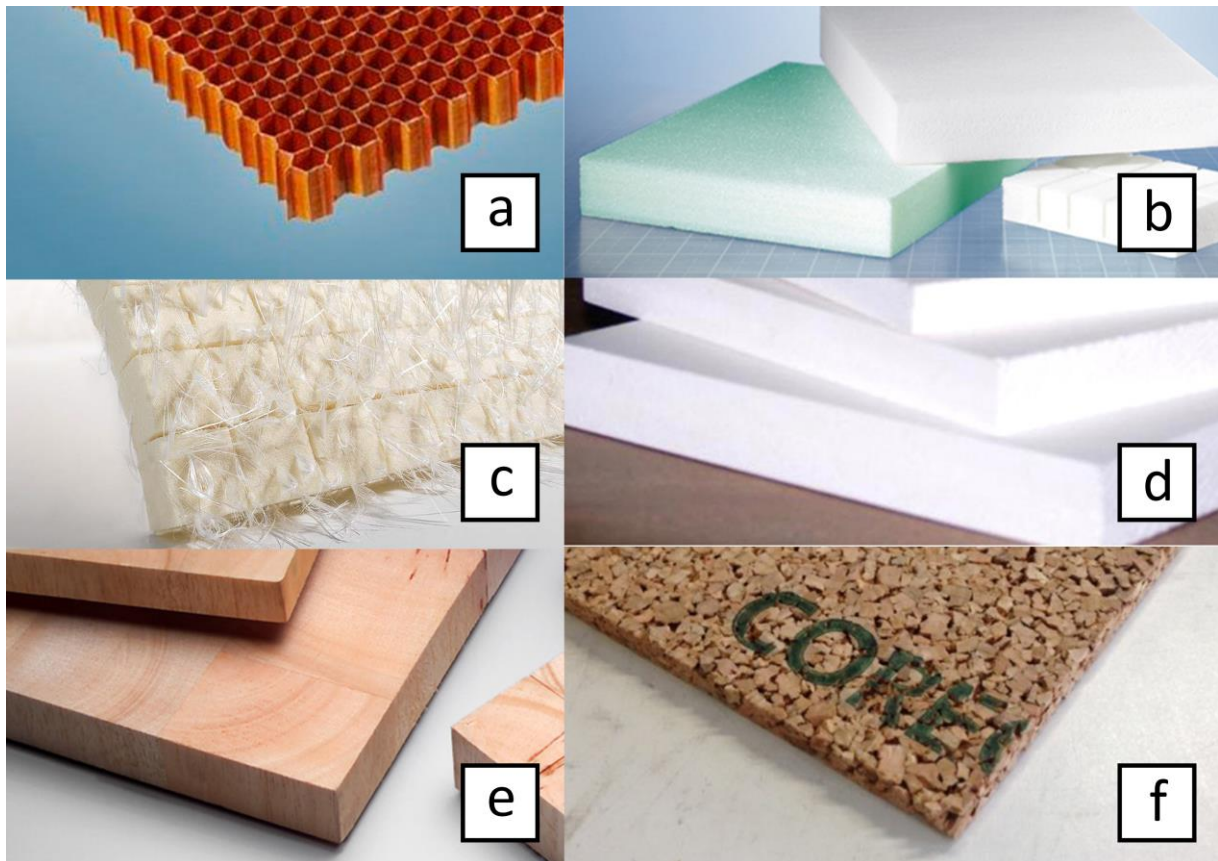


Figure 1.4: Different types of cores; a) honeycomb (Fatol, 2016), b) PET foam (Armacell, 2016), c) fibre reinforced SAN foam (Saertex, 2016), d) PVC foam (Quora, 2016), e) balsa wood (Airex, 2016) and f) cork (CastroComposites, 2016).

1.1.3 Failure of composite sandwich constructions

Composite sandwich constructions have advantages in stiffness and weight over non-sandwich composite panels, i.e. composite laminates. However, the failure of sandwich composites is more complex than the failure of composite laminates, since there are at least two different components; the composite skins and the core. This causes failure mechanisms that are specific to composite sandwich constructions. According to Craig A. Steeves, (2004), composite sandwich structures, during three-point bending, have four main failure mechanisms (Figure 1.5);

- Core shearing
- Microbuckling
- Indentation
- Face wrinkling

The first one, *core shearing* (Figure 1.5-a), is a failure of the core due to the large shear stresses in the core of sandwich construction. Since the core has worse properties than the facesheets, the core is the vulnerable point in the construction.

The second failure mechanism is *Microbuckling* (Figure 1.5-b). Microbuckling is also called face yielding, which occurs when the axial stresses in the facesheet exceed the limits and therefore fails. These failure types are predicted and expressed in lots of expressions, such as Tsai-Wu, Tsai-Hill, maximum stress criterion or Hashin damage criterion. The last one, *Hashin damage criterion*, is widely used in modelling software packages, because of its distinction between four kinds of failure including fibre compressive, fibre tension, matrix compressive and matrix tension. In this way it can be seen how and where the facesheet fails. This criterion is explained more detailed in Chapter 3.

The third failure mechanism is *indentation* (Figure 1.5-c). This failure type is also called elastic indentation, in which the facesheet deforms elastically and the core yields plastically.

The last failure mechanism is *face wrinkling* (Figure 1.5-d), where there's a short wavelength elastic buckling of the top facesheet which is resisted by the elastic core underneath, causing the facesheet to wrinkle. (Steeves C. F., 2004)

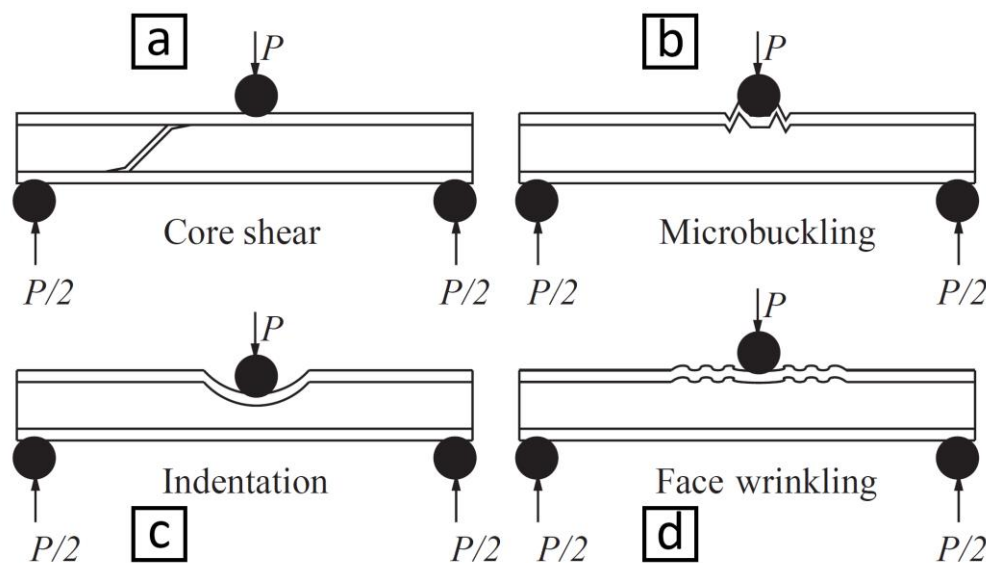


Figure 1.5: Different failure mechanisms of composite sandwich constructions (Steeves C. F., 2004).

1.2 Previous work

In literature, there are several studies which investigated the impact behaviour of composite sandwich panels. Castilho et al. (2014) investigated the impact behaviour of sandwich composites with different cores e.g. PVC, Cork and Balsa. He found that Balsa has the highest reaction (peak) force, but that Cork has the best ability to absorb impact energy by deforming instead of breaking. Hassan (2012) researched the influence of core properties on the perforation resistance in composite sandwich panels. He compared PET foam with linear PVC and crosslinked PVC and found that crosslinked PVC has the highest reaction force during impact. Wang (2013) studied low-velocity impact (LVI) behaviour of foam-cored composite sandwich panels. He found a relation between the skin thickness and the absorbed impact energy, the contact duration and the reaction force. When the skin thickness increases, the absorbed energy decreases as well as the contact duration, while the reaction force increases with increasing skin thickness. He also found that the damage state and impact response are independent of core thickness, which was tested with two different core thicknesses; 10 mm and 25 mm. Özdemir (2012) investigated the core material effect on impact behaviour of composite sandwich panels. He found that the shear strength and compressive strength values of core materials play a significant role on impact behaviour of specimens. Other result is that having a small core thickness compared to a thicker core with the same density, has a higher reaction force.

Moreover, there have been work which deal with the compression behaviour of sandwich panels after impact. Shipsha (2005) investigated the compression-after-impact strength of composite sandwich panels with core crushing damage. The experiments show that there is an influence of an impact on the compression strength of a composite sandwich panel. The difference was not significant, but there was a difference in compression strength. McQuigg (2012) researched the compression-after-impact strength of honeycomb composite sandwich panels. They found that the residual compressive strength reduction was highest in lightly damaged specimens, but increasing level of damage resulted in further reduction of the compression strength (with the reduction decreasing in magnitude). However, bending-after-impact has not been investigated yet in the available literature.

The full literature-table can be found in *Appendix B: Literature table*.

One of the main conclusions of this literature survey is that a Balsa, PVC and PET are really suitable for resisting impact in a sandwich panel, probably due to their shear strength and compressive strength. In this literature research, also one of the important conclusions was that PVC is the best foam core in comparison to other synthetic cores (Falk, 1994) (Hassan, 2012) (Shipsha A. B., 2000). It is conceivable that this is caused by its high shear modulus and tensile modulus (Young's Modulus). Furthermore, the literature shows that the top skin is most important in impact scenarios, which seems plausible because this is the first (and if strong enough the only) part in contact with the impactor (Wang, 2013). Another important conclusion in the literature is that a foam core can be strengthened by a 3D fibre reinforcement (Kim, 1999). In this way the fibre reinforced foam had a strength which is up to 10 times higher than the non-reinforced foam.

1.3 Research goal and objectives

The main goal of the research is to understand the mechanical behaviour of sandwich composites in bending after impact which has not been considered up to now in the literature discussed in section 1.2 *Previous work*. Therefore, there is ample room for conducting research on the residual mechanical performance of sandwich composites after impact in order to have a deeper understanding of the damage tolerance of these structures. The objectives of this study are:

- To identify the influence of an impact loading on the residual bending stiffness of a composite sandwich panel
- To determine the failure modes of sandwich composites after only impact loading as well as in bending after impact
- To illustrate the influence of core material type on the mechanical behaviour of the sandwich composites in bending after impact
- To demonstrate the effect of impact energy on the mechanical response of sandwich panels in bending after impact

An overview of the approach is shown in Figure 1.6. In order to gather insight and information, the literature research is done. Thereafter, two types of analyses are done; experimental analysis and Finite Elements Method (FEM) analysis. These two types are separated into three different tests; Impact-Only (IO), Bending-Only (BO) and Bending-after-Impact (BAI). The BO results will be compared with the Bending-after-Impact results in order to determine the influence of an impact on the mechanical response of composite sandwich panels. After this comparison the first three research questions can be answered. In order to answer the fourth question, an extensive FEM simulation is done in order to compare the results of the different impact energies.

1.4 Outline of the thesis

In Chapter 2 the materials (and the corresponding dimensions) used in this thesis are described in detail. Also the experimental set-ups used in this investigation, impact tests and three-point bending tests, are described extensively. In Chapter 3 the Finite Elements Method models are described in detail, which is separated in three sections; an impact-only model, multiple bending-only models and finally the bending-after-impact models. In Chapter 4 the results will be shown and discussed. This chapter is divided in the same sections as chapter 3; Impact-only, bending-only and bending-after-impact. In each section there will be a part with the experimental results and a part with the FEM results. Finally, in Chapter 5 the conclusions will be drawn and the future recommendations will be provided.

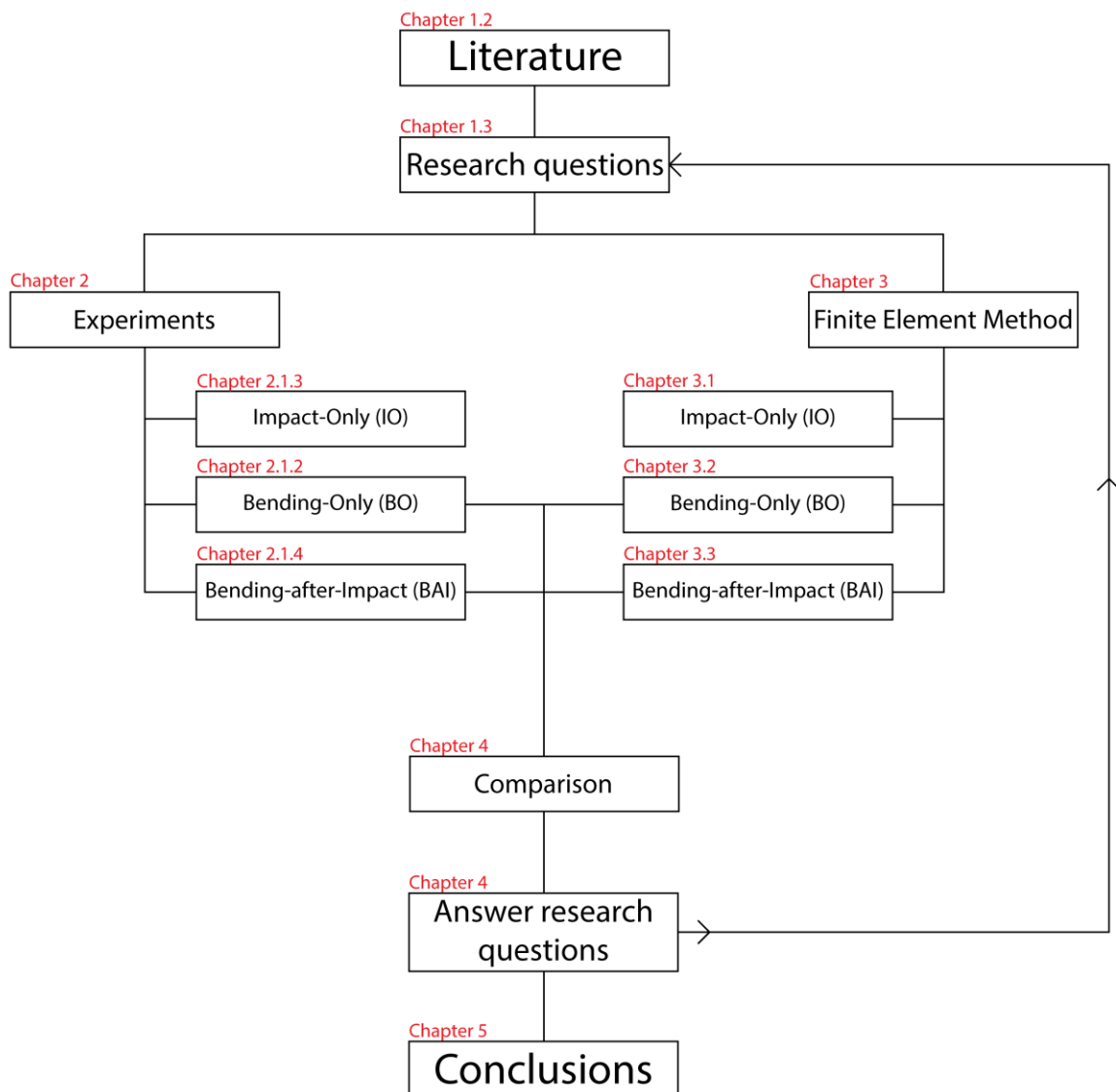


Figure 1.6: Overview of the approach in order to answer the research questions

2. Materials and experiments

In this chapter, the utilized materials are described in detail. In order to be able to understand the behaviour of composite sandwich materials during impact and bending after impact, certain practical tests are done. Three different experimental testing are carried out: Impact test (Impact-only; IO), 3-point bending test (Bending-Only; BO) and bending test after impact (Bending-after-Impact; BAI). The corresponding configuration of experimental set-ups are presented in detail. Figure 2.1 gives an overview of the experimental analysis.

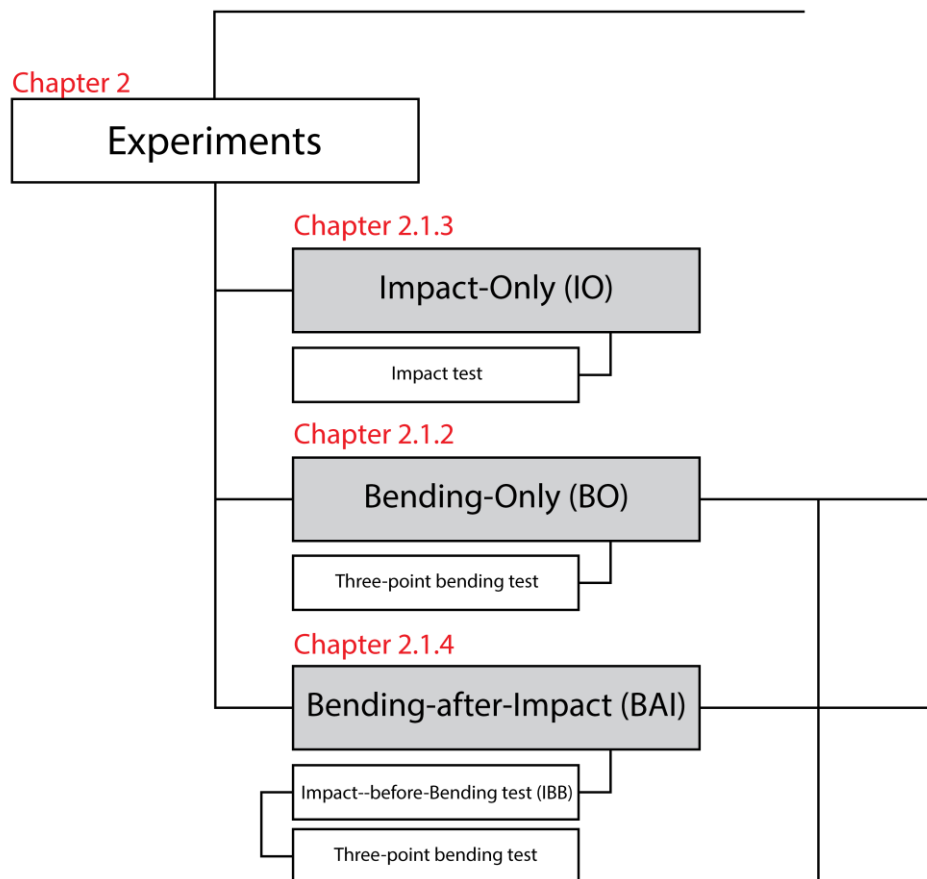


Figure 2.1: Overview of the experimental part of this thesis.

2.1 Experimental testing

In order to characterize the mechanical performance of the sandwich panels, several experiments tests are performed. First as a benchmark, a 3-point bending test and an impact test are carried out in order to determine and understand the basic mechanical behaviour during these loading scenarios. Afterwards, an impact test is performed on specimens, after which these same specimens are subjected to a 3-point bending test. In this way, the residual mechanical performance is determined.

The Balsa specimens are all cut out of one single panel, in order to ensure overall equality in properties. The PET and SAN specimens are made from a second panel, produced in one single infusion.

2.1.1 Materials

In this section the glass fibres and the layup will be described in detail, the resin and the core materials will be described briefly. The details of the briefly discussed materials and the production process can be found in *Appendix C: Materials*.

In the experiments, composite facesheets are made of glass fibres with an epoxy resin. The following glass fibres are used to produce the specimens:

- Saertex S32EQ260-00820-01270-450000 Quadraxial-glass-fabric 822 g/m² with PES tricot-warp stitching and with [0/-45/90/+45] layup

This type of fabric is quadraxial which means it has four different fibre directions inside one single ply. In Figure 2.2, it can be seen how these plies are build up. The single fibre orientations are stitched together with a PES tricot-warp stitching. One single layer including the stitches have a weight of 822 grams per square metre.

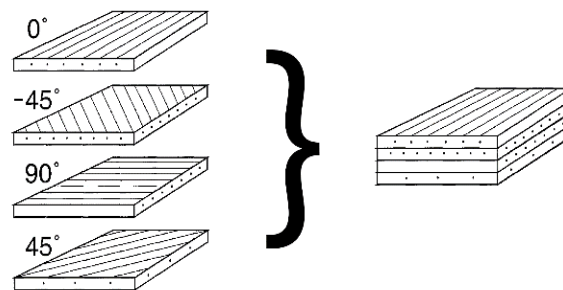


Figure 2.2: The layup of the quadrax glass fibre mat, made up of 4 single UD plies.

In the composite sandwich panels, use is made of three different core materials. The first core material is SAN foam with a density of 85 kg/m³. The second core material is PET foam with a density of 65 kg/m³ and the third core material is Balsa wood with a density of 155 kg/m³. The specifics of these core materials can be found in *Appendix C: Materials*.

The panels are build up in the mould with first three layers of quadraxial fibres. The core is placed on top of that and then again three layers of quadraxial fibres are placed on top of the core. The quadraxial fibres are orientated with the 0° layer faced towards the core, symmetric around the core. In Figure 2.3 an example is shown of the balsa panel layup.

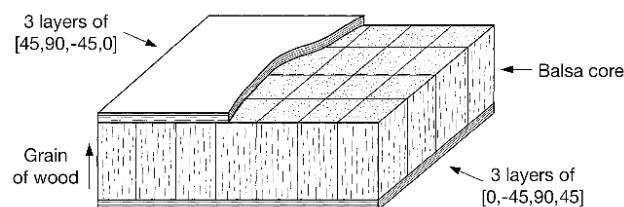


Figure 2.3: The layup of the composite sandwich panel; 3 layers of quadrax (with the 0° faced towards the core), then the core and on top again three layers of quadrax (with the 0° faced towards the core) symmetric with the core.

2.1.2 Bending testing setup

The specimens are cut into pieces of 200 mm x 75 mm with a thickness of 30.2 mm, as shown in Figure 2.4. The specimens are subjected to a three-point bending, a vertical displacement until the reaction force drops a certain percentage. This test is performed according testing standard *ASTM C393/C393M* on a *Zwick Z100* tensile testing machine, capable of performing forces up to 100 kN. The fixtures used in this test are three half-cylindrical shaped fixtures with a diameter of 50 mm, a width of 100 mm and a span of 150 mm according the testing standard. The test is performed with a vertical speed of 6 mm/min until the reaction force drops 50% or until the deformation is 20 mm, whichever is first. The complete setup is depicted in Figure 2.5.

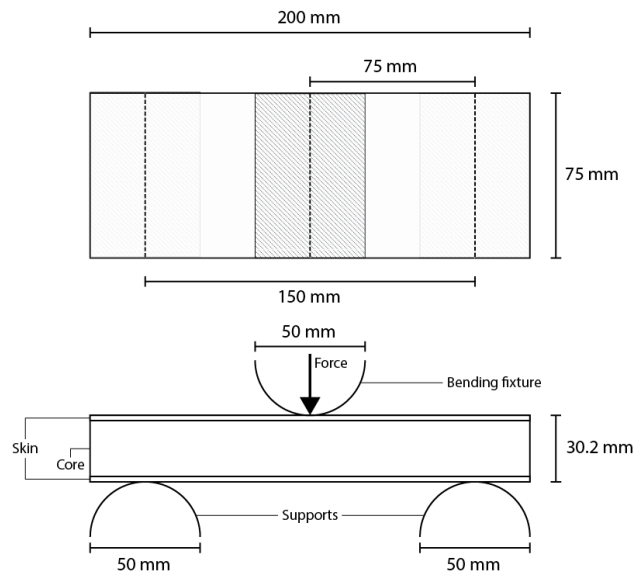


Figure 2.4: The dimensions of the bending test panels according testing standard *ASTM C393/C393M*.

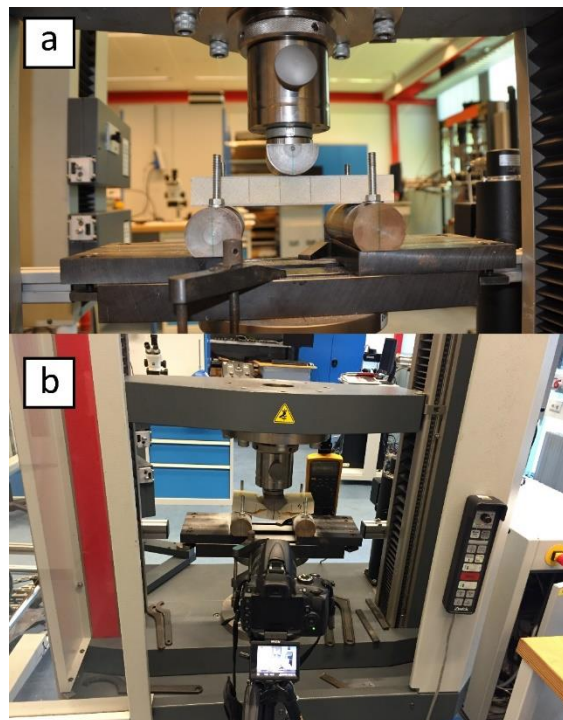


Figure 2.5: The testing setup of the bending tests according testing standard *ASTM C393/C393M*. In a) the setup of the three-point bending test and in b) the camera setup in order to capture the failure.

2.1.3 Impact testing setup

The specimens are cut into pieces of 150 mm x 100 mm with a thickness of 30.2 mm as shown in Figure 2.6. The specimens are subjected to an impact force of 3.4 m/s with a weight of 5.895 kg, from a height of 60 cm. The test is performed according testing standard *ASTM D7136/D7136M* on a *Dynatup 8250* falling weight impact machine. The specimens are impacted with a hemispherical tup of 16 mm diameter. The loading cell used in this test is a *Kistler 901 1A SN1530440*, capable of processing a 15 kN force. The impact-tup is attached to an extension beam, in order to enable the impact on the panel on the sub-plateau of the machine. The extension beam is attached to the added weight (4.95 kg). The complete setup (extension beam, bolts, tup, added weight), weights 5.895 kg. The specimens are clamped with four clamps to prevent the specimens from moving. After the impact has occurred two pneumatic support units move up, in order to prevent a second impact of the impact tup after bouncing. The complete setup is shown in Figure 2.7.

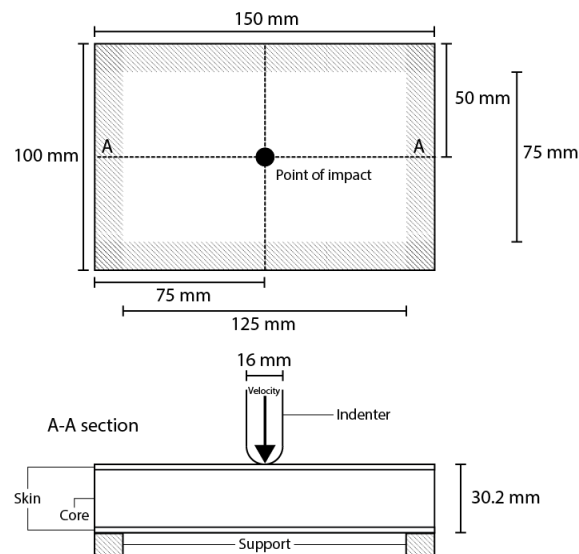


Figure 2.6: The dimensions of the impact test panels according the *ASTM D7136/D7136M* standard.

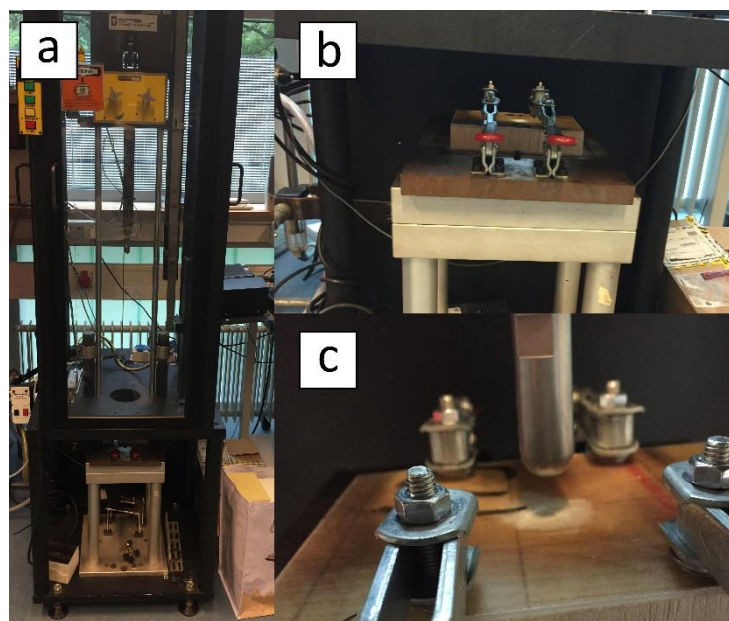


Figure 2.7: The impact test setup according testing standard *ASTM D7136/D7136M*. In a) the complete setup, in b) the fixture with a specimen and in c) the indenter of the impact setup.

2.1.4 Bending after impact testing setup

The specimens of this test are the same size as the static loading test (Section 2.1.2 *Bending testing setup*), 200 mm x 75 mm with a thickness of 30.2 mm as shown in Figure 2.8. The specimens are subjected to an impact (IBB; Impact-before-Bending) as described in 2.1.3 *Impact testing setup* and thereafter subjected to a static loading (BAI; Bending-after-Impact) as described in 2.1.2 *Bending testing setup*. The specimen's dimensions are shown in Figure 2.8 and the complete setup is shown in Figure 2.9.

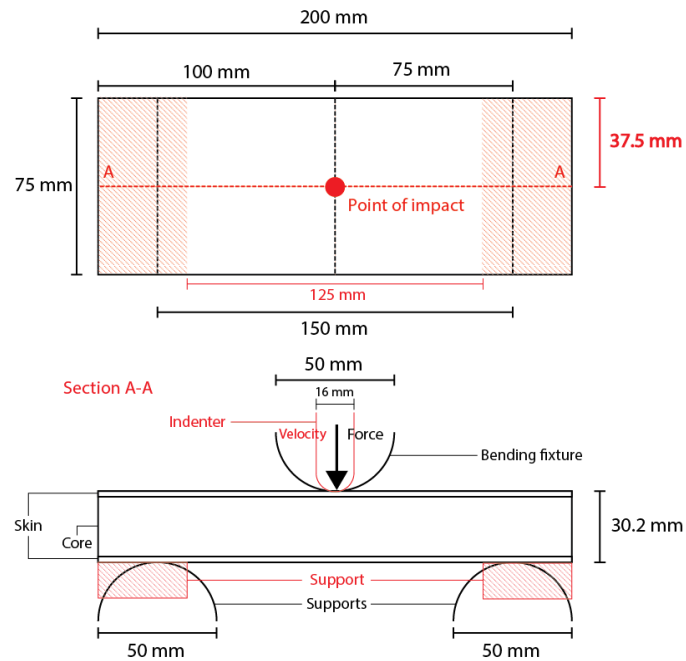


Figure 2.8: The dimensions of the BAI test panels, according to the testing standard for bending composite sandwich panels; ASTM C393/C393M. The black lines are related to the bending test and the red lines are related to the impact test.

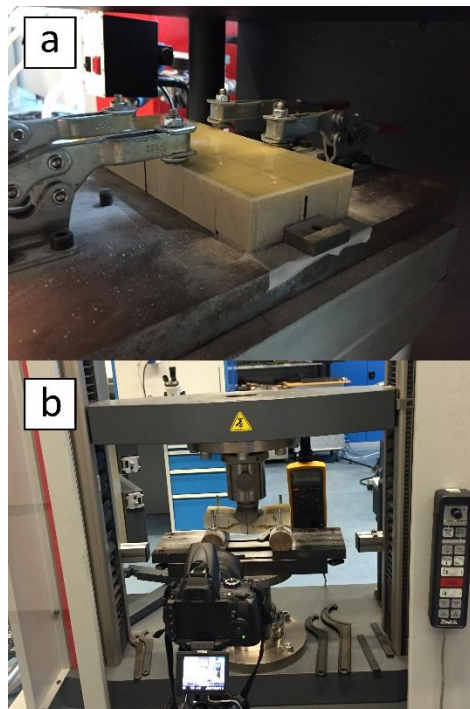


Figure 2.9: Bending-after-Impact testing setup with the impact test on top and below the three-point-bending test. In a) the impact (IBB) setup and in b) the bending (BAI) setup.

2.2 Analytical calculation of maximum stresses and shear stresses

Different papers describe how to calculate the maximum (shear) stresses in sandwich constructions during three-point bending. The utilized ASTM standard for three-point bending (ASTM-C393/C393M, 2012) describes as stated in Table 2.1. Arbaoui (2014) investigated the effect of the core thickness and intermediate layers on the mechanical properties of a polypropylene honeycomb sandwich panel. He also formulated a way to calculate the shear stress in the core during three-point bending. This formulae can also be found in Table 2.1. Chawla (1998) describes the shear stresses in non-sandwich laminates while bending, which is also stated in Table 2.1.

In the formulas in Table 2.1, the P represents the load at fracture, which is the maximum force in the three-point bending tests in the analyses in this thesis. The S represents the span, which is 150 mm in the three-point bending tests in this thesis. The b represents the width of the specimens (75 mm in this thesis), h is the overall thickness (30.2 mm in this thesis), h_s is the skin thickness (2.4 mm in this thesis), h_c is the core thickness (25.4 mm in this thesis) and d is the distance between the centrelines of the skins (27.8 mm in this thesis).

Table 2.1: Analytical equations for maximum stress and shear stress calculation.

Paper	Maximum shear stress
(ASTM-C393/C393M, 2012)	$\tau_{max} = \frac{P}{(h + h_c)b}$
(Arbaoui, 2014)	$\tau_{max} = \frac{P}{2bd}$
(Chawla, 1998)	$\tau_{max} = \frac{3P}{4bh}$

3. Finite Element Method analysis

In order to improve the understanding of the bending and impact situations, several FEM analyses are applied. In this chapter the FEM models for impact-only (IO), bending-only (BO) and bending-after-impact (BAI) are described in detail. The IO model is modelled in a 3D dynamic analysis, because the time is important in impact situations. The IO simulations are modelled in two different ways; with Damage Criteria (DC) of the skin and without DC of the skin. The BO model is modelled in three different ways; a 2D model, a simple 3D model and a more complex 3D model to justify the correct FEM implementation. Analytical calculations of (shear) stresses are performed in order to validate the models with the experiments. Finally, a 3D impact model is made (Impact-before-Bending; IBB), with the dimensions of a bending panel and thereafter implemented in a three-point bending simulation, i.e. BAI. An overview of this chapter is summarized in Figure 3.1.

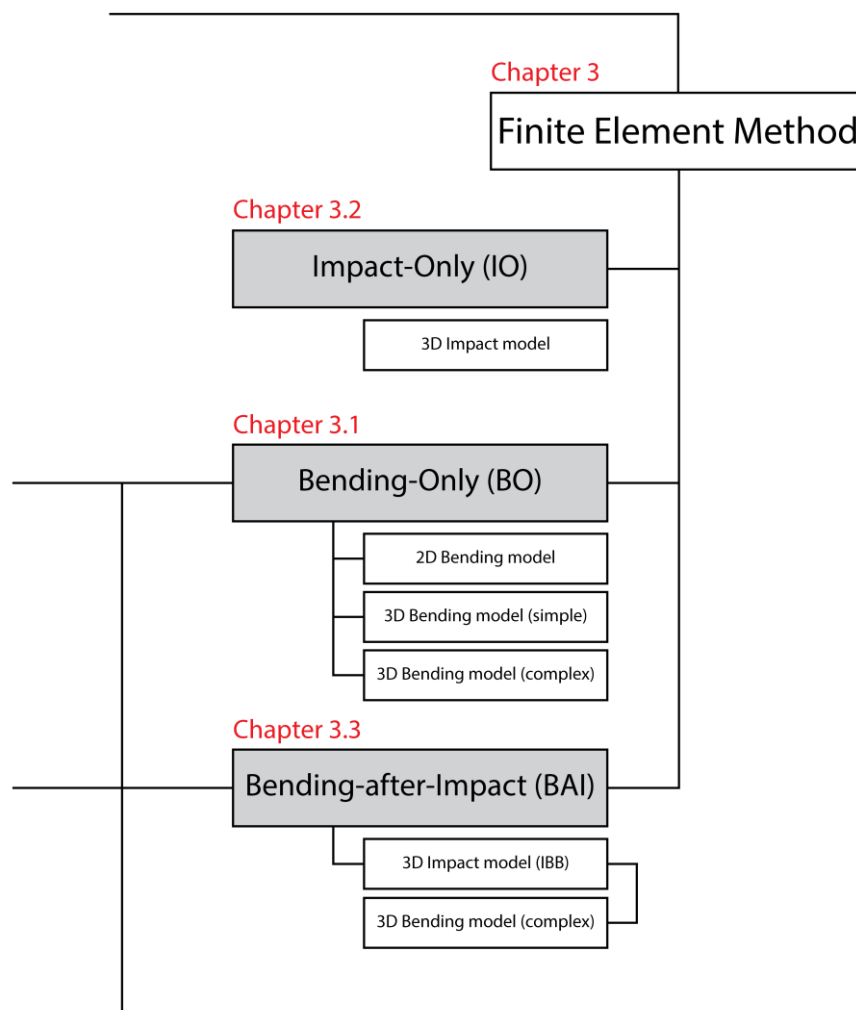


Figure 3.1: Overview of the FEM analysis with the three different situations divided into one or more models.

In the following sections the FEM models will be discussed. In these sections the terms in between brackets [...], are options available in the ABAQUS software package.

3.1 Bending-Only (BO) model

In order to model the bending problem, as in the experimental analysis, first a simple 2D model is made for its short computation time. Thereafter a simple 3D model is created, in order to have a working 3D model which could be compared to the reality and still has short computation time. Finally, a more complex 3D model is made which needed to have the same characteristics as the impact model, since the impact model needs to be used in the BAI simulations.

In Table 3.1 an overview is given of the differences in the different bending models. The models are also depicted in Figure 3.7 in which both 3D models have the same appearance.

Table 3.1: Comparing different bending models.

	Model 1	Model 2	Model 3
Model	<u>2D</u> , deformable with sections.	<u>3D</u> , deformable with sections (simple).	<u>3D</u> , deformable core with shell skins (complex).
Material model	Skins; engineering constants <u>without</u> failure type. Cores; isotropic <u>without</u> plasticity model.	Skins; engineering constants <u>without</u> Hashin failure type. Cores; isotropic <u>with</u> the Crushable foam model.	Skins; engineering constants <u>with</u> Hashin failure type. Cores; isotropic <u>with</u> the Crushable foam model.
Analysis type	Static general	Static general	Static general
Mesh type	Skins; plane stress Core; plane stress	Skins; <u>3D stress</u> Core; 3D stress	Skins; <u>Continuum shell</u> Core; 3D stress
Interactions	Skins-fixtures; surface-to-surface.	Skins-fixtures; surface-to-surface.	Skins-fixtures; surface-to-surface. Skins-core; Tie
Loading condition	displacement of upper fixture	displacement of upper fixture	displacement of upper fixture
Boundary conditions	Encastred bottom fixture, X-symmetry.	Encastred bottom fixture, X- and Z-symmetry.	Encastred bottom fixture, X- and Z-symmetry.
Geometry	<u>2D</u> Length: 100 mm Height: 30.2 mm (2.4 mm skin and 25.4 mm core)	<u>3D</u> Length: 100 mm Width: 75 mm Height: 30.2 mm	<u>3D</u> Length: 100 mm Width: 75 mm Height: 30.2 mm

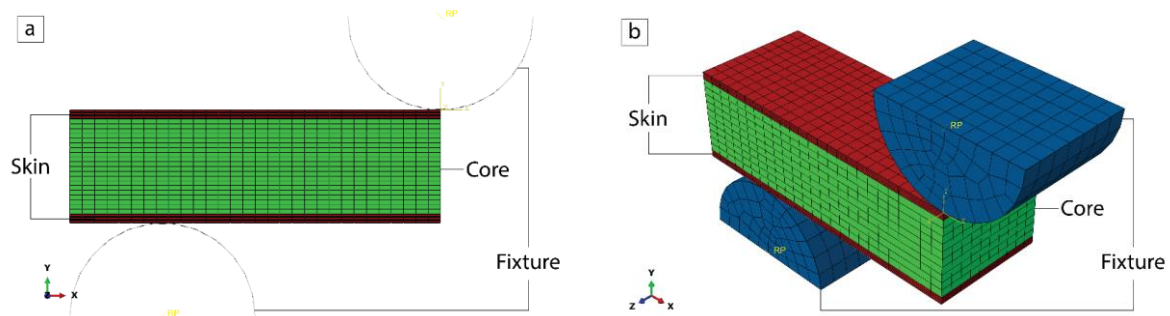


Figure 3.2: FEM models of a) model 1, the 2D model, b) model 2 and 3, the simple and complex models. Both models have 2.4 mm thick skins and a 25.4 mm thick core.

3.1.1 Material models

The material properties of the datasheets in *Appendix D: Datasheets* where not aligning with the experiments, therefore Table 3.2 provides datasheet values and the values fitted to the experiments. More details can be found in *Chapter 4*. The orthotropic properties of the facesheet are simulated using the Elastic Type [Engineering Constants], while the isotropic properties of the SAN, PET and Balsa cores are simulated using the Elastic Type [Isotropic].

In the first (2D) model no damage criteria and plasticity models are used since these are not possible in 2D modelling. In model 2 and 3, the plasticity model used for the core materials is [Crushable Foam] with [Crushable Foam Hardening] in order to simulate the plastic hardening of the cores. In model 3 the Damage Initiation type used for the glass facesheet is [Hashin Damage] with a [Damage Evolution] in order to simulate the failure of the facesheet.

Table 3.2: Properties of the used materials in the ABAQUS software package.

	Units	Glass facesheet	Model 1; SAN core		Model 2; PET core		Model 3; Balsa core	
		Datasheet	Fitted	Datasheet	Fitted	Datasheet	Fitted	Datasheet
Density	Kg/m ³	1,500		85		65		155
Young's Modulus E ₁	MPa	20,696	85	72	25	85	300	142
Young's Modulus E ₂	MPa	20,696	85	72	25	85	300	142
Young's Modulus E ₃	MPa	12,578	85	72	25	85	300	385
Poisson ratio ν_{12}		0.285		0		0		0.45
Poisson ratio ν_{13}		0.285		0		0		0.014
Poisson ratio ν_{23}		0.375		0		0		0.014
Shear Modulus G ₁₂	MPa	4,860		29		12		18
Shear Modulus G ₁₃	MPa	6,360		29		12		326
Shear Modulus G ₂₃	MPa	4,860		29		12		326
Longitudinal Tensile Strength σ_{1t}	MPa	272		1.62		1.5		6.5
Longitudinal Compressive Strength σ_{1c}	MPa	340	1.4	1.02	0.6	0.8	5.5	7.9
Transverse Tensile Strength σ_{2t}	MPa	207		1.62		1.5		6.5
Transverse Compressive Strength σ_{2c}	MPa	308	1.4	1.02	0.6	0.8	5.5	7.9
Longitudinal Shear Strength τ_{12}	MPa	100		1.09		0.5		2.5
Transverse Shear Strength τ_{13}	MPa	100		1.09		0.5		2.5

A continuum damage initiation criterion is defined for the glass facesheet which is based on [Hashin Damage] with a [Damage Evolution] option available in ABAQUS in order to simulate the failure of the facesheet. The Hashin damage criteria consist of 4 different criteria; the fibre tension (Eq. 3.1), matrix tension (Eq. 3.2), fibre compression (Eq. 3.3) and matrix compression (Eq. 3.4) criteria. When the failure criteria given in equations 3.1-3.4 is smaller than 1 there is no failure and when it is greater than 1 there exists a damage and a subsequent damage evolution using the linear degradation of elements. The degradation elements, i.e. the damage evolution, is defined using the linear fracture energy definition in ABAQUS. (Barbero, 2013)

$$F_f^t = \left(\frac{\sigma_{11}}{X^T}\right)^2 + \alpha \left(\frac{\tau_{12}}{S^L}\right)^2 \quad \text{Eq. 3.1}$$

$$F_m^t = \left(\frac{\sigma_{22}}{Y^T}\right)^2 + \left(\frac{\tau_{12}}{S^L}\right)^2 \quad \text{Eq. 3.2}$$

$$F_f^c = \left(\frac{\sigma_{11}}{X^C}\right)^2 \quad \text{Eq. 3.3}$$

$$F_m^c = \left(\frac{\sigma_{22}}{2S^T}\right)^2 + \left[\left(\frac{Y^C}{2S^T}\right)^2 - 1 \right] \frac{\sigma_{22}}{Y^C} + \left(\frac{\tau_{12}}{S^L}\right)^2 \quad \text{Eq. 3.4}$$

Where σ_{11} is the normal stress in the X-direction (fibre direction), σ_{22} is the normal stress in the transverse direction (Y-direction), τ_{12} is the in-plane shear stress in the XY-plane, X^T is the longitudinal tensile strength (σ_{1t} in Table 3.2), Y^T is the transverse tensile strength (σ_{2t} in Table 3.2), X^C is the longitudinal compressive strength (σ_{1c} in Table 3.2), Y^C is the transverse compressive strength (σ_{2c} in Table 3.2) and S^L is the longitudinal shear strength (τ_{12} in Table 3.2).

Since the directions and the properties of the skins are important because of the failure criteria, the coordinate system is changed (1-direction = X, fibre direction, 2-direction = Y, out-of-plane transverse direction, 3-direction = Z, in-plane transverse direction) which can be seen in Figure 3.3.

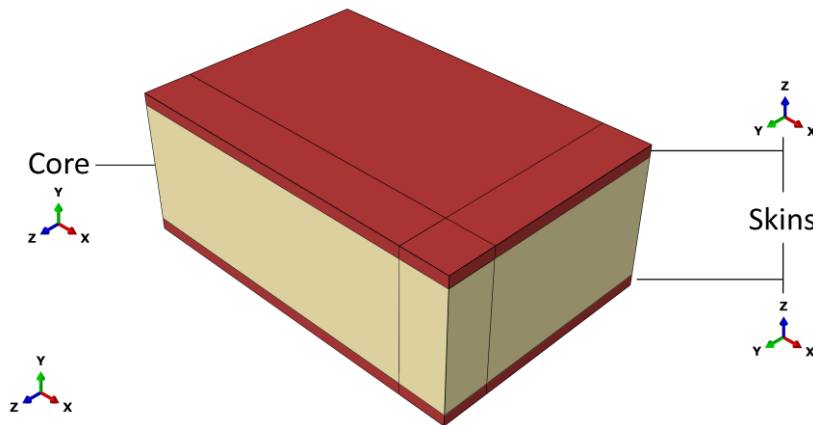


Figure 3.3: Different coordinate systems in the FEM models.

The material model used for the core materials is [Crushable Foam] with [Crushable Foam Hardening] in order to simulate the plastic hardening of the cores. Actually balsa core has orthotropic properties, but the isotropic properties are used, since the crushable foam requires isotropic instead of orthotropic properties in ABAQUS. For the [Crushable Foam Hardening], the materials plasticity values of stress and strain are required. The plasticity of polymer foam materials is described in several studies in literature such as (Panduranga, 2007) and (Vries, 2009). Polymer foams behave, when compressed, elastically up to a certain (yield) point (Figure 3.4-a), after this yield point it behaves plastically (resulting in a plateau) up to a certain point (Figure 3.4-b). Compressing it even further results in densification of the foam, which means that the small cells in the foam are all packed together until the foam fails (Figure 3.4-c). This behaviour can be seen when the stress-strain curve is plotted during a compression test of a foam based core material, which can be seen in Figure 3.4.

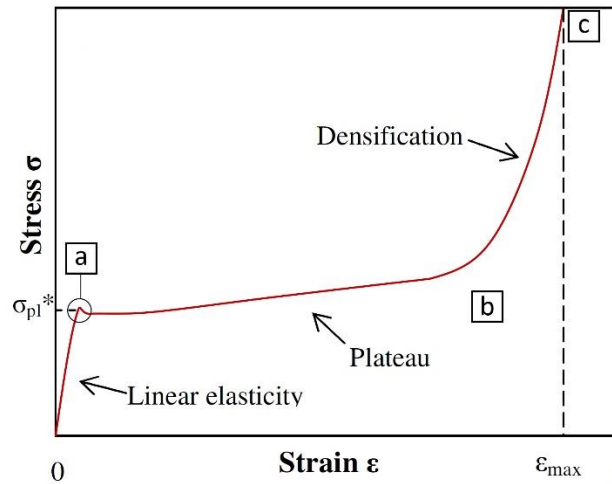


Figure 3.4: Stress-strain curve of a polymer foam in a compression test. (Vries, 2009)

The different cores used in this thesis have, obviously, different values for these critical points. RapraTechnology (2007) describes the forming process of different polymer foams. In (RapraTechnology, 2007) it is also described how SAN foam behaves during compression, which can be seen in Figure 3.5-a, in which SAN (0.067 g/cm^3) is in the same order of magnitude as the SAN foam used in this thesis. Sakly (2016) researched the low velocity impacts on composite sandwich constructions and also described the compression behaviour of PET foam, which is depicted in Figure 3.5-b, in which the blue curve is in the same order of magnitude as the PET foam used in this thesis. Vural (2003) investigated the microstructural aspects and modelling of naturally porous composites, in which the balsa was investigated. He describes the compression behaviour of balsa during a compression test, which is shown in Figure 3.5-c, in which the B-curve is in the same order of magnitude as the balsa used in this thesis.

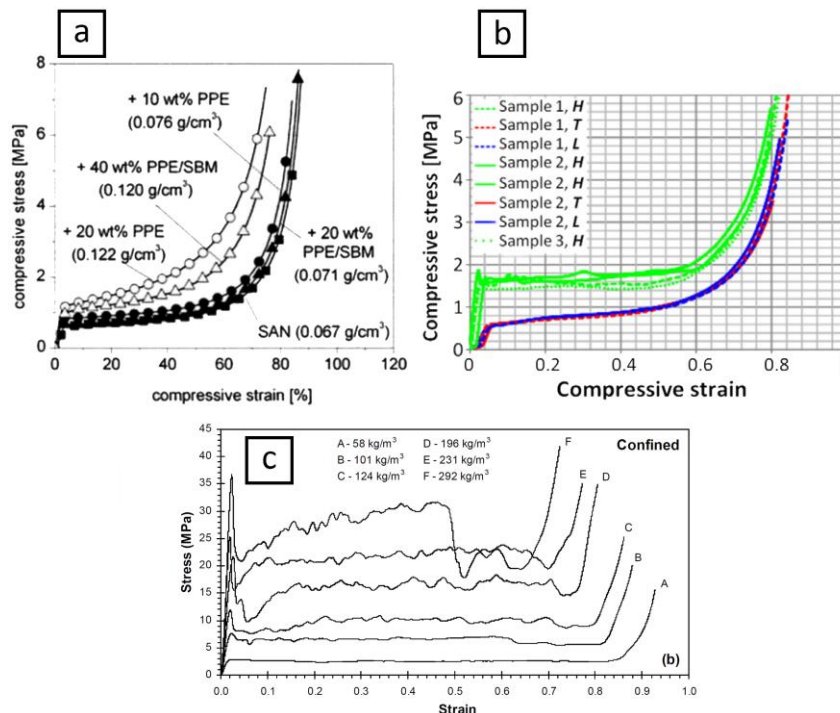


Figure 3.5: Plasticity curves of a) SAN foam (RapraTechnology, 2007), b) PET foam (Sakly, 2016) and c) balsa wood (Vural, 2003).

In this thesis, the crushable foam parameters are defined based on literature and fitted to the experimental results. The corresponding parameters that define the crushable foam material model (Figure 3.4) in ABAQUS are summarized in Table 3.3.

Table 3.3: Plasticity values used in the ABAQUS software package in order to simulate the Crushable Foam.

	SAN foam		PET foam		Balsa	
	Stress (MPa)	Plastic strain	Stress (MPa)	Plastic strain	Stress (MPa)	Plastic strain
Yield point (1)	1.40	0.0	0.60	0.0	5.50	0.0
End plateau (2)	30.0	0.7	0.65	0.7	5.70	0.8
End densification (3)	35.0	1.0	5.0	1.0	15.0	1.0

3.1.2 Analysis type

In order to simulate the 2D and 3D bending, a [Static General] type is performed, since it is a static situation. The simulation time period was 1 second with [Non-linear Geometry] switched off.

3.1.3 Mesh type

Model 1

The mesh of the facesheets and the core are [Standard] type [Plane Stress] elements (**CPS4R**) with [Linear Geometric Order]. The elements have [Default Hourglass Control], [Default Element Deletion], [Default Max Degradation] and no [Second-order Accuracy]. The element type that is used is [Structured Quad-dominated].

The fixtures have a standard type [Discrete Rigid Element] mesh type with [Linear Geometric Order].

Model 2

The mesh of the facesheets and core are [Standard] type [3D Stress] elements (**C3D8R**) with [Linear Geometric Order]. [Default Hourglass Control], [Default Element Deletion], [Default Max Degradation] and no [Second-order Accuracy]. The element type that is used is [Hex], stacked from the top plane.

The mesh of the fixtures are [Standard] type [3D Stress] elements (**C3D8R**) with [Linear Geometric Order]. No [Second-order Accuracy], [Default Distortion Control], [Default Hourglass Control], [Default Element Deletion] and [Default Max Degradation]. The element type that is used is [Sweep Hex], stacked from the front plane.

Model 3

The mesh of the facesheets are [Standard] type [Continuum Shell] elements (**SC8R**) with [Linear Geometric Order]. No [Second-order Accuracy], [Default Distortion Control], [Default Hourglass Control], [Default Element Deletion] and [Default Max Degradation]. The element type that is used is [Structured Hex], stacked from the top plane.

The mesh of the cores are [Standard] type [3D Stress] elements (**C3D8R**) with [Linear Geometric Order]. No [Second-order Accuracy], [Default Distortion Control], [Default Hourglass Control], [Default Element Deletion] and [Default Max Degradation]. The element type that is used is [Structured Hex], stacked from the top plane.

The mesh of the fixtures is the same as the mesh in model 2.

The skin consists of 300 elements in the 2D model and of 6,000 elements in the 3D models. The core contains 600 elements in 2D and 6,000 elements in 3D. Together this results in 1,200 elements in the 2D model and 18,000 elements in the 3D models.

The fixtures are built of 14 elements in 2D (wire) and of 336 elements in 3D.

3.1.4 Interactions

All models have a [Surface to surface] contact interaction between the skins and the fixtures with [Finite sliding], in which the fixtures are the master surfaces and the skins are the slave surfaces. This contact is modelled as a [Hard contact]. In model 2 and 3, the fixtures are constrained with a [Rigid body] constraint. In model 3 the skins and the core are bonded using a [Tie] interaction in order to ensure rigid bonding. This means that the slave surface makes the exact same movement as the master surface at each node. Since the load presses from the top, it is decided that the upper fixture is the master surface and the skin-surface underneath is the slave surface and for the bottom surface pair the bottom fixture is the master surface and the skin is the slave surface.

3.1.5 Loading and boundary conditions

The models are loaded by the upper fixture with a displacement of 2.5 mm in the vertical direction, which is represented by the Y-direction in Figure 3.6 (green edge/surface). The boundary conditions are shown in Figure 3.6, in which can be seen that the bottom-fixture is encastred (blue edge/surface), which means that all degrees of freedom are fixed. Furthermore, the 2D panel is imposed with x-symmetry on the right edge, which means the panel is mirrored in this edge (red edge) and the 3D panels are imposed with Y-symmetry as well (yellow surfaces in Figure 3.6).

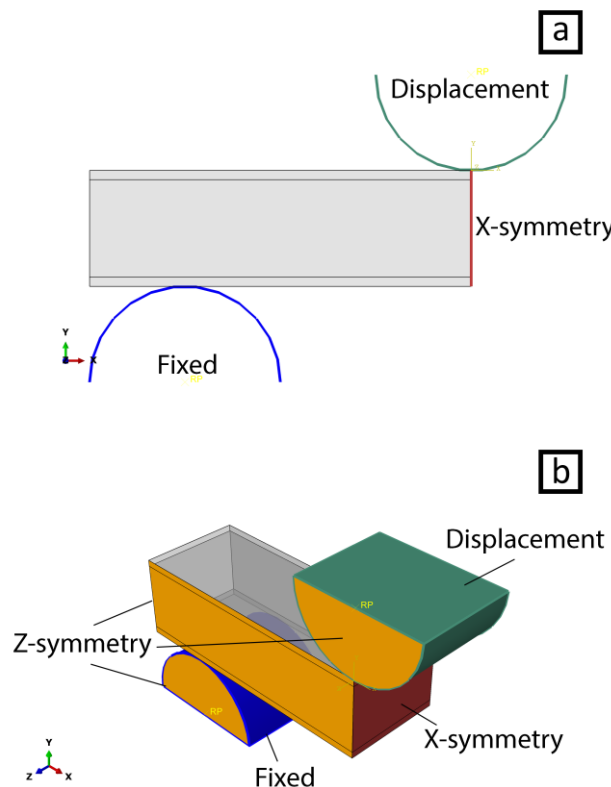


Figure 3.6: Loading and boundary conditions of the FEM bending models in the ABAQUS software package, with a) the 2D-model boundary conditions, b) the 3D-simple-model boundary conditions and c) the 3D-complex-model boundary conditions

3.2 Impact-Only (IO) model

In order to model the impact problem, the sandwich panel used in the impact tests, i.e. 150 mm length and 100 mm width, is modelled in the ABAQUS software package. Due to symmetry condition, only a quarter of the panel is modelled, which results in reduction of computational cost. The composite sandwich model consists of two 2.4 mm thick facesheets with a 25.4 mm thick core in between, resulting in a 30.2 mm thick panel. The finite elements model of this panel is shown in Figure 3.7.

In order to simulate the impact behaviour, two situations are chosen to be simulated; 1) impact without failure criteria of the skins and 2) impact with failure criteria of the skins. The first situation, without the failure criteria, is chosen in order to decrease calculation time since the model is more simple than the one with the damage criteria. The second situation, the one with the failure/damage criteria, is chosen in order to better simulate the real situation. The most important differences are summarized in Table 3.4.

Table 3.4: Differences between the two impact models for the skin. Note that the core model is the same in Model 1 and Model 2.

	Model 1	Model 2
Material model	No damage criteria	Hashin damage criteria
Mesh type	3D stress	Continuum shell

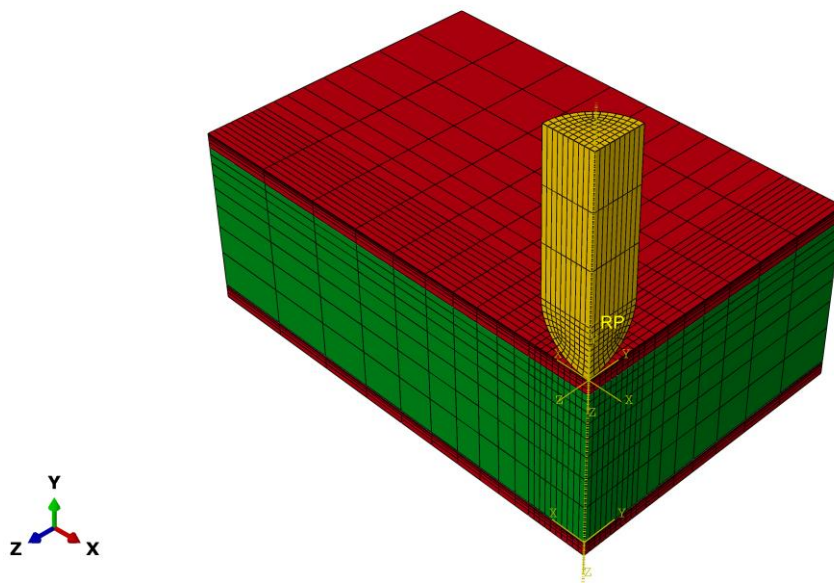


Figure 3.7: FEM model of the impact test in the ABAQUS software package with in green the core, in red the skins and in orange the indenter.

3.2.1 Material models

The material properties are the same as in the BO simulation in section 3.1 *Bending-Only (BO) model*. The IO analysis is done using two different models; one model with (Hashin) damage criteria of the skin and one model without damage criteria of the skin.

3.2.2 Analysis type

In order to simulate the three-dimensional impact loading, a [Dynamic Explicit] type is performed. An explicit analysis is a dynamic analysis, which means that time plays an important role unlike in the implicit (static) analysis. The simulation time period was 0.02 seconds with a [Non-linear Geometry].

3.2.3 Mesh type

The mesh of the facesheets are explicit type [Continuum Shell] elements (**SC8R**) with [Linear Geometric Order]. [Stiffness] enhanced [Hourglass Control] and [Element Deletion] are switched on. [Default Max Degradation] and no [Second-order Accuracy]. The element type that is used is [Hex], stacked from the top plane.

The mesh of the cores is made of explicit type [3D Stress] elements (**C3D8R**) with [Linear Geometric Order] and [Average strain] of Kinematic Split. No [Second-order Accuracy] and [Distortion Control] was switched on. [Stiffness] enhanced [Hourglass Control] and [Element Deletion] are switched on and Default [Max Degradation]. The element type that is used is [Hex], stacked from the top plane.

The mesh of the indenter is made of explicit type [3D Stress] elements (**C3D8R**) with [Reduced Integration], [Linear Geometric Order] and [Average strain] of Kinematic Split. [Distortion Control] and [Element Deletion] are switched on. [Stiffness] enhanced [Hourglass Control] and Default [Max Degradation]. The element type that is used is [Hex], stacked from the top plane.

The skins contain 9,000 elements, with smaller elements at the impact location and increasing element size towards the edges. The skins contain 10 elements in the thickness direction.

The core contains 4840 elements, with as in the skin, smaller elements at the impact location and increasing element size towards the edges. Furthermore, the element size in the thickness of the foam is also increasing towards the bottom.

The indenter contains 966 elements with smaller elements at the tip and larger elements in the cylindrical part.

3.2.4 Interactions

The interface between the facesheets and the core is considered as a perfect mechanical contact for simplicity. Therefore, the core is bonded with the facesheets by using a [Tie] surface-to-surface constraint, in order to ensure rigid bonding. This means that the slave surface makes the exact same movement as the master surface at each node. Since the impact strikes from the top, it is decided that the upper surface is the master surface and the surface underneath is the slave surface in each surface pair.

Furthermore, [Hard Contact] is defined between the indenter and the panel. The Hard contact relationship minimizes the penetration of the skin-surface into the indenter-surface and does not allow the transfer of tensile stress across the interface. (Simulia, 2016)

3.2.5 Loading and boundary conditions

The sandwich panel is loaded by an impact of 3.4 m/s with a weight of 5.895 kg using an initial velocity applied to the indenter (green surfaces and edges). The boundary conditions are shown in Figure 3.8. It can be seen that the side surfaces of the panel are encastred (blue surfaces), which means that the movement in X-, Y- and Z- direction is clamped and also the rotations are clamped. This boundary condition is chosen in order to simplify the boundary conditions from the experiments.

There is chosen to simulate a realistic boundary condition, shown in Figure 3.9, in order to predict the outcome more accurately. In this boundary condition, the bottom is supported only in the Y-direction and the blue area at the side surface is fixed, since this is the point at which the clamp is positioned (see Figure 2.7-c).

Furthermore, the inner surfaces are constrained with the X- and Z-symmetry, meaning that the panel is mirrored in these axis (red and orange surfaces).

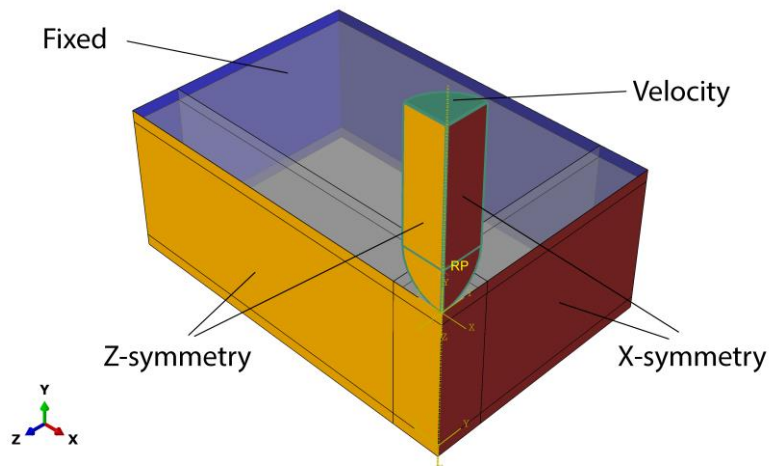


Figure 3.8: Boundary and loading conditions of the FEM impact test setup in the ABAQUS software package

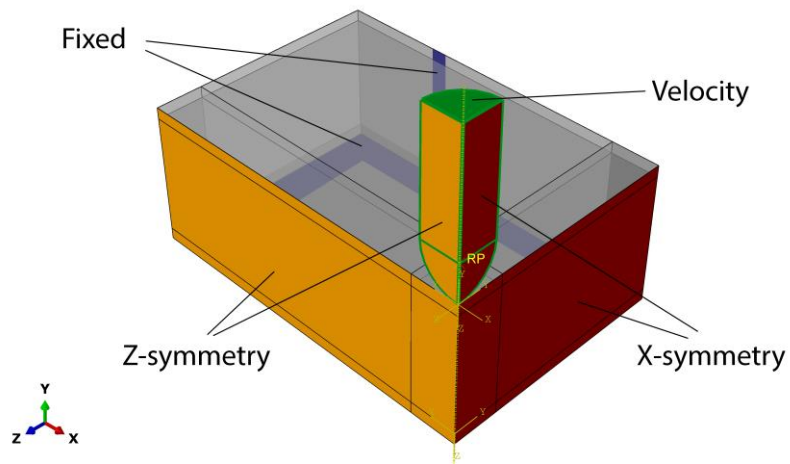


Figure 3.9: Realistic boundary condition of the FEM impact test setup.

3.3 Bending-after-Impact (BAI) model

In order to model the three-point bending situation after impact, a quarter of the specimen with the bending dimensions (Figure 2.4) is modelled and loaded with an impact. The quarter of the panel of the Impact-before-Bending (IBB) situation is imported and subjected to a displacement of the top fixture of 2.5 mm. Since a bending simulation requires different dimensions than an impact simulation, first an impact simulation is done on a (quarter) panel with the dimensions of the bending panel, which are 100 mm width, 37.5 mm length and a height of 30.2 mm. The panel is modelled for a quarter, in order to reduce calculation time. After the impact simulation, the panel needs to be imported in a bending simulation. This is done by importing the impacted panel as an initial state (deformation field together with the 3D stress field) in the ABAQUS software. In this way the explicit (dynamic) model of the impact simulation can be imported in an implicit (static) simulation of the bending in order to solve the three-point bending situation. The IBB model is shown in Figure 3.10.

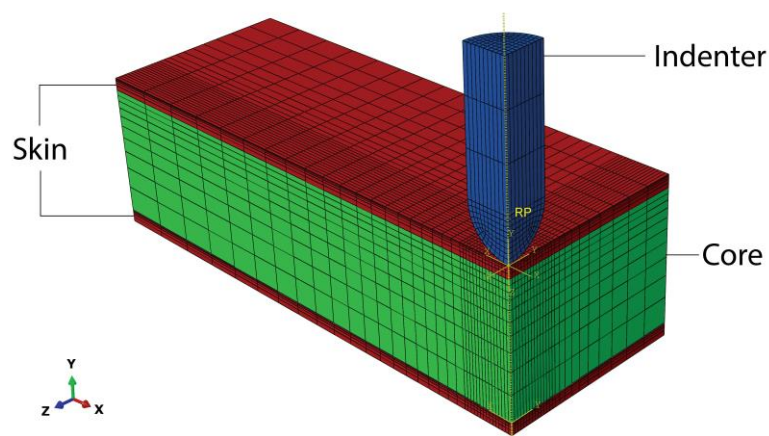


Figure 3.10: FEM model of the BAI test setup of the impact test.

The BAI model can be seen in Figure 3.11.

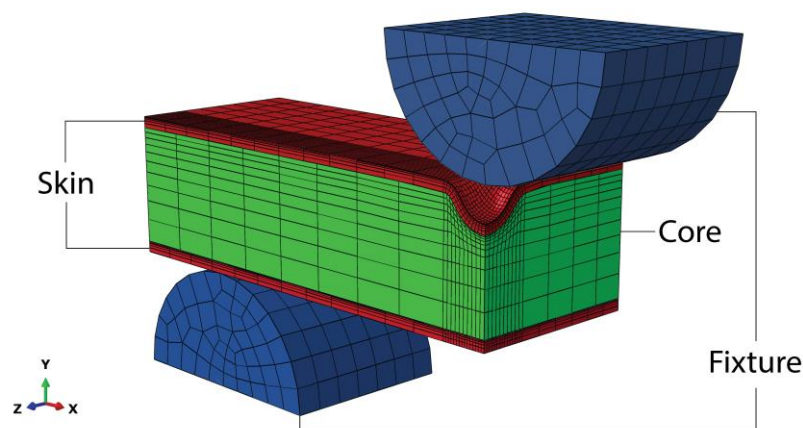


Figure 3.11: FEM model of the BAI test setup in the ABAQUS software package.

3.3.1 Material properties

The material properties of the sandwich panels are the exact same properties as used in the bending simulation in section 3.1 *Bending-Only (BO) model*.

3.3.2 Analysis type

In order to simulate the three-dimensional bending, a [Static General] analysis is performed. The simulation time period was 1 second with no [Non-linear Geometry].

3.3.3 Mesh type

The mesh is the exact same mesh as the impact simulation, because the panels are imported after these impact simulations.

The mesh of the fixtures are standard type [3D Stress] elements (**C3D8R**) with [Linear Geometric Order]. No [Second-order Accuracy], [Default Distortion Control], [Default Hourglass Control], [Default Element Deletion] and [Default Max Degradation]. The element type that is used is [Sweep Hex], stacked from the front plane.

3.3.4 Interactions

The core is bonded with the facesheets by using a [Tie] surface-to-surface constraint, in order to ensure rigid bonding.

Furthermore, there's chosen to simulate a [Hard Contact] between the indenter and the panel and the fixtures are constrained with a [Rigid body] constraint.

3.3.5 Loading and boundary conditions

The boundary conditions of the IBB model are shown in Figure 3.12. The only difference with the IO model in section 3.2 *Impact-Only (IO) model* is the fixed area, which is smaller in the IBB model since the dimensions are different. The boundary conditions of the BAI model are the same as the boundary conditions of the BO model in section 3.1.5 *Loading and boundary conditions*. The only difference is that the composite panel is imposed with an [Initial State] predefined field.

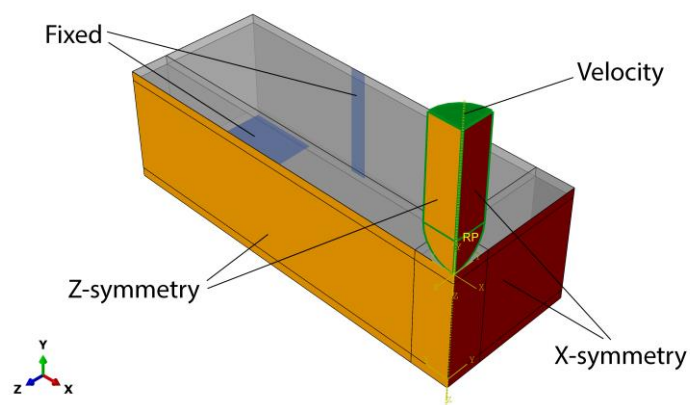


Figure 3.12: Boundary conditions of the IBB panel.

4. Results & Discussion

The most important part of this study are the results from both the FEM analysis and the experimental analysis. It is also important that these two different components verify each other. In this section of the thesis the results of both analyses will be discussed. First the BO results will be discussed comprehensively, which is divided into experimental analysis and FEM analysis. Thereafter the IO tests will be discussed, which will be a reference for the Impact-before-Bending (IBB) since the IBB specimens are not according the testing standard. This section is also split into experimental analysis and FEM analysis. Then, the Bending-after-Impact results will be discussed, also divided in the same sections as the IO and BO sections; experimental and FEM. These sections are then also divided into Impact-before-Bending (IBB) and Bending-after-Impact (BAI).

Finally, some further investigations are discussed, in which different impact-energies are simulated to determine the influence of the impact energy on the shear stress distribution, the displacement and the reaction force. These impacted specimens are also loaded in a bending simulation afterwards in order to determine the influence of impact energy on the residual stiffness of a composite sandwich panel.

In the following results, the different specimens are discussed. In this section the first three letters of each specimen represent the core material, the number after these letters represent the specimen number of that specific test, for example BAL2 is the second balsa specimen of that specific test.

4.1 Bending-Only (BO)

First, a three-point bending test is performed on the produced specimens, in order to determine the stiffness and failure behaviour of the reference specimens. To ensure reliable results, the test is performed according testing standard *ASTM C393/C393M*.

4.1.1 Experimental analysis

The three-point bending is performed and the force is plotted against the displacement of the upper fixture, which can be seen in Figure 4.1. It can be concluded that the balsa panel has the highest stiffness as expected. It can bare up to twice as much force as the SAN foam and up to four times the force of the PET foam. The force-drop after the peak cannot be seen when the drop is higher than 50%, because this force-drop stops the test and therefore there's no data available after the force-drop and it cannot be shown in the graphs. An overview of maximum force and displacement values is given in Table 4.1. In this table there are corrected values, which will be explained in the following.

In Figure 4.1 it can also be seen that the first part of the curves is linear, which represents the initial stiffness of the panels. After some displacement the graph increases less, which shows that there is a certain plastic deformation in the panels. For the Balsa and the SAN foam specimens this plastic zone can be seen around 2 mm, for the PET foam this zone start around 3 mm.

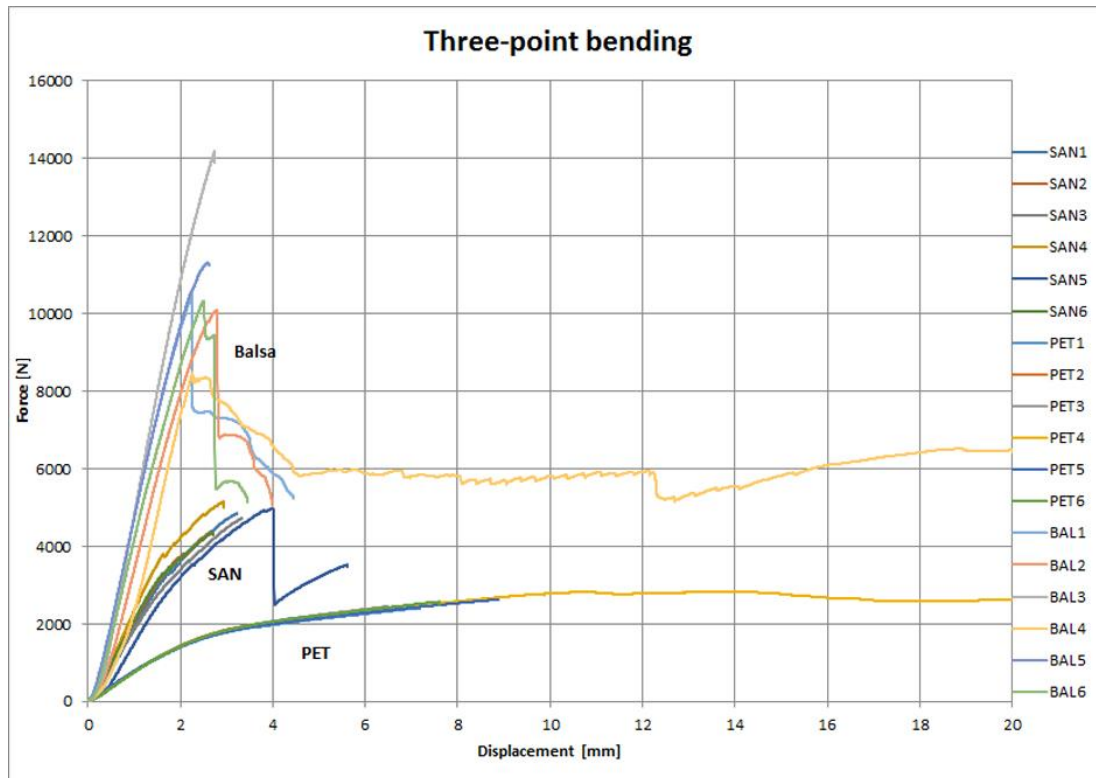


Figure 4.1: Force-displacement graphs of the bending tests.

Table 4.1: Maximum force and maximum displacement of the different BO specimens after the bending test.

Sample		BO-SAN	BO-PET	BO-BAL
1	Max force (N)	4,847	2,409	10,505
	Max displacement (mm)	3.23	7.18	2.25* (4.44)
2	Max force (N)	4,359	2,262	10,080
	Max displacement (mm)	2.64	5.43	2.76* (3.99)
3	Max force (N)	4,720	2,452	14,176
	Max displacement (mm)	3.33	6.48	2.74
4	Max force (N)	5,153	2,818	8,477
	Max displacement (mm)	2.93	13.86* (20.00)	2.26* (20.00)
5	Max force (N)	4,975	2,630	11,322
	Max displacement (mm)	4.02* (5.62)	8.88	2.60
6	Max force (N)	4,356	2,575	10,319
	Max displacement (mm)	2,71	7.61	2.49* (3.45)
Avg	Max force (N)	4,735	2,524	10,813
	Max displacement (mm)	3.14	8.24	2.52

*corrected value with the initial value in between brackets

The values of Table 4.1 are summarized in the bar plots of Figure 4.2 and Figure 4.3. In Figure 4.2 the maximum force is plotted of all specimens during the three-point bending test. In Figure 4.3 the maximum displacement is plotted for all specimens during this test.

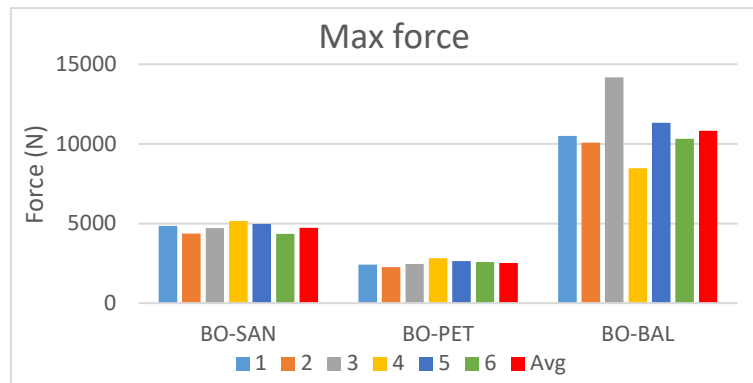


Figure 4.2: Bar plot of the maximum force during the three-point bending test in the BO specimens.

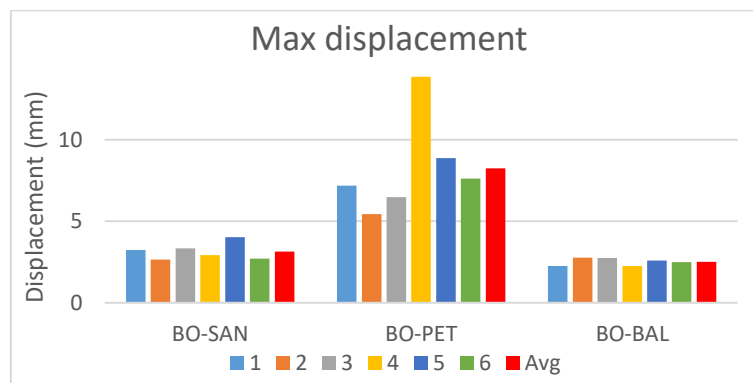


Figure 4.3: Bar plot of the maximum displacement during the three-point bending test in the BO specimens.

When looking at the specimens in Figure 4.4, it can be seen that the main failure mechanism during these bending tests is core shearing. In Figure 4.4-a the SAN3 specimen is shown, in Figure 4.4-b the PET2 specimen is shown and in Figure 4.4-c the BAL2 specimen is shown. As can be seen, these three specimens have the core shearing failure. In Figure 4.4d the corresponding force-displacement graph is plotted.

Almost all specimens had this type of failure (core shearing) except for PET4, which will be discussed in the following paragraph.

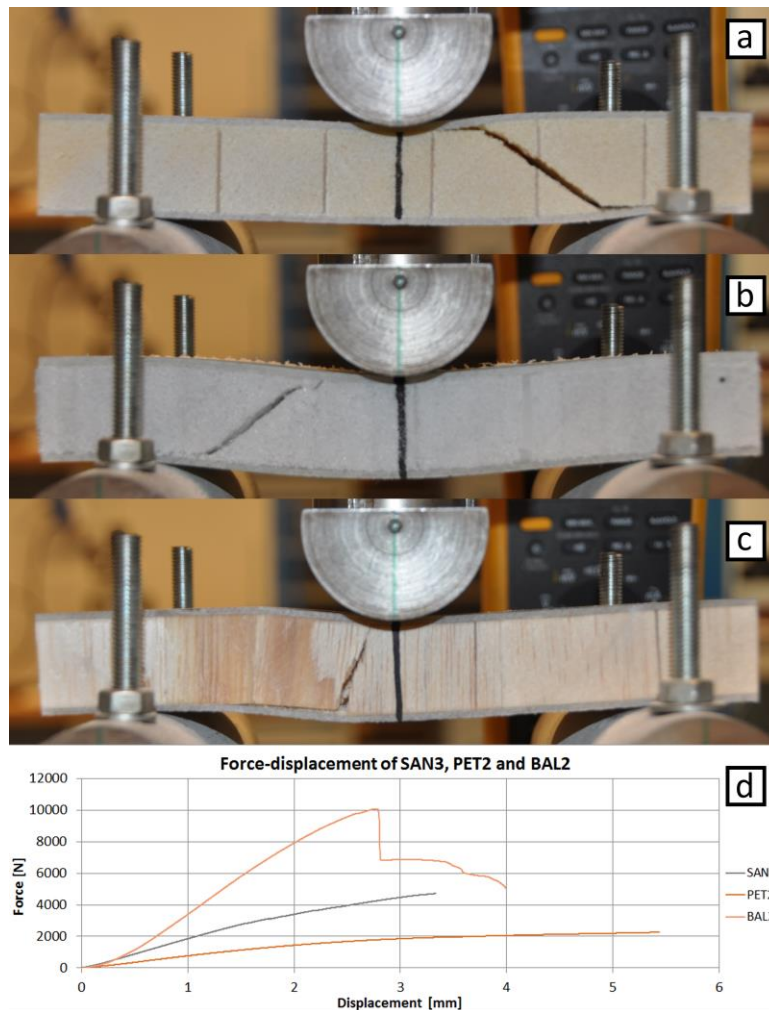


Figure 4.4: Visible damage of the bending tests of the a) SAN3 specimen, b) PET2 specimen and c) BAL2 specimen. In d) the force-displacement graph of these panels is provided.

One specimen of the PET foam sandwich panels (PET4) has a failure mechanism of indentation (Figure 4.5), which means that the core is compressed instead of sheared apart. This can be seen in the graph in Figure 4.1, in which the PET4 specimen has a high degree of displacement without a drop in the force.

In the graph of Figure 4.1 it can also be seen that the BAL4 specimen has a high degree of displacement. The cause of this large displacement are the settings of the three-point bending test. In the settings it is stated that the force-drop needs to be 50% or more in order to stop the test, when the force drop is (slightly) below 50%, the test keeps continuing. This also happened in the BAL4 specimen, in which the force drop was below 50%, which caused the test to continue instead of stopping. This specimen had an initial failure mechanism of core shearing at ± 2.2 mm displacement (peak in the force-displacement graph), but after continuing the test (since the force drop was not over 50%) there was also core-skin debonding (Figure 4.6 and Figure 4.7). After the first failure mechanism, which was core shearing, the specimen lost its stiffness. Therefore, the maximum displacement is corrected to the first peak after which the stiffness only decreases; 2.26 mm. The corrected value can also be seen in Figure 4.7. This correction is also done for other specimens (SAN5, PET4, BAL1, BAL2 and BAL6) in order to ensure reliable results.

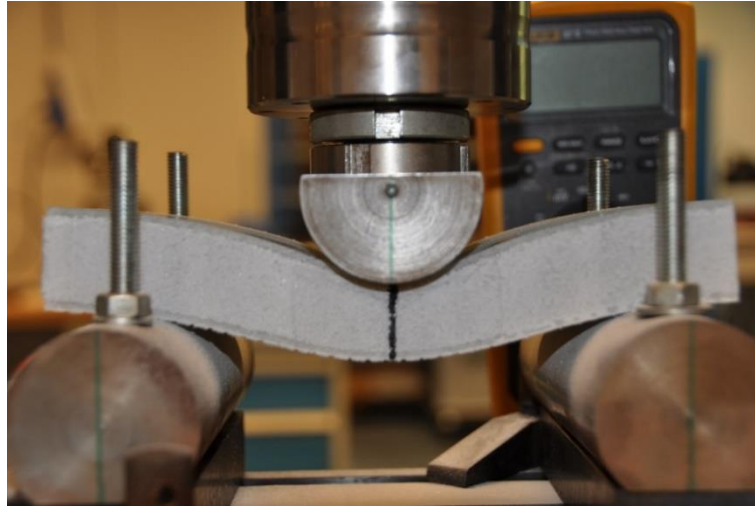


Figure 4.5: Indentation failure mechanism of the PET4 specimen.

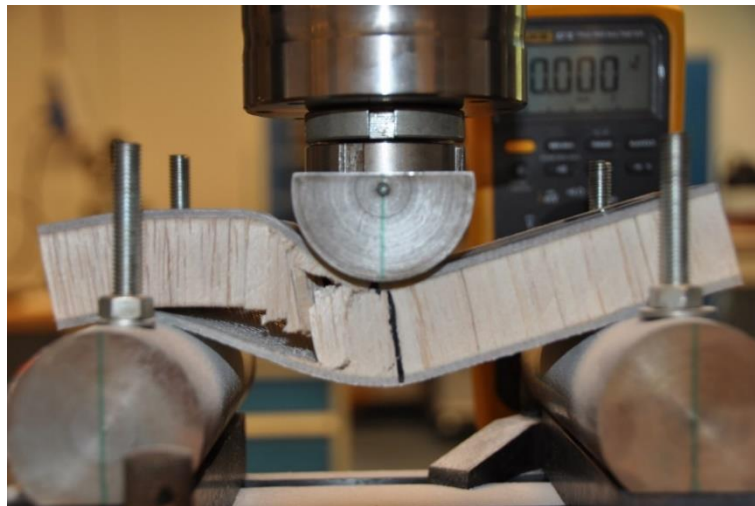


Figure 4.6: Core shearing and core-skin debonding failure mechanisms in the BAL4 specimen.

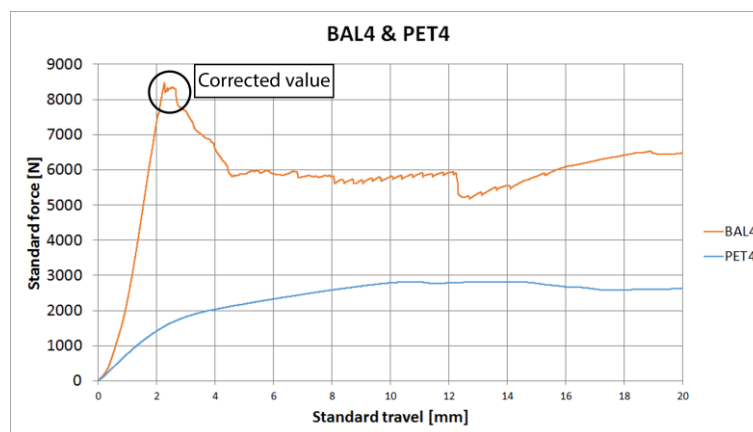


Figure 4.7: Force-displacement graphs of the PET4 and BAL4 BO specimens. The corrected value is also shown.

4.1.2 FEM analysis

After the practical three-point bending tests, the three developed FEM models are simulated and compared with each other and with the experiments in Figure 4.8. It can be seen that the values of the 2D model have the same inclination, which means that the initial stiffness is the same. Furthermore, the different 3D FEM models are of the same order of magnitude (some of them are even overlapping), which concludes that these models are representative for each other. It can be seen that the forces are in the same order of magnitude as the experimental values and therefore can be assumed to be correct.

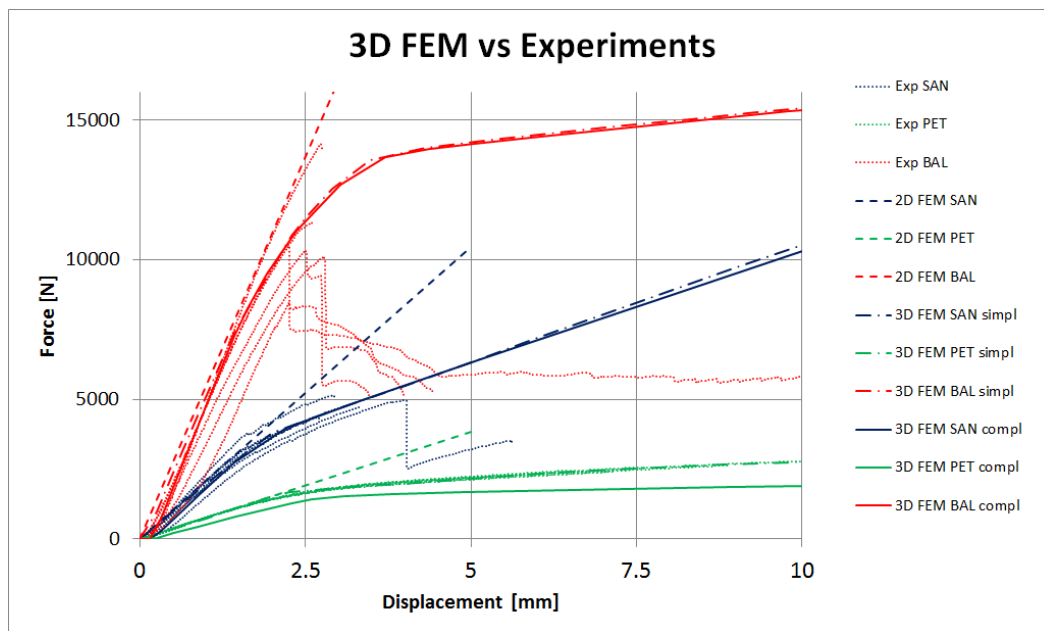


Figure 4.8: Force-displacement graphs comparison between FEM and experimental three-point bending tests.

In Figure 4.8 it can be seen that the plasticity values are estimated sufficiently, since it fits the experimental data. The plasticity values used for the three different cores are summarized in Table 3.3. These values do not match with the values in the literature or the datasheets, which could indicate that the production process has an influence on the plasticity behaviour of the core materials.

When investigating the shear stresses in the cores of the 2D models in Figure 4.9, it can be seen that the shear stresses are highest in between the side- and the middle fixtures. The shear stresses are (theoretically) highest in the centre of the core, therefore the maximum shear stress values in the red boxes in Figure 4.9 are considered to be the stresses of interest. These stresses are then compared to the shear stresses of the complex 3D bending models in Figure 4.10.

It can be seen that in the 3D models that there is a large amount of shear stress in the contact area near the fixtures. This can be explained by the high rate of contact forces in these relatively small areas. These shear stresses are not the shear stresses which are catastrophic for the core, but the shear stresses in the middle of the core (the red boxes) are of interest. Therefore, it is wise to investigate the shear stresses at the middle of the core within the red boxes in Figure 4.10.

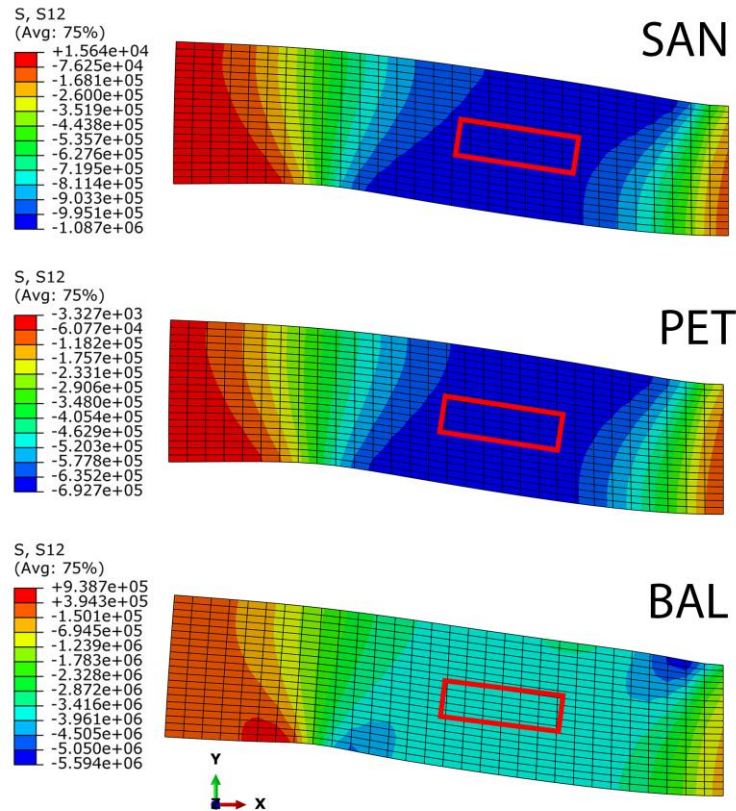


Figure 4.9: Shear stress distribution at 2.5 mm displacement in the different cores in the 2D three-point bending test in the ABAQUS FEM software.

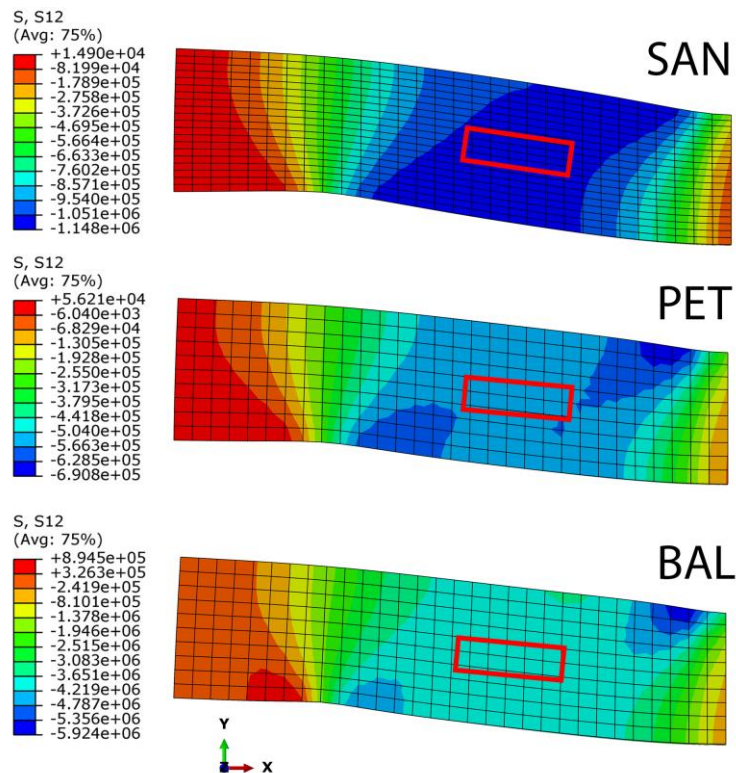


Figure 4.10: Shear stress distribution in the different cores in a 3D three-point (simple) bending simulation.

When investigating the maximum shear stresses, it can be seen that also these stresses are in the same order of magnitude for all bending models. The values of the maximum shear stresses of the three different bending models are compared in Table 4.3.

Table 4.2: Maximum shear stresses at 2.5 mm displacement in the different FEM models.

	Model 1; 2D	Model 2; 3D (simple)	Model 3; 3D (complex)
SAN	± 1.1 MPa	± 1.1 MPa	± 1.1 MPa
PET	± 0.4 MPa	± 0.4 MPa	± 0.3 MPa
BAL	± 3.2 MPa	± 3.0 MPa	± 3.0 MPa

In order to compare the experimental results with the FEM results, the maximum force is needed of the experimental results. With these maximum forces, the (shear) stresses can be calculated according equations 2.1 – 2.6 (section 2.2 *Analytical calculation of maximum stresses and shear stresses*).

The maximum forces of the experimental tests are retrieved from Table 4.1, after which the maximum (shear) stresses are calculated. For the maximum force of the FEM analysis, the forces of the complex-3D-bending model at the time of the 2.5 mm displacement of the middle fixture are used. The maximum (shear) stresses are also retrieved from this point (the 2.5 mm displacement) of the simulation. It should be noted that the shear stresses at the centre of the sandwich panel are used for comparison analysis since the analytical shear stress calculations are treated at the neutral line of the beam.

The comparison of both the maximum force (at 2.5 mm displacement) and the shear stresses is shown in Table 4.3.

Table 4.3: Comparing Experimental values and FEM Analysis values of the maximum force at 2.5 mm displacement and the maximum shear stress.

		Experimental	FEM	Difference
Force at 2.5 mm displacement	SAN	± 4,197 N	± 4,200	+ 0.1 %
	PET	± 1,654 N	± 1,700 N	+ 2.8 %
	BAL	± 10,019 N	± 11,300	+ 12.8 %
Shear stress	SAN	1.28 MPa	1.1 MPa	- 14.1 %
	PET	0.69 MPa	0.4 MPa	- 42.0 %
	BAL	2.92 MPa	3.0 MPa	+ 2.7 %

Investigating these values, it can be seen that Balsa has a higher degree of disparity than the SAN and PET values. This can be declared by the fact that Balsa is a natural product with more diversity in its properties. The large difference can thus be devoted by the weaker spots in the balsa wood, causing the balsa core to fail premature in comparison to its FEM simulation.

4.2 Impact-Only (IO)

After the BO test, an impact test is done as a reference for the impact test of the combined test (IBB). In order to determine whether the impact test in the combined test is sufficient, an impact test is done according testing standard *ASTM D7136/D7136M* and thereafter the FEM analysis is done of the same situation.

4.2.1 Experimental analysis

First the experimental impact tests are done. A hemispherical indenter with a weight of 5.895 kg falls from a height of 600 mm and hits the panel. The falling time, velocity and impact energy can be calculated according the following equations:

$$t = \left(\frac{s}{\frac{1}{2} \cdot g} \right)^{\frac{1}{2}} \quad \text{Eq. 4.1}$$

$$v = g \cdot t \quad \text{Eq. 4.2}$$

$$E = m \cdot g \cdot s \quad \text{Eq. 4.3}$$

In which t is the falling time, s is the distance, g is the gravity acceleration (9.81 m/s^2), v is the velocity and m is the mass.

The panels are hit with a velocity of 3.4 m/s with an impact energy of 34.7 J , calculated using equation 4.3. In Figure 4.11 the velocity is plotted over time of the first Balsa impact test. The reaction force is calculated by the software and plotted over the deformation which can be seen in Figure 4.12.

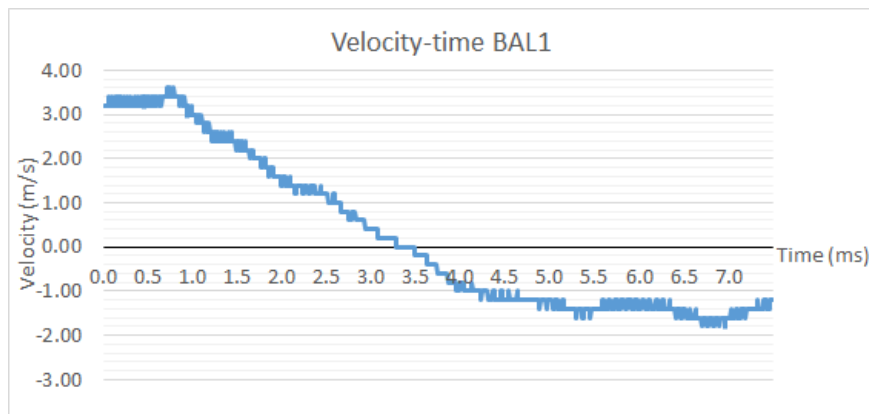


Figure 4.11: Velocity-time graph of the first Balsa specimen

It can be concluded that the balsa sandwich panel is the strongest panel, since the first peak load (the load to penetrate the upper skin) is highest for the balsa panels. The balsa panels have a high degree variety in the values. This can be explained by the balsa being a natural product having a great diversity in the properties of the wood. In contrast with the PET and SAN cored sandwich panels, which are far more alike, shown in Figure 4.12.

Looking at the graph in Figure 4.12-c, it can be seen that one balsa sample (Balsa3) has a plateau in the force-displacement graph. This can be explained by the force-cell settings, in which a maximum force of 10 kN is used. Therefore, the maximum force which can be processed is 10 kN, which causes the plateau of Balsa3 in Figure 4.12-c.

Examining the panels after the impact tests, it can be seen that all panels have visible damage (Figure 4.13). The PET foam core sandwich panels have the least visible damage and the SAN and Balsa panel have about the same amount of visible damage. This can be explained by the lower elastic modulus (see Table 3.2) of the PET foam which generated less reaction force. The foam absorbs the energy by deforming instead of breaking like the balsa wood which can be seen in the graphs of the tests. The PET sandwich panels have much more deformation than the Balsa specimens and the SAN specimens.

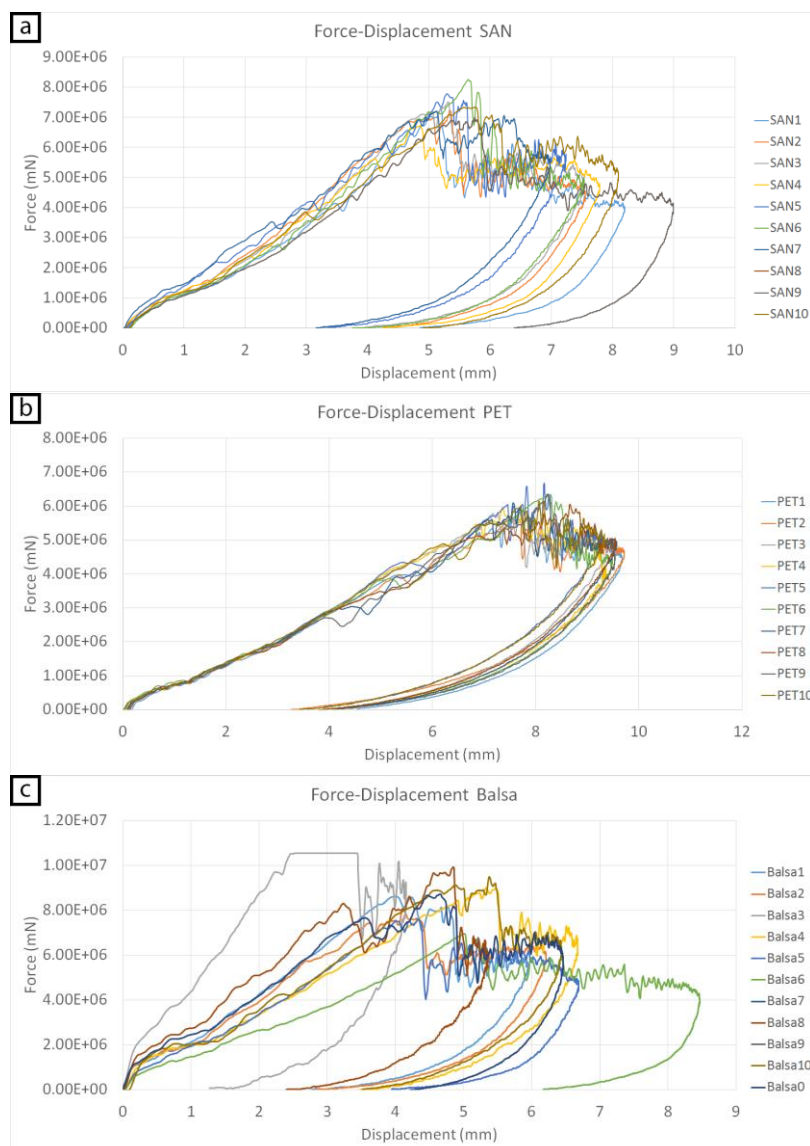


Figure 4.12: Force-displacement graphs of a) SAN foam cored panels, b) PET foam cored panels and c) Balsa wood cored panels.

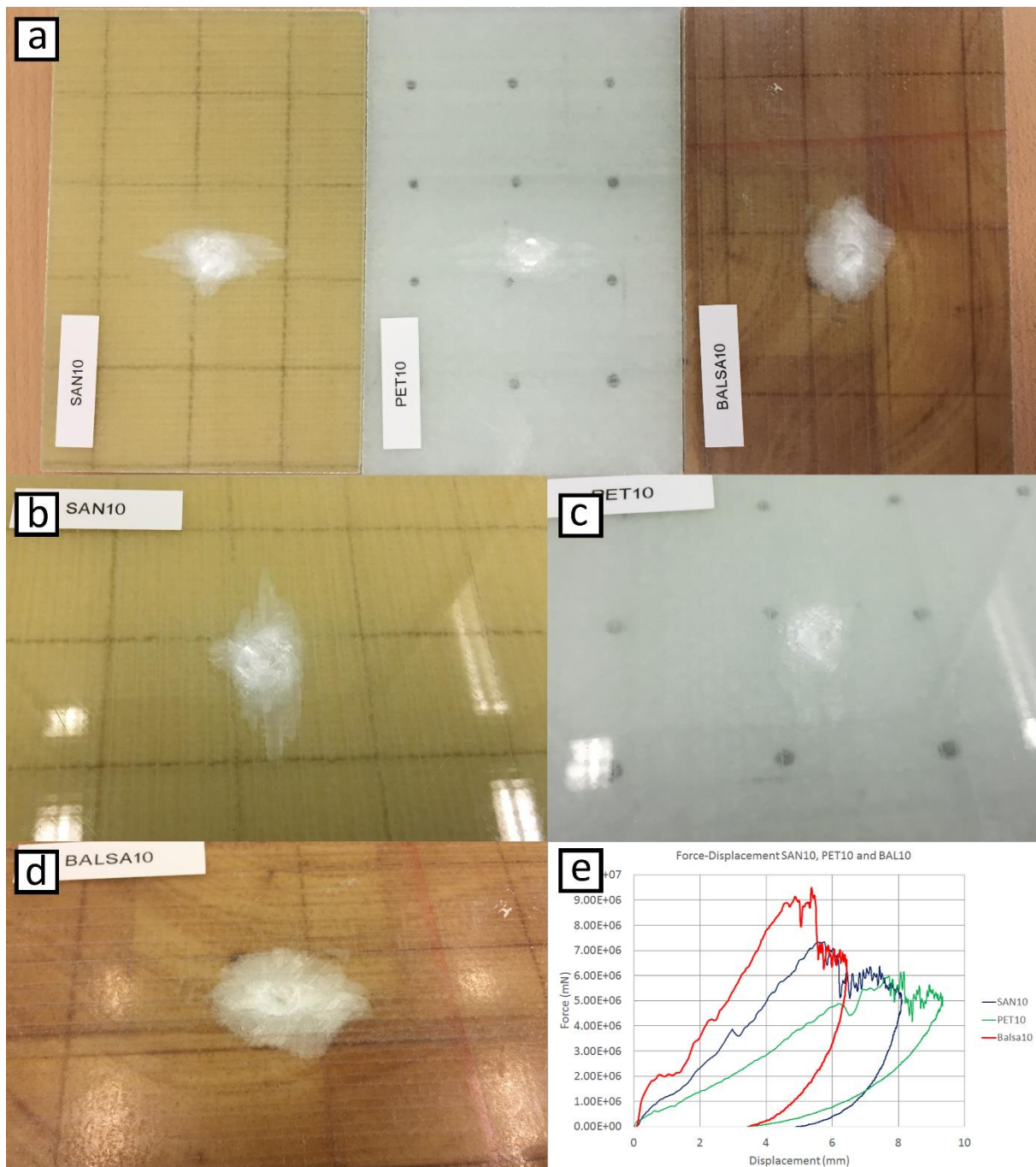


Figure 4.13: Visible damage of the different cored panels; a) all panels, b) the SAN10 panel, c) the Balsa10 panel, d) the PET10 panel and e) the corresponding force-displacement graph.

Examining the bottom of the impact panels in Figure 4.14, it can be seen that the Balsa panels have some sort of failure (probably debonding/delamination) underneath (Figure 4.14-c). It seems that the core and the skin start debonding, probably due to the out-of-plane shearing behaviour of Balsa. The bottoms of the panels are shown in Figure 4.14, in which depicted clearly that the Balsa panel has debonded in a circle around the impact area.

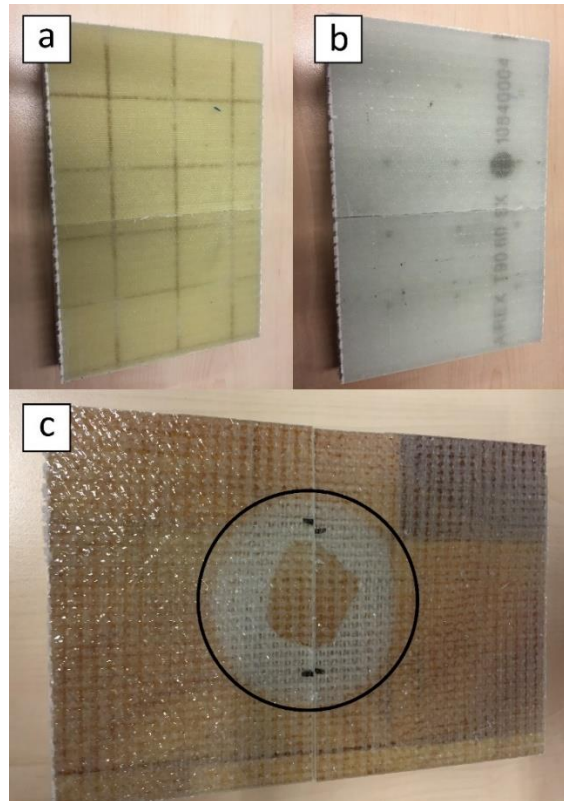


Figure 4.14: The bottom of the impact panels; a) SAN10, b) PET10 and c) Bal9

In order to investigate this behaviour, the panels are cut in half (in the middle of the impact point) and then examined through an optical microscope (the VXH 5000) with a lens which is able to magnify 100-1000 times. The debonding in between the core and the bottom skin in the BAL9 panel is clear and is depicted in Figure 4.17. In the specimens with the other core materials, the SAN and PET cored specimens, it can be seen that there is no debonding in between the bottom skin and the core (Figure 4.15 and Figure 4.16). More details about the microscopic analysis can be found in *Appendix E: Microscopic analysis*.

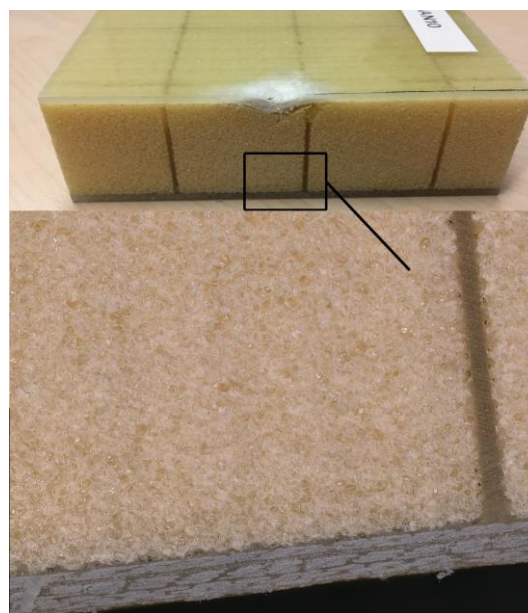


Figure 4.15: Microscopic image of the bottom skin-core interface of the SAN IO specimen.

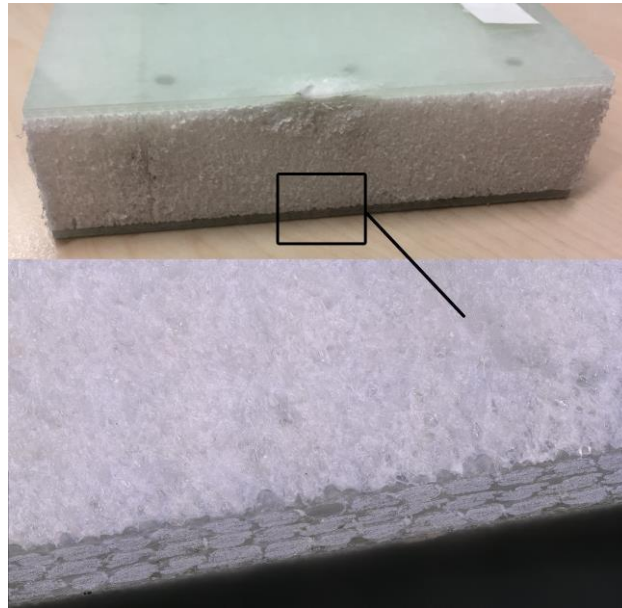


Figure 4.16: Microscopic image of the bottom skin-core interface of the PET IO specimen.

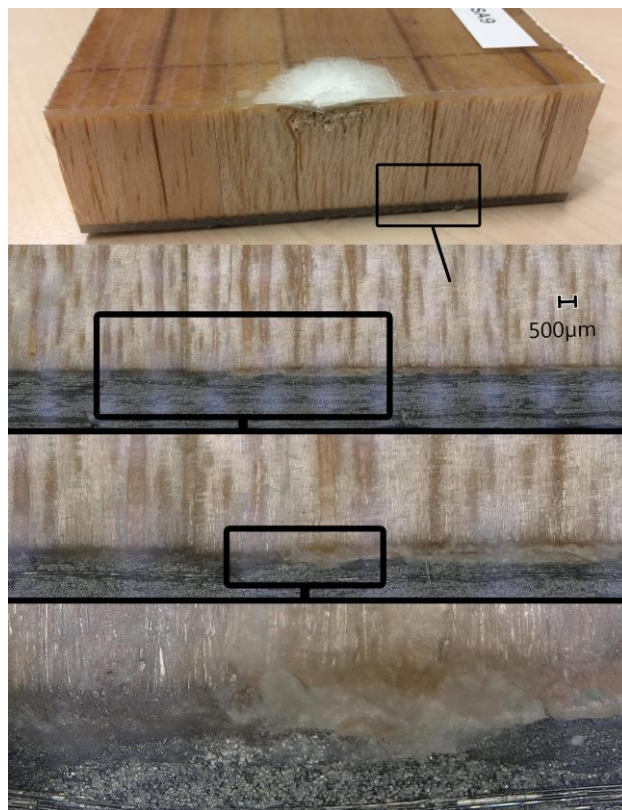


Figure 4.17: Microscopic image of the bottom skin-core interface of the Balsa IO specimen.

4.2.2 FEM analysis

After the experimental tests, a FEM analysis is done in order to better understand the behaviour of the panel during the impact test. The FEM analysis is done with two different approaches; without damage criteria and with damage criteria, as described in section 3.2 *Impact-Only (IO) model*. In Figure 4.18 the difference between a Balsa cored specimen without damage criteria (Figure 4.18-a) and a Balsa cored specimen with damage criteria (Figure 4.18-b) is shown (15 ms after impact). Obviously, the model without the damage criteria has less indentation depth than the model with the damage criteria. This can be explained by the element degradation in the model with the damage criteria. When an element is damaged, the properties of that element deteriorate, which causes the complete model to loose stiffness and strength.

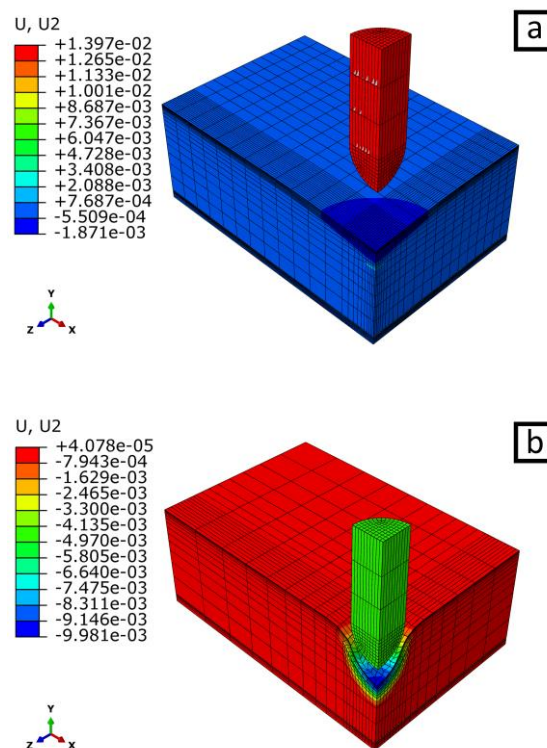


Figure 4.18: FEM impact models of a) Balsa cored panel without damage criteria and b) Balsa cored model with damage criteria. U2 is the deformation in the vertical direction (Y-direction) 15 ms after impact.

In the simulation results seen in Figure 4.19, it can be seen that there is a lot more deformation in the simulations with the damage criteria, than in the simulations without damage criteria (9.98 mm over 1.87 mm). It can be seen, comparing these values with the experimental values, that the simulations without using a damage criteria are closer to reality than the simulations with damage criteria.

When looking at the force-displacement graphs in Figure 4.19, it can be seen that there is not only a significant difference in the displacement between the two different models (with damage criteria; _DC, and without damage criteria; noDC), but that there is also a large difference in the maximum reaction force during the impact. In Figure 4.19 the two boundary conditions are also shown; the dotted lines are the simple boundary conditions (Figure 3.8) and the solid lines are the realistic boundary conditions (Figure 3.9).

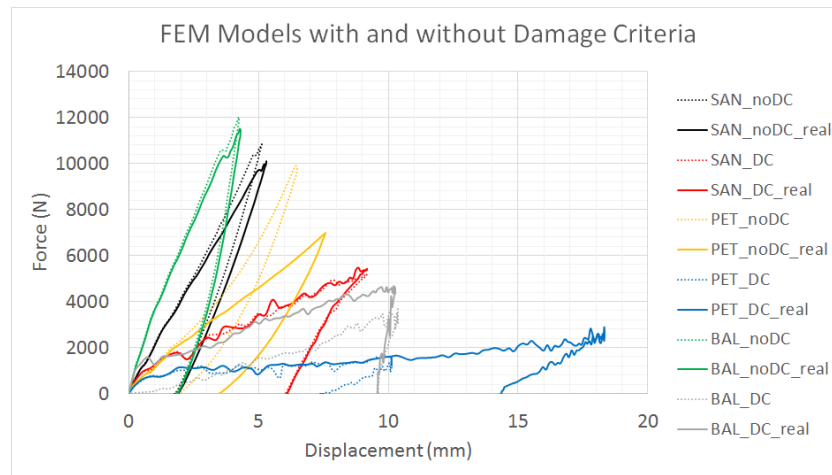


Figure 4.19: Force-displacement graphs of all different FEM impact models.

In Figure 4.19 it can be seen that there is some noise in the graphs of the simulations with the damage criteria. This can be explained by the degradation of the elements after damage. When an element is damaged, it loses (part of) its stiffness and strength, which causes a drop in the force. When the next (undamaged) element is loaded, the force again increases and then rises up to the point where the element gets damaged and again deteriorates.

As described, the indentation depth is smaller if there are no damage criteria in the upper skin, since no elements are (partially) degraded and therefore retain their stiffness and strength causing a higher reaction force and less displacement. This can also be seen in the force-displacement graphs in Figure 4.20, when putting the two analyses, i.e. FEM and experimental, of all the different core materials next to each other. The comparison between FEM and experimental is shown in Figure 4.20-a of the SAN foam core, in Figure 4.20-b of the PET foam core and in and Figure 4.20-c of the balsa core.

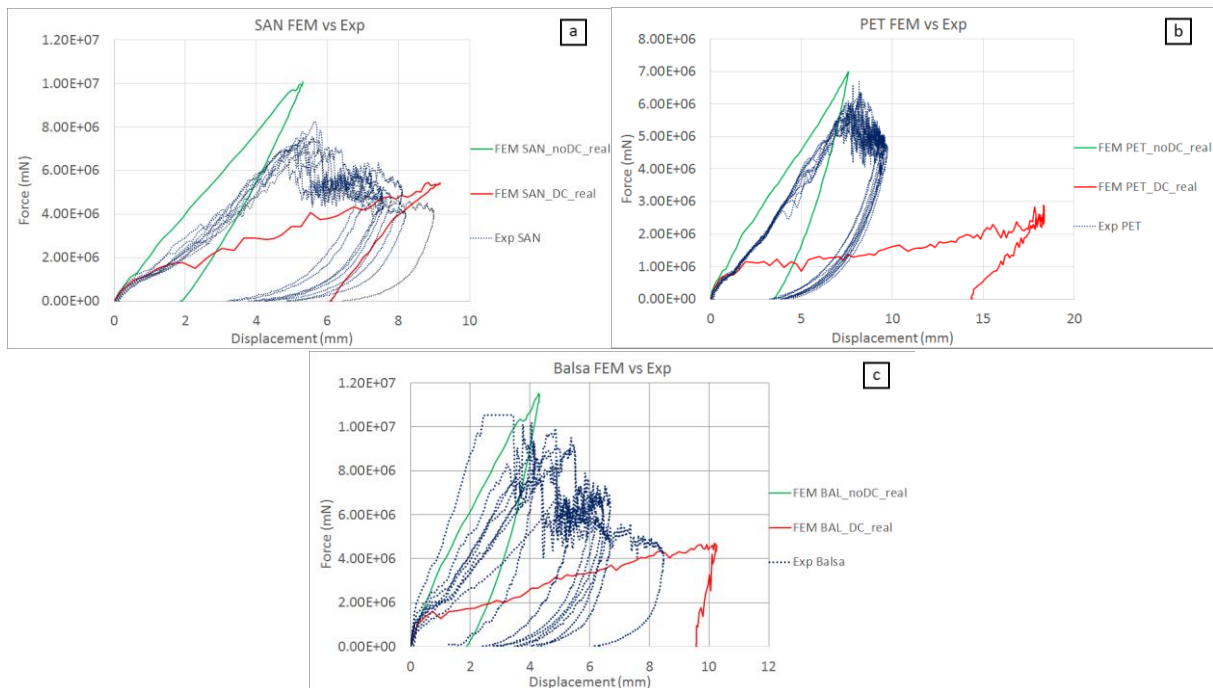


Figure 4.20: Comparison of the force-displacement graphs of a) SAN, b) PET and c) the balsa specimens of the impact tests in which the green lines are the FEM models without damage criteria, the yellow lines are the FEM models with damage criteria and the blue lines are the experimental values.

From these graphs, it can be seen that all cores have sufficient approximation in the simulations without damage criteria, since the displacement at the maximum force, matches the first peak of the experimental results. It can be concluded that the damage criteria are not sufficient accurate in order to predict the behaviour in impact situations.

Investigating the normal stress distribution of the panels in Figure 4.21, it can be seen that there is a difference of a decade between the simulations with damage criteria and the ones without damage criteria. Also the shear stress distributions in Figure 4.22 have a difference of a decade between the simulations with and without damage criteria. It can also be seen that the simulations without damage criteria have a different (shear) stress distribution compared to the simulations with damage criteria. It can be seen that the simulations without damage criteria have more stress distribution on the rest of the core, while the simulations with damage criteria have most of the shear stress in the indentation zone.

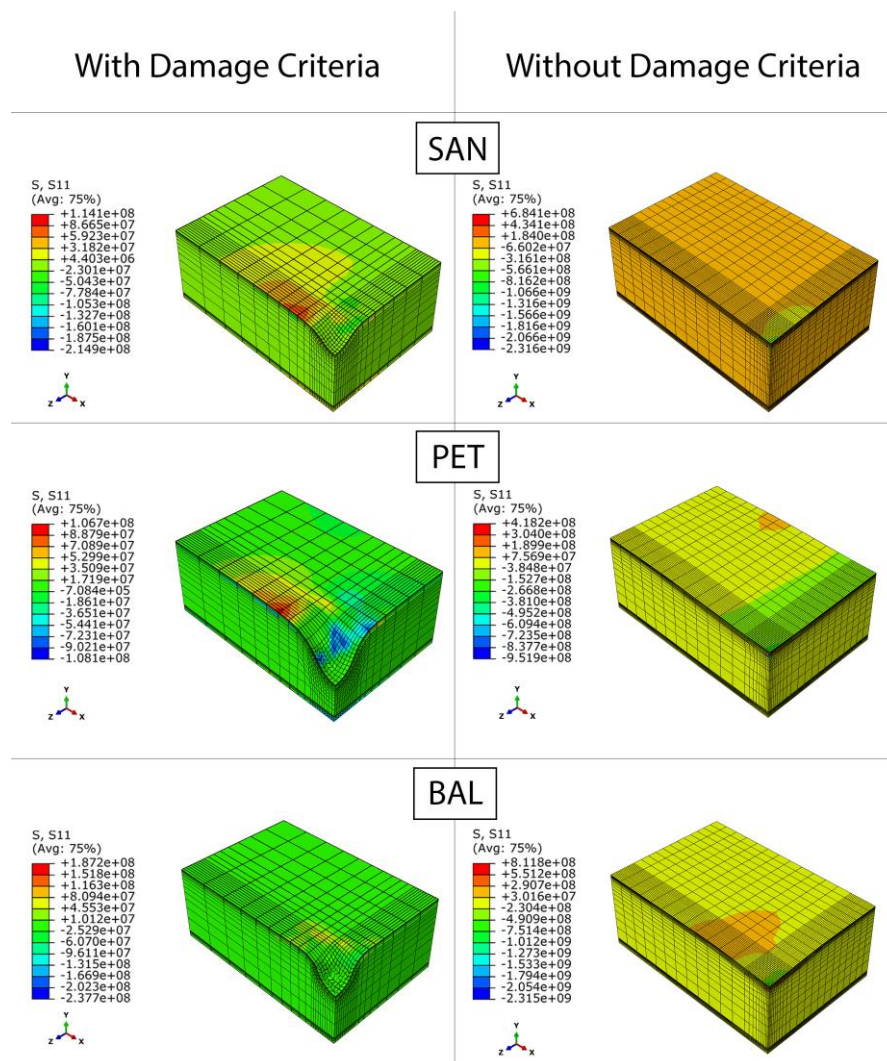


Figure 4.21: Difference between the simulations with and without damage criteria of all different cores.

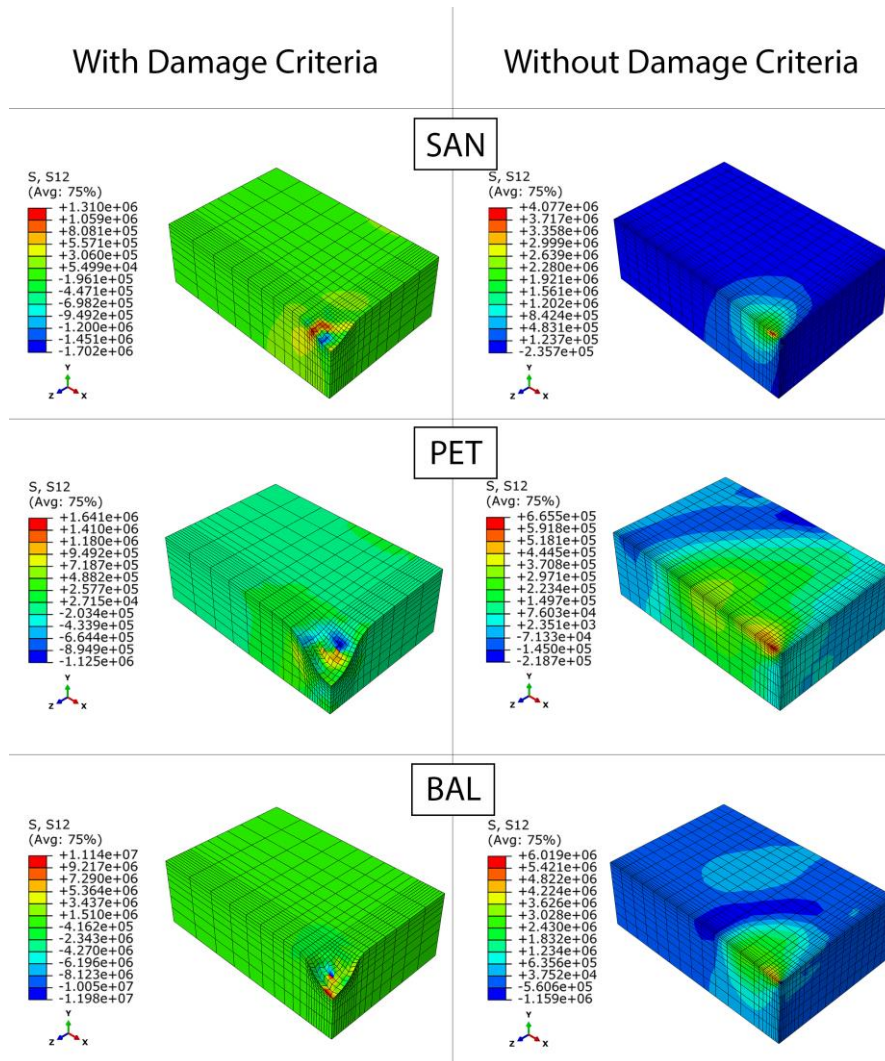


Figure 4.22: Shear stress distribution comparison between the simulations with and without damage criteria.

Please consider that investigating these stresses, the core and the skins have different coordinate systems as shown in Figure 3.3. Direction Z and direction Y are switched in these different sections, i.e. S22 in the skins is the same as S33 in the core and vice versa. In Table 4.4, it is shown how these different properties can be compared.

Table 4.4: Differences between the different coordinate systems of the different parts in a model.

	Skins	Core
Fibre direction	11 (X)	11 (X)
Transverse direction	22 / 33 (Y / Z)	33 / 22 (Z / Y)
In plane	12 (XY)	13 (XZ)
Transvers In-plane	13 (XZ)	12 (XY)

The investigation of the experimental specimens showed that the balsa cored specimens had debonding in between the core and the bottom skin. In the FEM results of the Balsa simulations, there was also a sign of (shear) stresses on top of the bottomskin which might cause this debonding between the core and the bottomskin. This can be seen in Figure 4.23, in which the in-plane shear stresses (S12) in the bottomskin are displayed in comparison with the debonding of a Balsa IO specimen. The magnitude of these shear stresses is almost 0.4 MPa, which is about 16% of the maximum shear stress for the balsa core according to *Appendix D: Datasheets*.

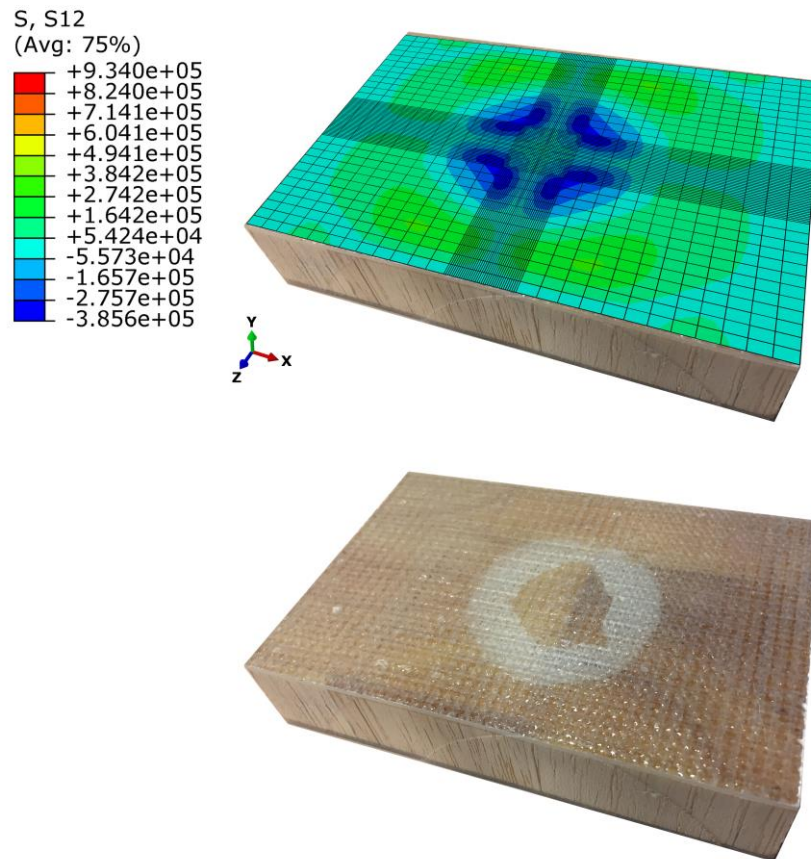


Figure 4.23: Comparison between the shear stress in the bottomskin and the debonding in the experimental impact specimen.

From the microscopic analysis in section 4.2.1 *Experimental analysis*, the impact-affected zone can be determined. When comparing these zones to the PEEQ (Plastic strain equivalent) zones in the simulations it can be seen that the simulations without damage criteria give a better approximation than the simulations with damage criteria. This can be seen in Figure 4.24 in which the top picture is the experimental specimen with the real plastic deformed zone highlighted, the middle picture is a representation of the PEEQ zone of the simulation without damage criteria and the bottom picture is a representation of the PEEQ zone of the simulation with damage criteria.

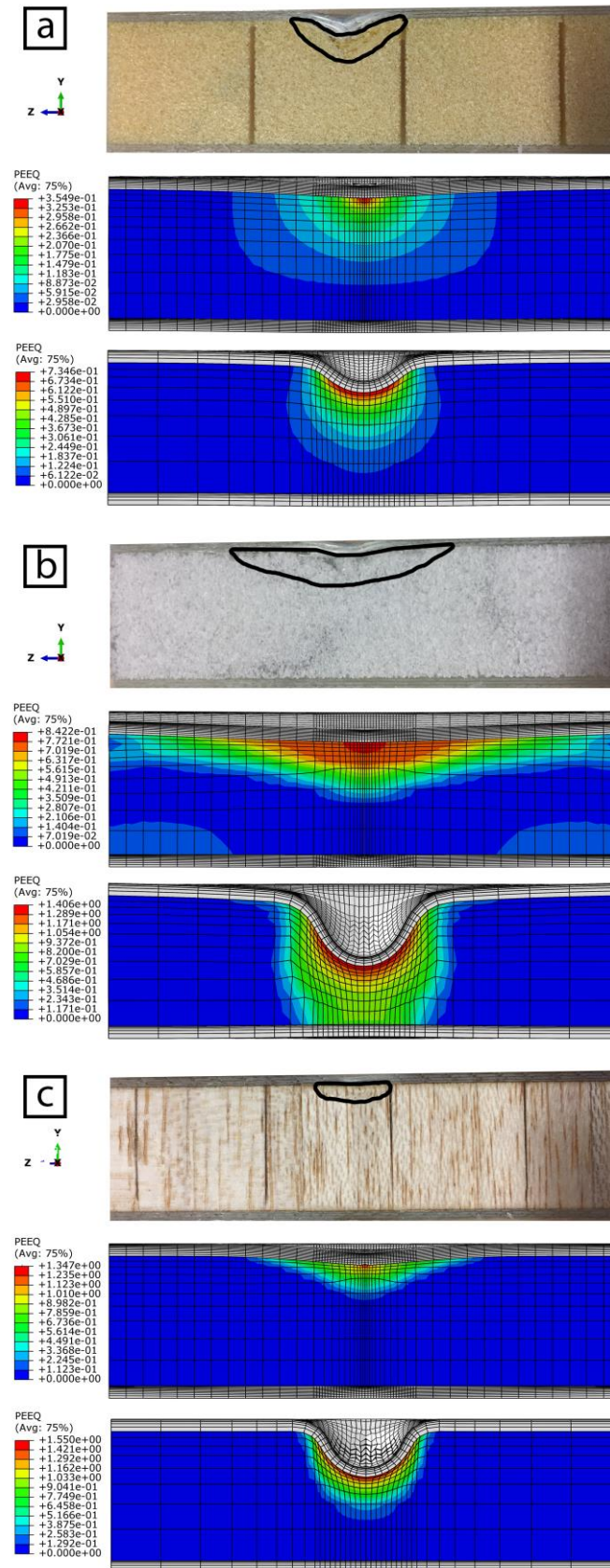


Figure 4.24: Impact-affected area versus the Plastic strain Equivalent zone in the ABAQUS FEM software, in a) the SAN foam, b) the PET foam and c) the Balsa. In each material the first image is the experimental result, the second image is the one without damage criteria and the third image is the one with damage criteria.

4.3 Bending after impact

In order to test the mechanical behaviour of the sandwich panels in bending after impact, first an impact needs to be done on the specimens after which the specimens are subjected to a three-point bending test.

4.3.1 Experimental analysis

Impact test

This impact test is done in a similar way as the IO tests in section 2.1.3 *Impact testing setup*; a hemispherical indenter with a weight of 5.895 kg falls from a height of 600 mm resulting in a speed of 3.4 m/s and an impact energy of 34.7 J. The only difference is the dimensions of the panel, which are the same dimensions as in the bending test as described in section 2.1.2 *Bending testing setup*.

The results of the impact on the bending specimens (Impact-before-Bending; IBB) will be compared to the specimens of the IO specimens. The results of this comparison can be seen in Figure 4.25, in which the red lines are the BAI specimens and the blue lines are the IO specimens.

It can be seen that in both Balsa and SAN specimens, the values match up with the values of the IO test. On the other hand, the PET specimens show a bit less reaction force and a higher degree of displacement. This can be declared by the support underneath the specimens. As can be seen in Figure 2.8, the support of the fixture is only underneath the left and right edges, which is in comparison to the IO specimens less support area. Considering PET has a high degree of deformation, the BAI specimens are able to deform more due to the less support area.

Observing these graphs, it can be concluded that the Balsa and SAN specimens are definitely representative concerning the impact tests, while the PET specimens leave room for discussion.

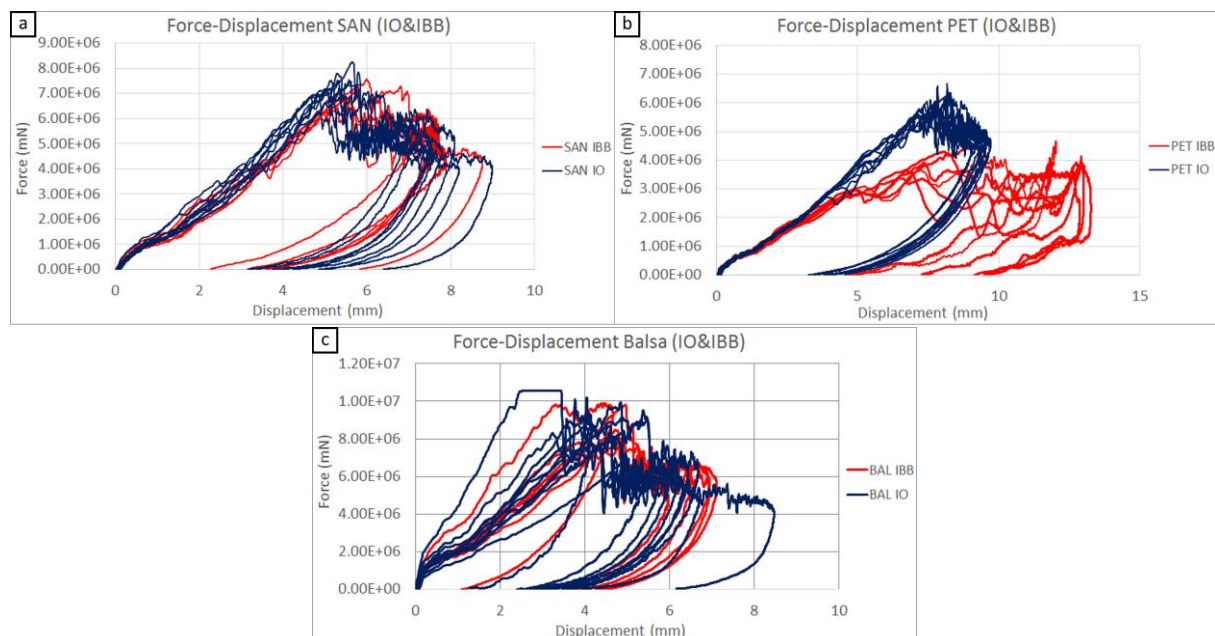


Figure 4.25: Comparison of the force-displacement graphs of the IO and IBB specimens impact tests of; a) the balsa wood cored specimens, b) the SAN foam cored specimens and c) the PET foam cored specimens.

Bending test

In order to be able to compare the BO and the BAI results, a bending test is done with the impacted bending specimens. The force-displacement graphs and values of these tests are shown in Figure 4.26 and Table 4.5. From Figure 4.26 and Table 4.5 it can be seen that the balsa core still is the stiffest core. It can also be seen that there is a lot more variety in the BAI values due to the impact (the blue lines). The BAI test values are shown in Table 4.5 and summarized in Figure 4.27 and Figure 4.28.

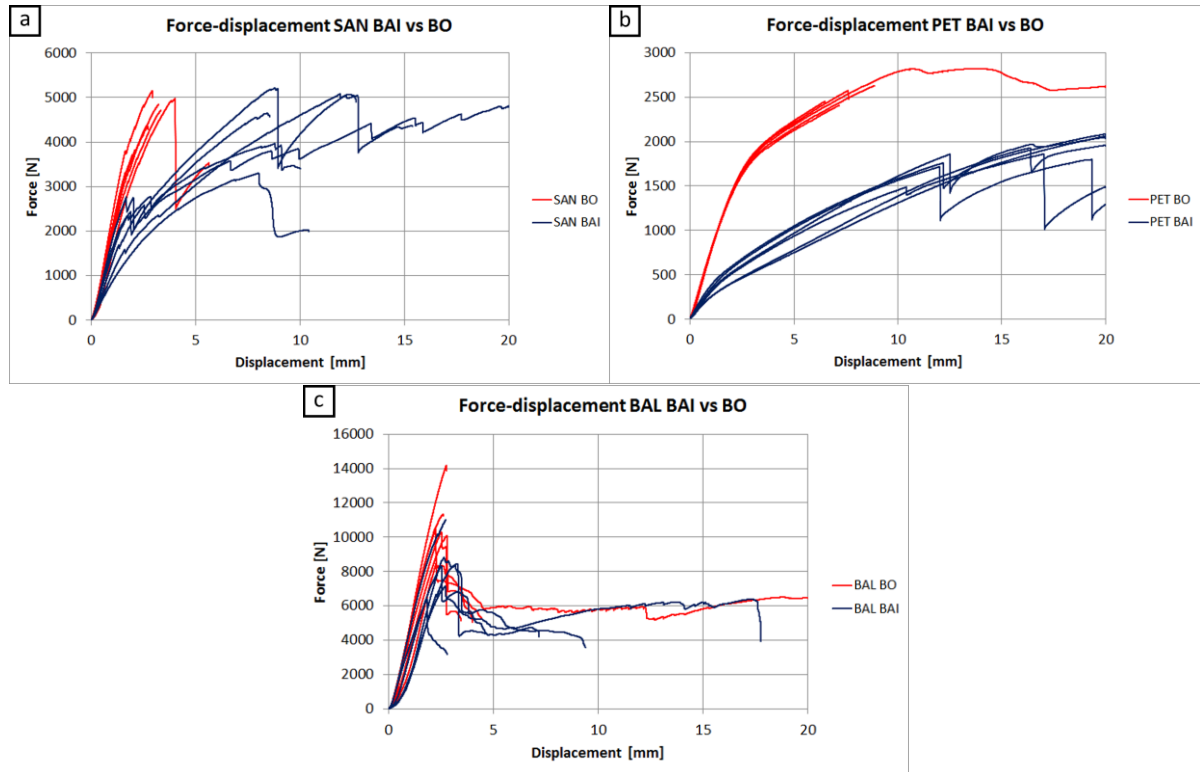


Figure 4.26: Comparison between the force-displacement graphs of the different specimens; a) SAN foam cored specimens, b) PET foam cored specimens and c) Balsa cored specimens. The red lines represent the BO results and the blue lines represent the BAI values.

Table 4.5: Values of the bending test of the BAI specimens.

Sample		BAI-SAN	BAI-PET	BAI-BAL
1	Max force (N)	1,591* (5,077)	1,860	11,023
	Max displacement (mm)	1.61* (12.69)	17.04* (20.00)	2.73
2	Max force (N)	3,157* (3,300)	2,060	8,393
	Max displacement (mm)	6.86* (10.41)	19.99* (20.00)	3.16* (7.17)
3	Max force (N)	2,751* (5,218)	1,759* (2,084)	7,151
	Max displacement (mm)	1.68* (15.39)	12.16* (20.00)	2.71* (9.38)
4	Max force (N)	2,592* (4,809)	1,718* (1,798)	6,399
	Max displacement (mm)	2.54* (20.00)	12.02* (20.00)	1.83* (2.78)
5	Max force (N)	2,775* (3,962)	1,856* (2,049)	8,296
	Max displacement (mm)	2.83* (10.02)	12.50* (20.00)	2.51* (17.75)
6	Max force (N)	2,438* (4,652)	1,925* (1,959)	8,817
	Max displacement (mm)	1.89* (8.55)	16.38* (20.00)	2.63* (4.66)
Avg	Max force (N)	2,551	1,863	8,347
	Max displacement (mm)	2.90	15.02	2.59

*Corrected value with the initial value in between brackets.

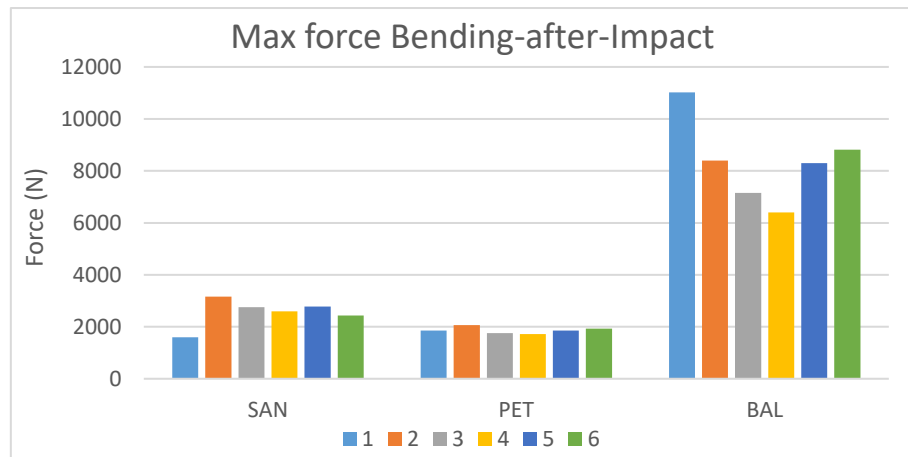


Figure 4.27: Bar plot of the maximum force in the BAI three-point bending test.

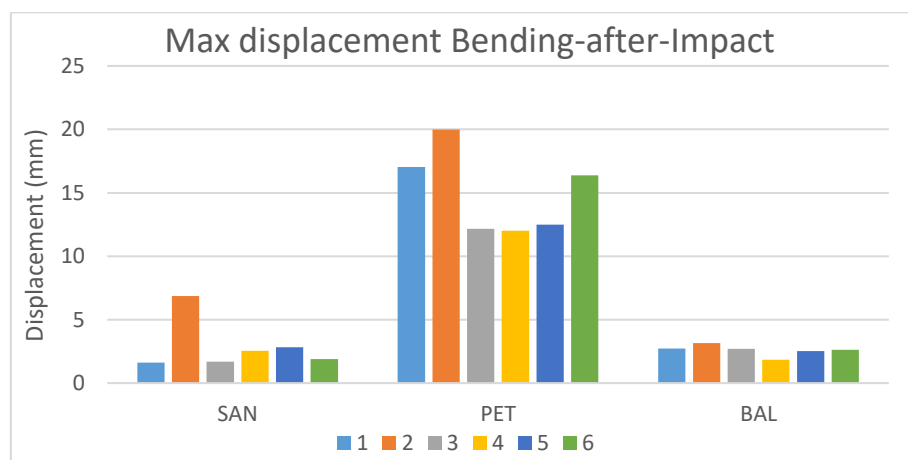


Figure 4.28: Bar plot the maximum displacement of every single specimen in the BAI three-point bending test.

In Table 4.5 it can also be seen that some of the values need correction as discussed in section 4.1.1 *Experimental analysis*. This can be devoted to the loss of stiffness in the specimens due to the impact. Many specimens lost stiffness in a certain way and therefore the force did not drop 50% or more. The values are corrected to the value at which the first *major failure mode* occurs; the failure mode after which the specimen only deteriorates and loses its stiffness. Investigating the specimens, it can be concluded that in most specimens the initial failure mechanism again was core shearing. During the tests it can clearly be seen that miniature cracks start to occur in early stages of the tests as shown in Figure 4.29, which was also the case in SAN2, SAN4 and all the PET specimens.

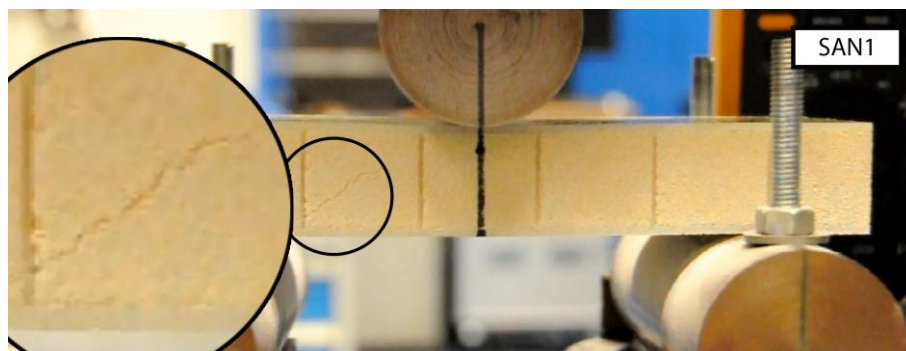


Figure 4.29: Mini-crack during the bending test of the BAI-SAN1 specimen.

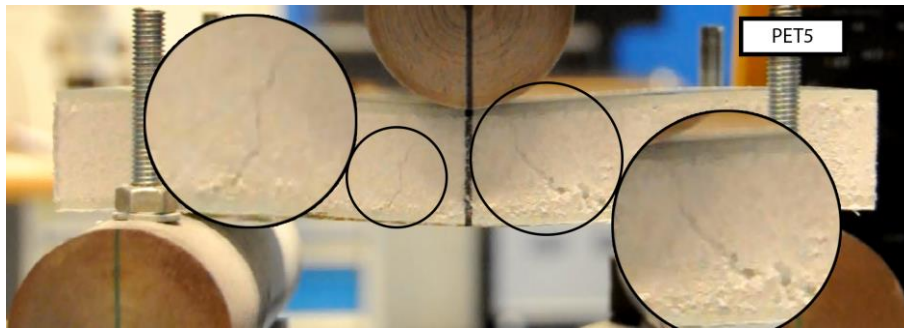


Figure 4.30: Mini-crack during the bending test of the BAI-PET5 specimen.

As mentioned, most of the BAI specimens suffer from the core shearing failure mechanism as can be seen in Figure 4.31. These specimens (SAN3, PET3 and BAL1) had little to none small cracks prior to the main failure mechanism.

There is only one specimen which has a different failure mechanism, namely SAN5. SAN5 has the (skin-core) debonding failure mechanism, which can be seen in Figure 4.32. This specimen has debonding of the skin and the core, but has also a little core shearing as can be seen at the right side in the magnification in Figure 4.32.

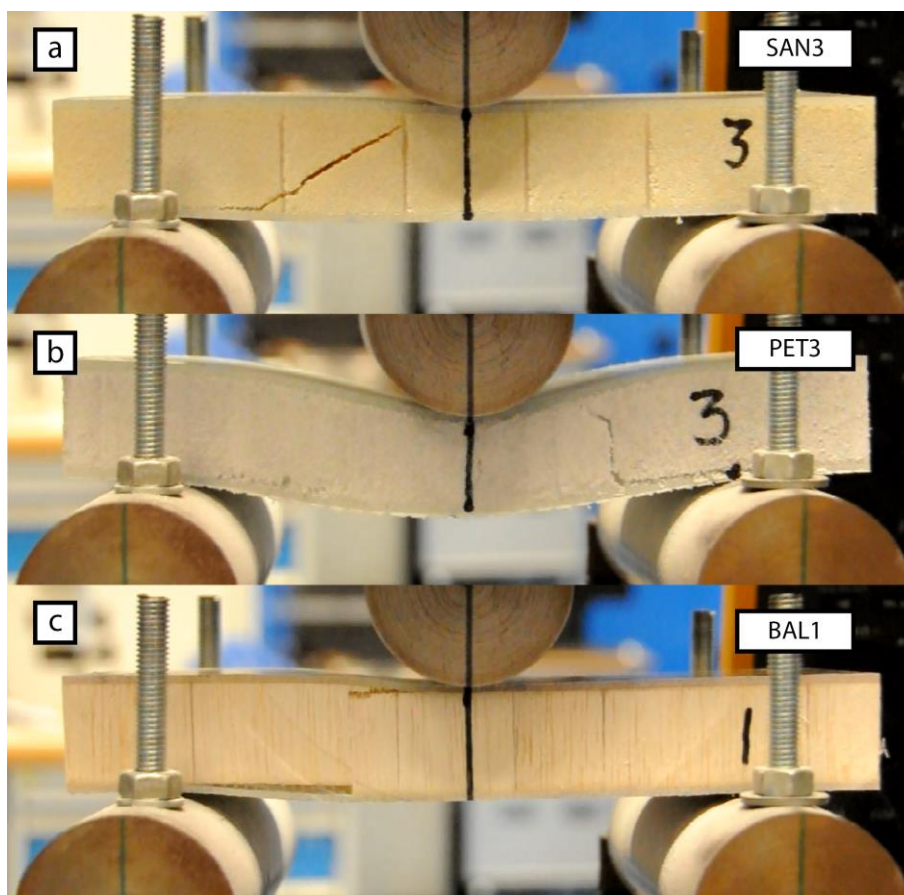


Figure 4.31: Core shearing failure mechanism in the SAN3, PET3 and BAL1 specimens.

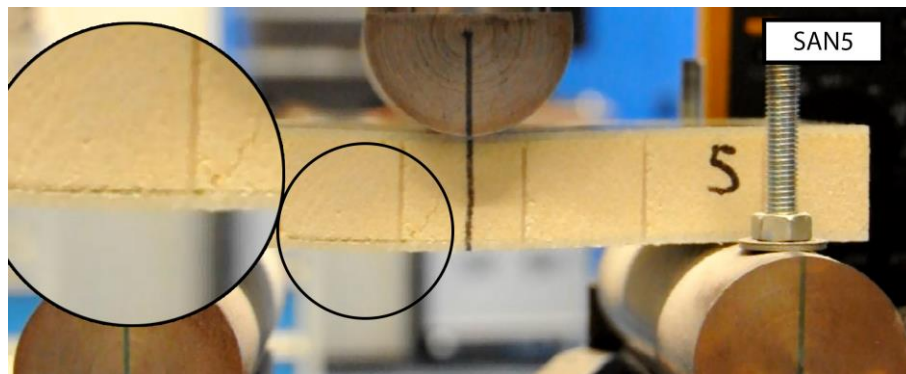


Figure 4.32: Debonding failure mechanism in the SAN5 specimen.

When comparing all failure modes of all specimen, in general there can be seen that balsa has sudden failure of core shearing/debonding and SAN and PET first have small internal cracks and thereafter sudden failure. In Table 4.6, a comparison is made between the failure modes of the BO specimens and the BAI specimens. It can be concluded that after the impact, the specimens show more small internal cracks than the BO specimens except for the Balsa cored specimens. This can probably be devoted to the fact that the core suffers small damage inside the core and therefore cracks when loaded.

Table 4.6: Most common failure modes in the different cored specimens.

	Bending-Only	Bending-after-Impact
SAN	Sudden failure <ul style="list-style-type: none"> Core shearing Debonding 	Pre-cracking <ul style="list-style-type: none"> Small internal cracks Sudden failure <ul style="list-style-type: none"> Core shearing Debonding
PET	Sudden failure <ul style="list-style-type: none"> Core shearing 	Pre-cracking <ul style="list-style-type: none"> Small internal cracks Sudden failure <ul style="list-style-type: none"> Core shearing Debonding
BAL	Sudden failure <ul style="list-style-type: none"> Core shearing Debonding 	Sudden failure <ul style="list-style-type: none"> Core shearing Debonding

Now all the bending tests are done, a comparison between the BO specimens and the BAI specimens can be made. The values are compared in Table 4.7 in which the different (average) values are compared and expressed in a percentage difference. It can be concluded that the SAN specimen lose 46.1% stiffness in terms of maximum force, but have 7.6% less maximum displacement. The PET specimen lose 25.7% stiffness in terms of maximum force and have an increase of 82.3% in terms of maximum displacement, which can be explained by the fact that the PET has less stiff material left which results in more displacement and a lower force. The Plastic Strain Equivalent (PEEQ) distribution, discussed in Figure 4.24, has also influence on this behaviour, since the affected area of the PET foam is distributed wider than the SAN foam and Balsa specimen. The Balsa specimen have a stiffness decrease of 19.1% in terms of maximum force and an increase of 2.8% in terms of maximum displacement. This is summarized in two bar plots in Figure 4.33 and Figure 4.34.

Table 4.7: Comparison of the values of the bending tests of the BO specimens and the BAI specimens.

		Bending-Only (BO)	Bending-after-Impact (BAI)	Difference (%)
SAN	Max force (N)	4,735	2,551	- 46.1%
	Max displacement (mm)	3.14	2.90	- 7.6%
PET	Max force (N)	2,508	1,863	- 25.7%
	Max displacement (mm)	8.24	15.02	+ 82.3%
BAL	Max force (N)	10,813	8,347	- 19.1%
	Max displacement (mm)	2.52	2.59	+ 2.8%

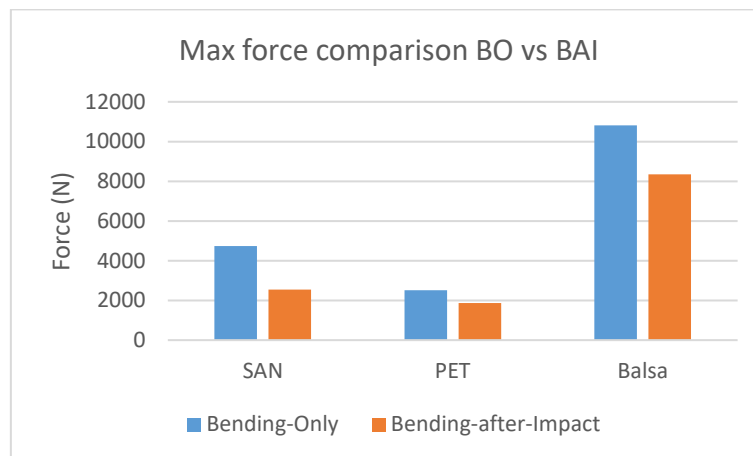


Figure 4.33: Bar plot of the maximum force in the three-point bending tests in which the BO is compared with the BAI.

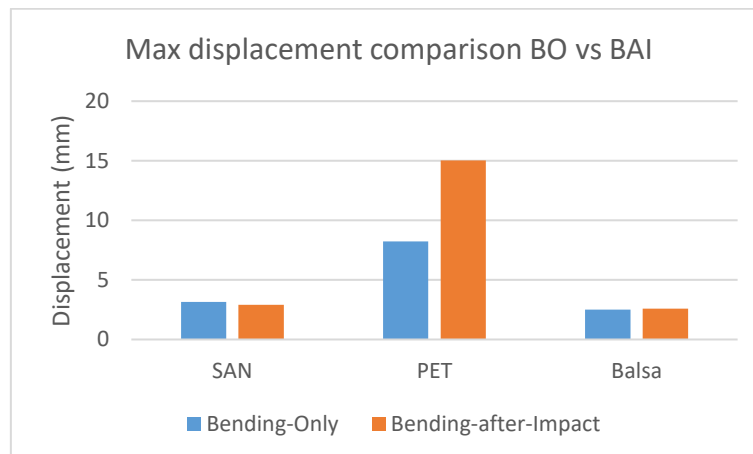


Figure 4.34: Bar plot of the maximum displacement in the three-point bending tests in which the BO is compared with the BAI.

Filling in the maximum forces in the analytical equations of section 2.2 *Analytical calculation of maximum stresses and shear stresses*, gives the following average values for maximum shear stress for the different cores shown in Table 4.8 and summarized in a bar plot in Figure 4.35.

Table 4.8: Average maximum stress and maximum shear stress in the different cores and a comparison expressed in percentage.

		Bending-Only	Bending-after-Impact	Difference
SAN	Max shear stress (MPa)	1.28	0.69	-46.1 %
PET	Max shear stress (MPa)	0.69	0.51	-26.2 %
BAL	Max shear stress (MPa)	2.92	2.25	-23.0 %

Full table in Appendix F: Stress table.

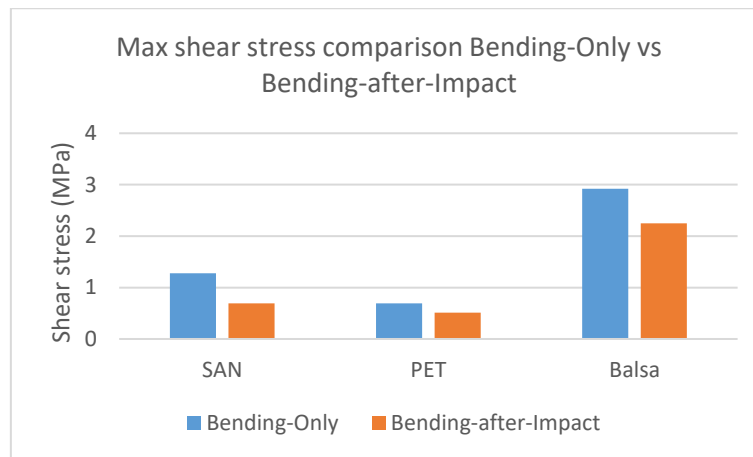


Figure 4.35: Bar plot of the maximum shear stress in the three-point bending tests, in which BO is compared with BAI.

In Table 4.8 it can be seen that the maximum stress and the maximum shear stress both decrease with the same values, except for the Balsa, in which both values are still in the same order of magnitude. The maximum (shear) stress in the SAN specimens decrease most, with a percentage of 46.1%. The maximum (shear) stress in the PET specimens decrease with 26.2% and in the Balsa specimens, the maximum stress decreases with 22.8% and the shear stress decreases with 23.0%. These reductions in (shear) stress are related to the drop in force, which are also in the same order of magnitude. Therefore, it can be concluded that due to the impact on the specimens, the specimens have a lower (shear) stress limit for failure.

4.3.2 FEM analysis

The FEM analysis of the BAI situation consists of two parts; Impact-before-Bending (IBB) and Bending-after-Impact (BAI). Like the experimental analysis of the BAI situation, the IBB is the same as the impact situation described in section 3.2 *Impact-Only (IO) model* with as difference the dimensions of the bending model (Figure 2.4) instead of the dimensions of the impact model (Figure 2.6).

After validating both the impact model and the bending model separately, there is no need to validate the BAI model also. Since the BO and IO results showed that the simulations without damage criteria fitted best compared to the ones with damage criteria, the simulations in the BAI section will only make use of the simulations without damage criteria. In order to do a BAI simulation, first an Impact simulation needs to be done on the bending specimens i.e. the IBB simulation. Thereafter, the BAI simulation can be done.

In this section the results of the FEM analysis of both the IBB and the BAI will be compared with the experimental values. Then the stress distributions will be studied and compared to the BO simulation results.

In Figure 4.36 the steps in the simulation are shown with first the impact simulation and then the bending simulation with the impacted panel as an initial state, which includes the residual impact stresses/strains and the residual deformed state.

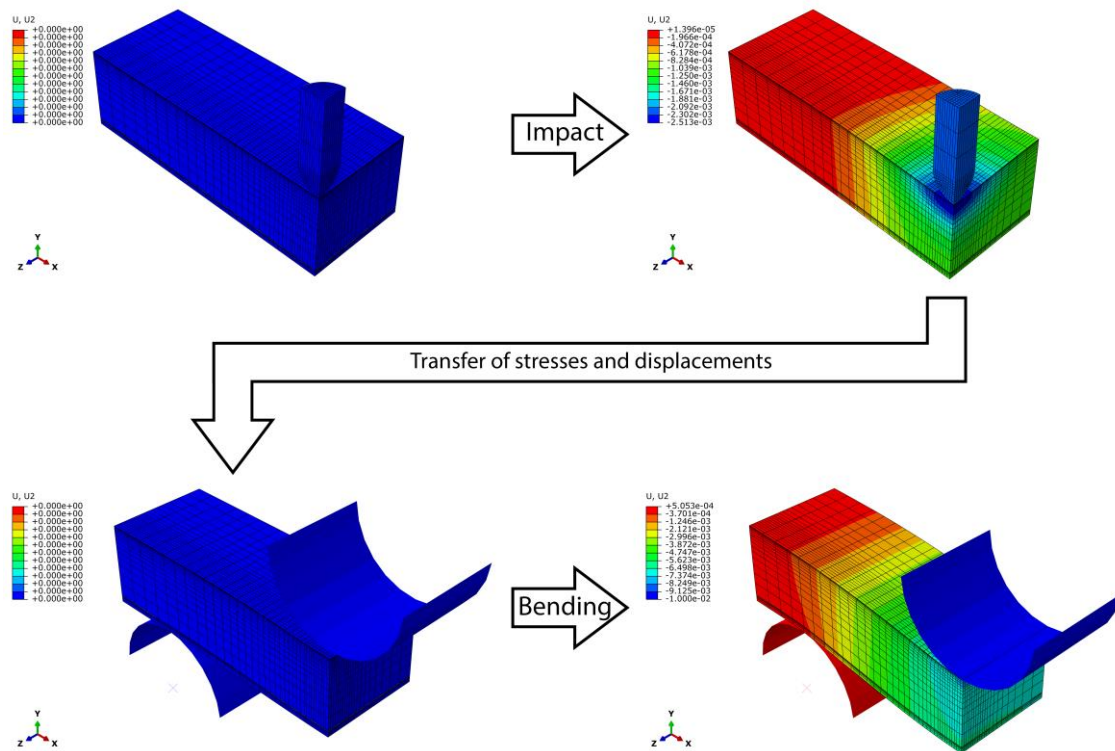


Figure 4.36: BAI simulation of SAN with the initial state in as starting position and afterwards the bended impact specimen expressed in deformation in the Y-direction.

In Figure 4.37 the force-displacement graphs of the IBB simulations are compared to the force-displacement graphs of the IO simulations. It can be seen that the IBB is subjected to more deformation, which can be explained by the support underneath the panel. Compared to the IO models, the IBB models have less support underneath, due to the geometry of the support fixture (shown in Figure 2.4 and Figure 2.6). Furthermore, it can be seen that the height of the force is in the same order of magnitude, which implies that the impact simulation can be assumed to be sufficient.

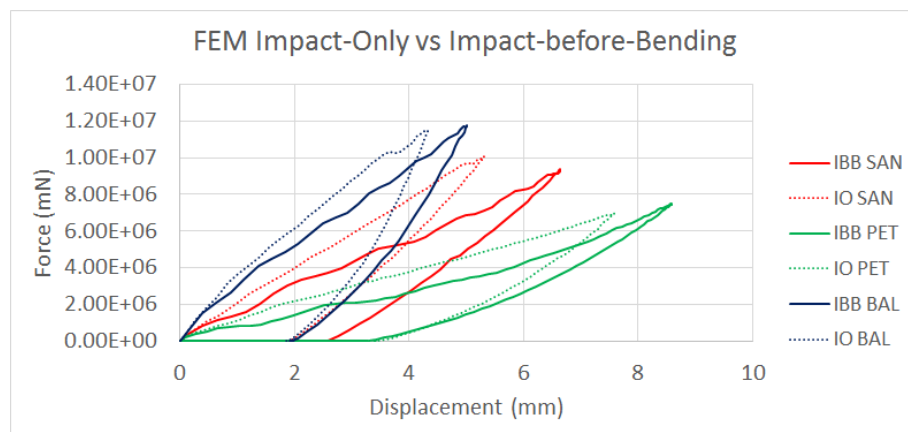


Figure 4.37: Comparison of the force-displacement graphs of the IO versus the IBB simulations.

In Figure 4.38 the simulations are compared with the experimental results. It can be seen that the initial stiffness of the IBB simulations approaches the experimental results better than the IO results, since the inclinations of the graphs are closer to the experimental values.

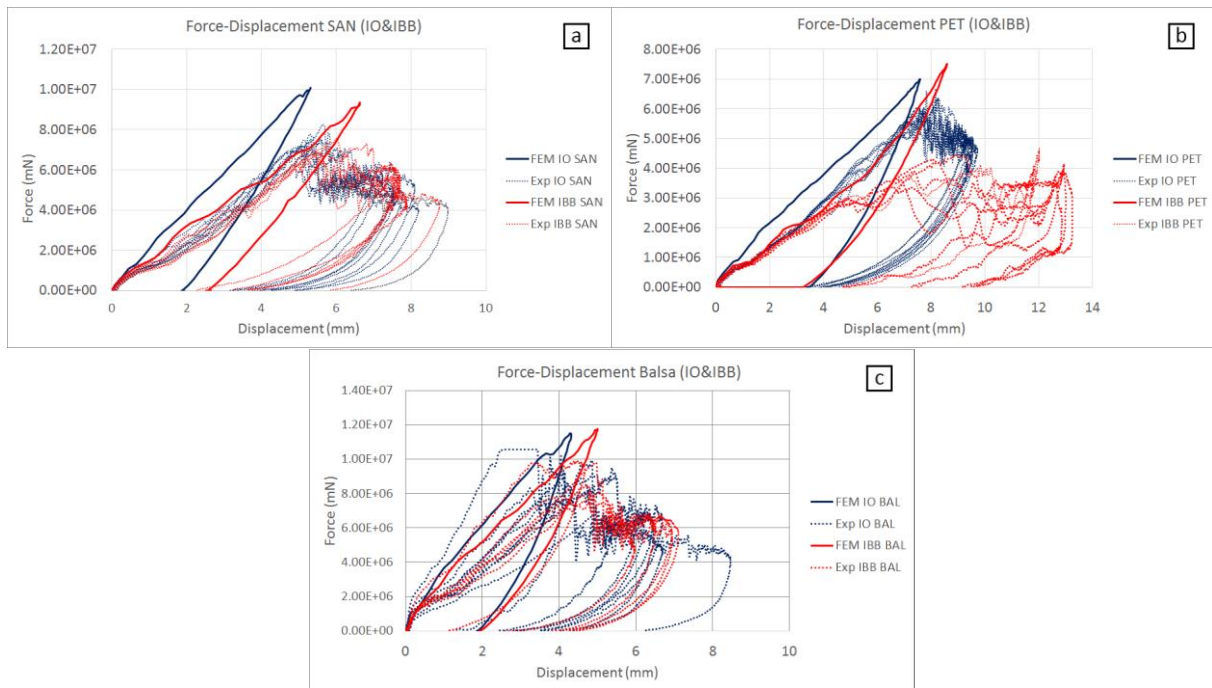


Figure 4.38: Force-displacement graphs in which the FEM results of the IO and the IBB simulations are compared to the corresponding experimental tests.

Investigating the velocity in the velocity-time graph in Figure 4.39, it can be seen that from moment of contact ($t = 0$ s), the initial velocity is accurate. After more indentation the simulation results show faster velocity decrease than the experimental tests which can be explained by the lack of damage criteria, so there is no perforation (or degradation of elements) of the skin causing the skin to remain stiff and strong during the entire simulation.

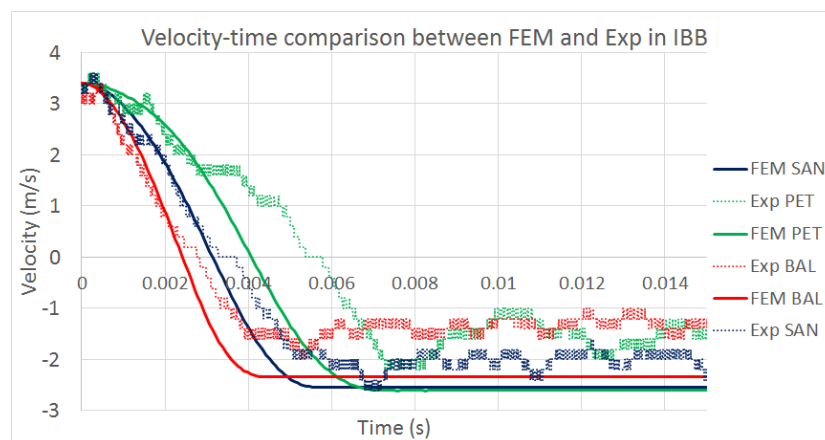


Figure 4.39: Velocity-time graphs of the IBB simulations and experimental tests in which $t=0$ is the moment of impact.

After the impact simulations, the bending simulations are performed with the impact results as an initial state. In Figure 4.40 it is shown that the SAN specimen has an initial stress distribution before bending which changes after bending. It can be seen that the BAI simulation starts with a panel which has residual stresses of the impact simulation as shown in Figure 4.36. Figure 4.40 shows a clear difference in the distribution of the normal stresses before and after bending (BAI).

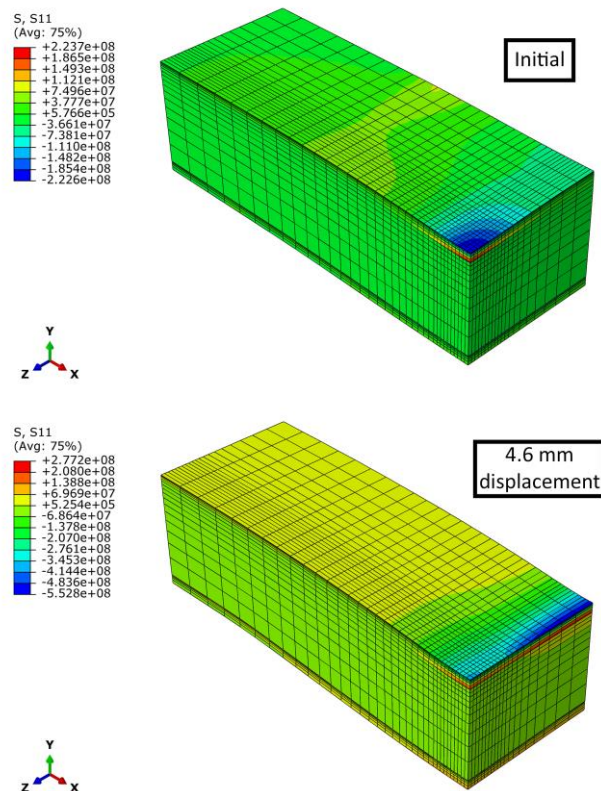


Figure 4.40: Stress state of a SAN specimen before and after the bending simulation in a BAI situation

After simulating the BAI situation, a comparison can be made between the BAI results and the BO results, discussed in section 4.1.2 *FEM analysis*. In Figure 4.41 a comparison between the two situations is made in which the shear stress (S12) in the core is investigated. Due to the software limitations, not every core is compared with equal displacement. The values which are used are close to the values of the experimental analysis at point of failure, except for the PET core in which the maximum displacement is used. A clear difference can be distinguished in terms of shear stress distribution, since the BAI started with an initial (shear) stress state. These residual (impact) stresses are in favour of the bending stresses, since both are in opposite direction, resulting in a lower shear stress in the BAI simulations compared to BO simulations.

The maximum shear stresses displayed in the legend in Figure 4.41 are not the maximum shear stresses which are of interest. The most important shear stresses are the shear stresses in the centre of the core, as already explained in section 4.1.2 *FEM analysis* in Figure 4.9 and Figure 4.10. Therefore, these sections are investigated which results in the maximum shear stresses in Table 4.9. In this table, also a comparison is made between the experimental values and the FEM results.

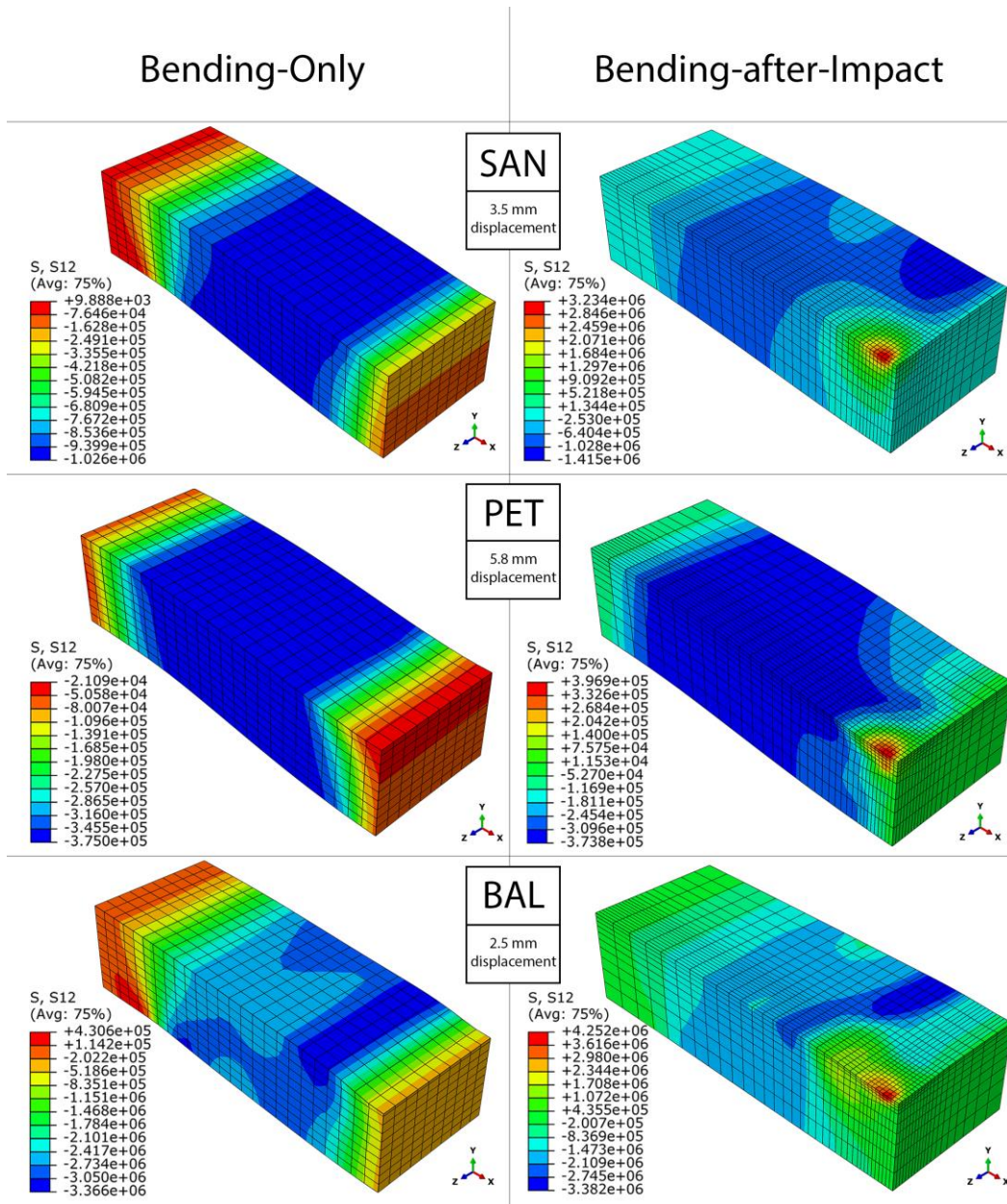


Figure 4.41: Shear stress comparison in the cores during bending.

Table 4.9: Maximum shear stresses of interest in the BO versus the BAI FEM simulations.

	Bending-Only	Bending-after-Impact	Difference
	FEM		
SAN	1.01 MPa	0.90 MPa	- 10.9%
PET	0.37 MPa	0.37 MPa	- 0.4%
BAL	3.00 MPa	2.17 MPa	- 27.7%
	Experimental		
SAN	1.28 MPa	0.69 MPa	-46.1 %
PET	0.69 MPa	0.51 MPa	-26.2 %
BAL	2.92 MPa	2.25 MPa	-23.0 %

Investigating the maximum forces in BAI in Figure 4.42, it can be seen that the initial stiffness of the BAI simulations is lower than the BO simulations. Despite the fact that the elements did not lose stiffness (due to the lack of damage criteria), this can be devoted to the contacting area of the upper fixture with the upper skin. Due to the impact on the panel, the deformation ensures that the panel has less contacting area with the upper fixture at the start of the BAI simulation. It can also be seen that, after reaching the complete contact area, the stiffness is equal to the initial stiffness again. This can be explained by the PEEQ distribution, which is only concentrated around the point of impact. The critical part of the core is in between the bottom fixture and the upper fixture (as shown in Figure 4.10), which is only little affected by the impact. After more displacement, the BAI simulations are approaching the BO simulations.

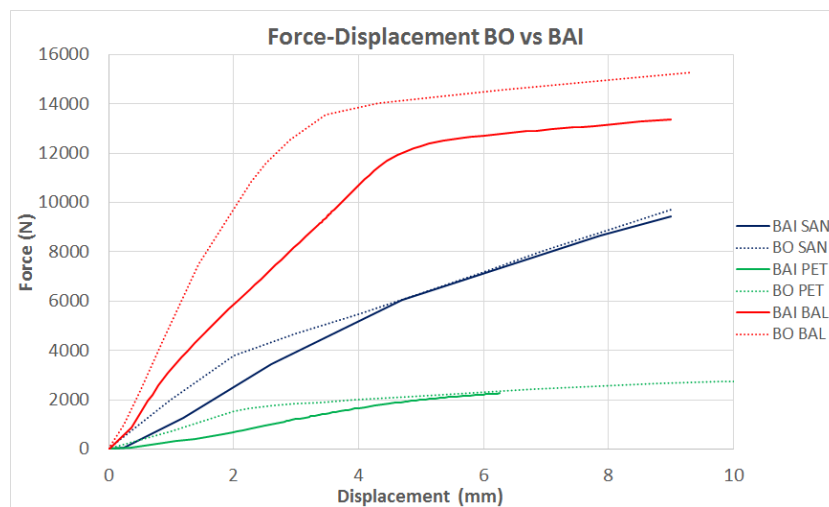


Figure 4.42: Force-displacement graph of the Bending simulations in which BO is compared with BAI.

Comparing these forces to the experimental results in Figure 4.43, it can be seen that the initial stiffness of the BAI simulations is in the same order of magnitude as the experimental tests. After more displacement, the upper fixture makes more contact with the panel and the panel becomes as stiff as the BO panel again, due to the lack of damage criteria and the small amount of damage to the critical part of the core (the centre of the core in between the fixtures).

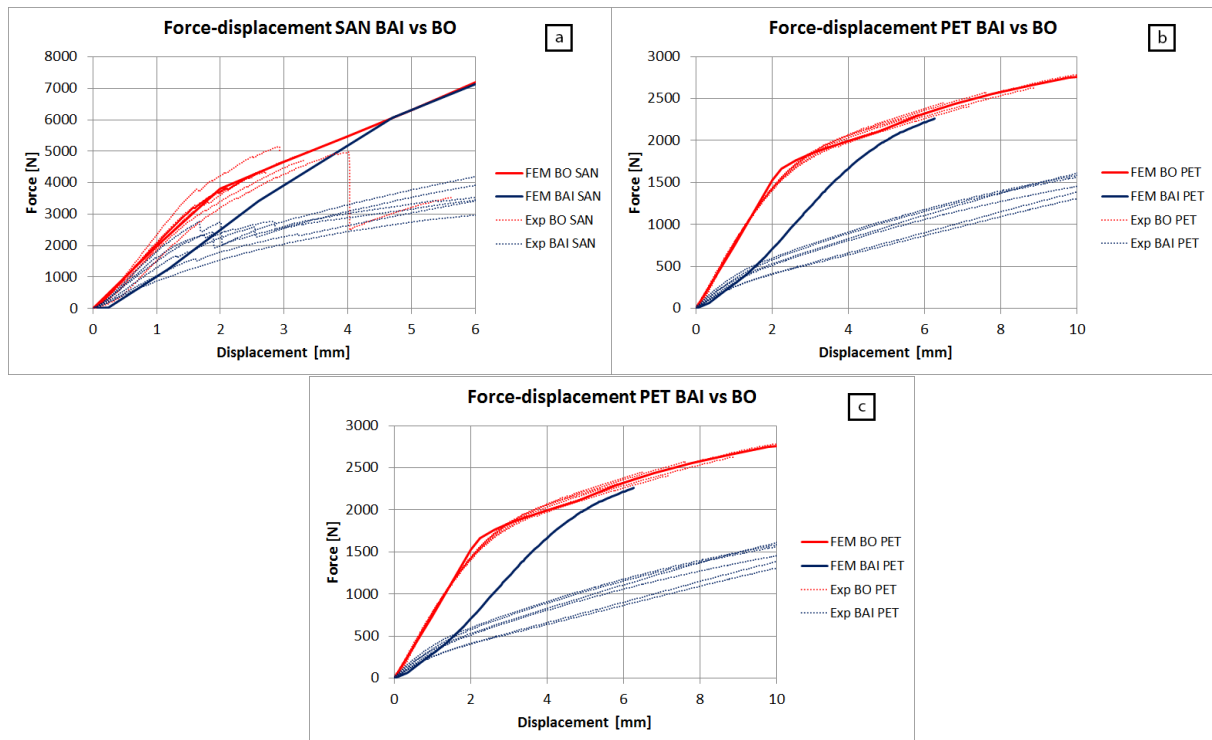


Figure 4.43: Force-displacement graph comparison between BO and BAI of the a) SAN foam core, b) PET foam core and c) Balsa core

In Figure 4.44 it can be seen that the contact area is small (about 50%) when the bending starts and increases until the contacting area is near 100% at 4 mm bending. In the force-displacement graph, this can also be seen in Figure 4.43-c, in which the BAI curve (solid blue line) starts to approach the BO curve (solid red line) at around 4 mm.

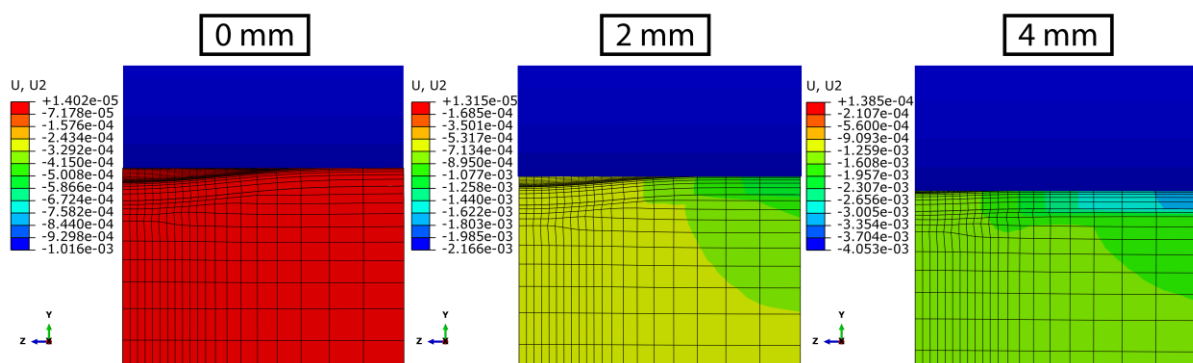


Figure 4.44: Contact area between the upper fixture (blue) and the Balsa cored panel (Red/Yellow/Green)

4.4 Effect of impact energy

In order to investigate the influence of the impact energy on the mechanical behaviour in bending after impact of the composite sandwich panels, a parameter study is done. In this parameter study, a number of different impact energies are investigated. In Table 4.10 the different simulations are shown with the corresponding impact energies and velocities of the indenter.

Table 4.10: Different iterations of impact energies in order to study the influence of impact energy on the mechanical behaviour of the different composite sandwich panels.

	Velocity (m/s)	Impact energy (J)
Reference	3.4	34.7
First iteration	2.9	25.0
Second iteration	4.1	50.0
Third iteration	5.8	100.0

The different velocities are plotted in Figure 4.45 in velocity-time graphs. It can be seen that the higher the starting velocity is, the faster the velocity decreases, which can be explained by the lack of damage criteria in the skin. Since the skin cannot be damaged, the indenter bounces back instead of perforating. It can also be seen that the Balsa panel (Figure 4.45-c) has earlier velocity decrease than SAN (Figure 4.45-a) and PET (Figure 4.45-b), which can be traced back to the superior properties of the Balsa. The PET panel has (naturally) the smallest velocity decrease, since the PET foam has poor properties and therefore deforms more easy.

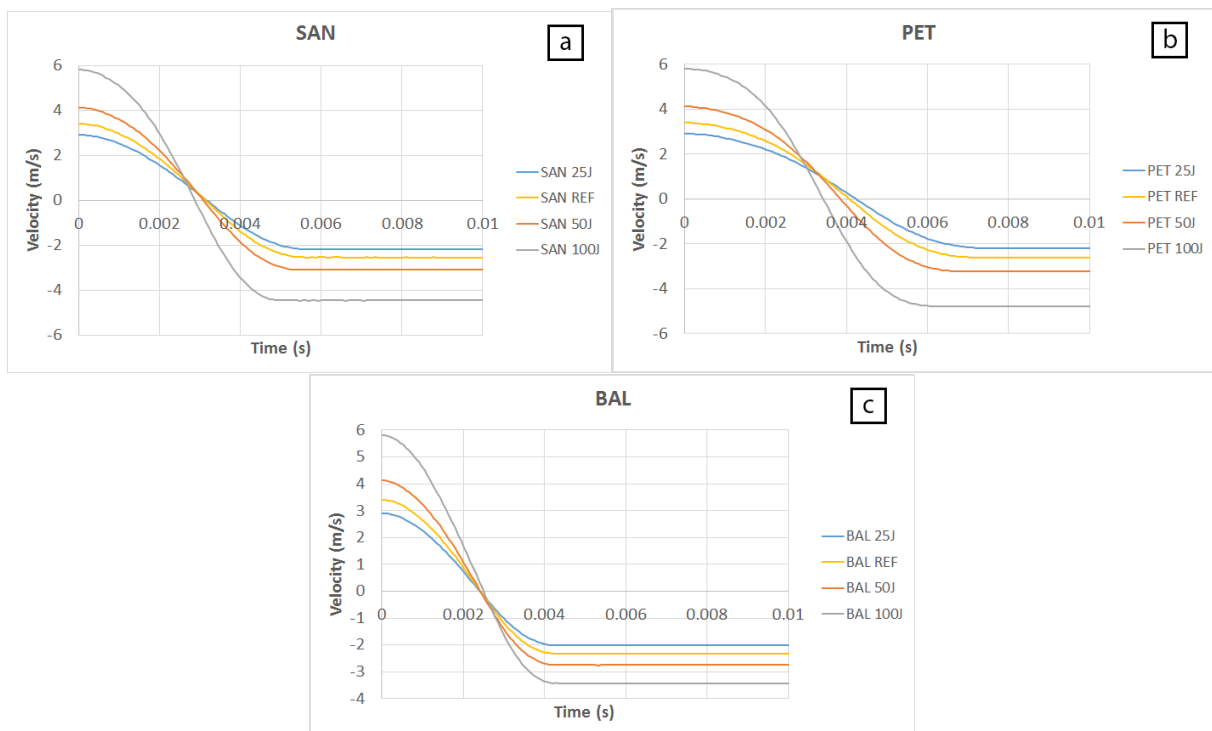


Figure 4.45: Velocity-time plots of the different impact energies of a) the SAN panels, b) the PET panels and c) the Balsa panels.

As can be seen in the force-displacement graphs of the IBB simulations of the different energies in Figure 4.46, the initial stiffness is the same in the different impact energies. Logically, higher impact energies result in higher deformation, both elastic and plastic deformation.

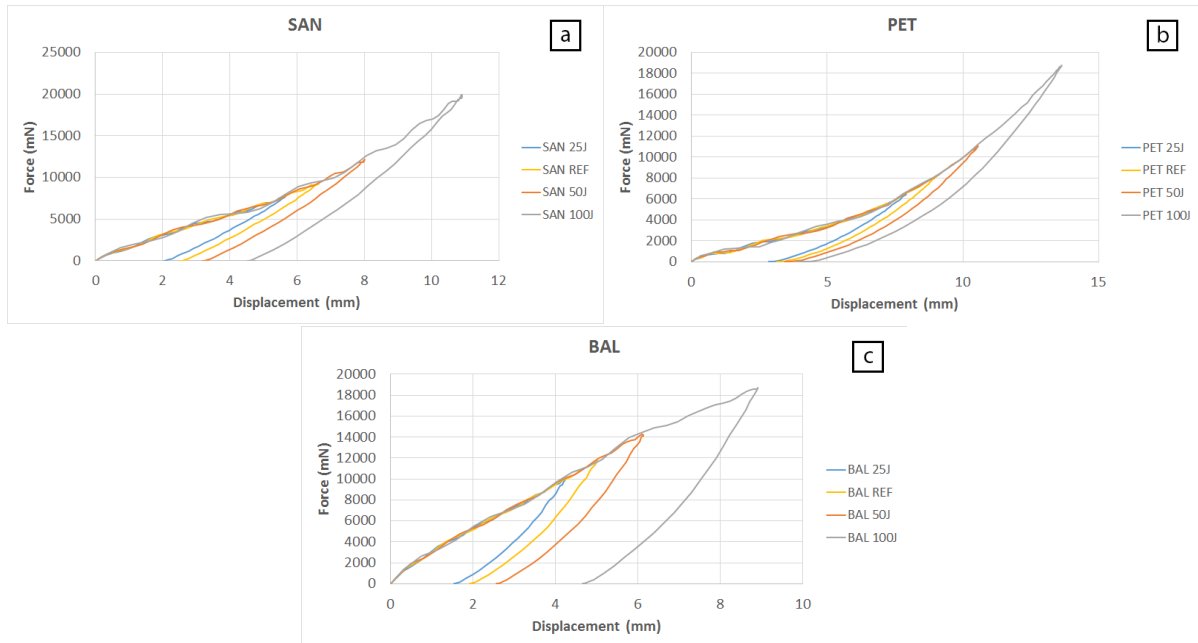


Figure 4.46: Force-displacement graphs of the IBB simulations with different impact energies of a) the SAN foam core, b) the PET foam core and c) the Balsa core.

The influence of the different impact energies, expressed in plastic strain equivalent (PEEQ), is shown in Figure 4.47. The PEEQ of the SAN foam increases from 0.26 to 0.49 when the impact energy is increased from 25J to 100J. The PEEQ of the PET foam increases from 0.82 to 1.0 and the PEEQ of the Balsa increases from 1.1 to 1.3 when raising the impact energy from 25J to 100J. In Figure 4.47 it can be seen that the increase in impact energy has the greatest influence on the PET foam core concerning the PEEQ distribution, which can be explained by the poor properties of this foam; the more the material can bend, then more effect a higher impact energy has. The impact energy has the least influence on the PEEQ distribution of the Balsa core, since the balsa core is the core with the highest properties.

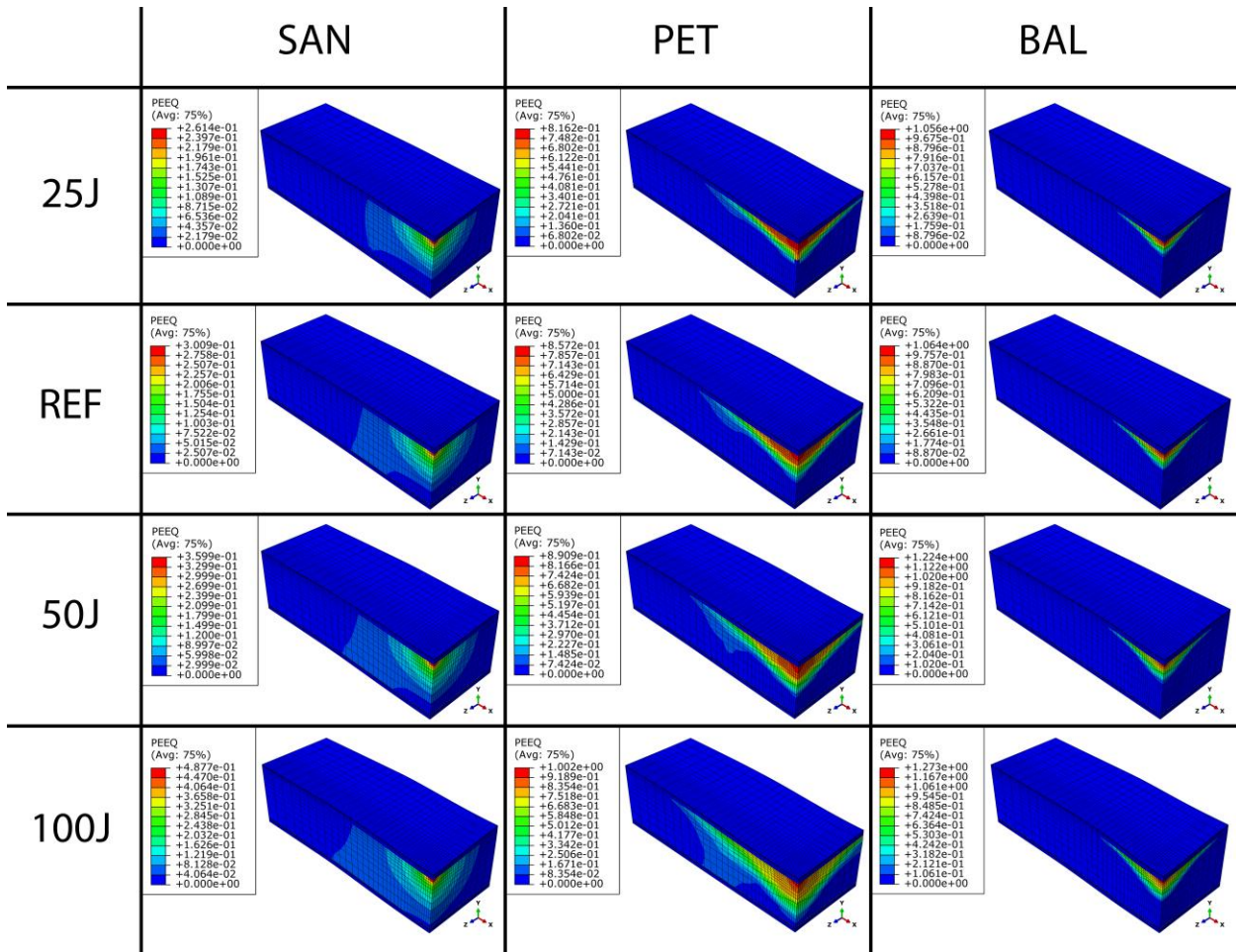


Figure 4.47: The influence of the impact energy on the Plastic strain Equivalent (PEEQ) in the different cores.

When investigating the influence of the different impact energies on the residual bending stiffness in Figure 4.48, it can be seen that in both PET in Figure 4.48-b and balsa in Figure 4.48-c, the influence of the different impact energies can be distinguished in contrast to the SAN foam cores in Figure 4.48-a, in which the different impact energies have no significant influence on the residual bending stiffness of the panel. This might be caused by the contacting area of the upper fixture during the three-point bending simulations. In Figure 4.49 the contact normal forces are shown of the SAN foam and the balsa cored specimens, showing that the contact area of the SAN remains the same while the contact area of the balsa becomes less with higher impact energies.

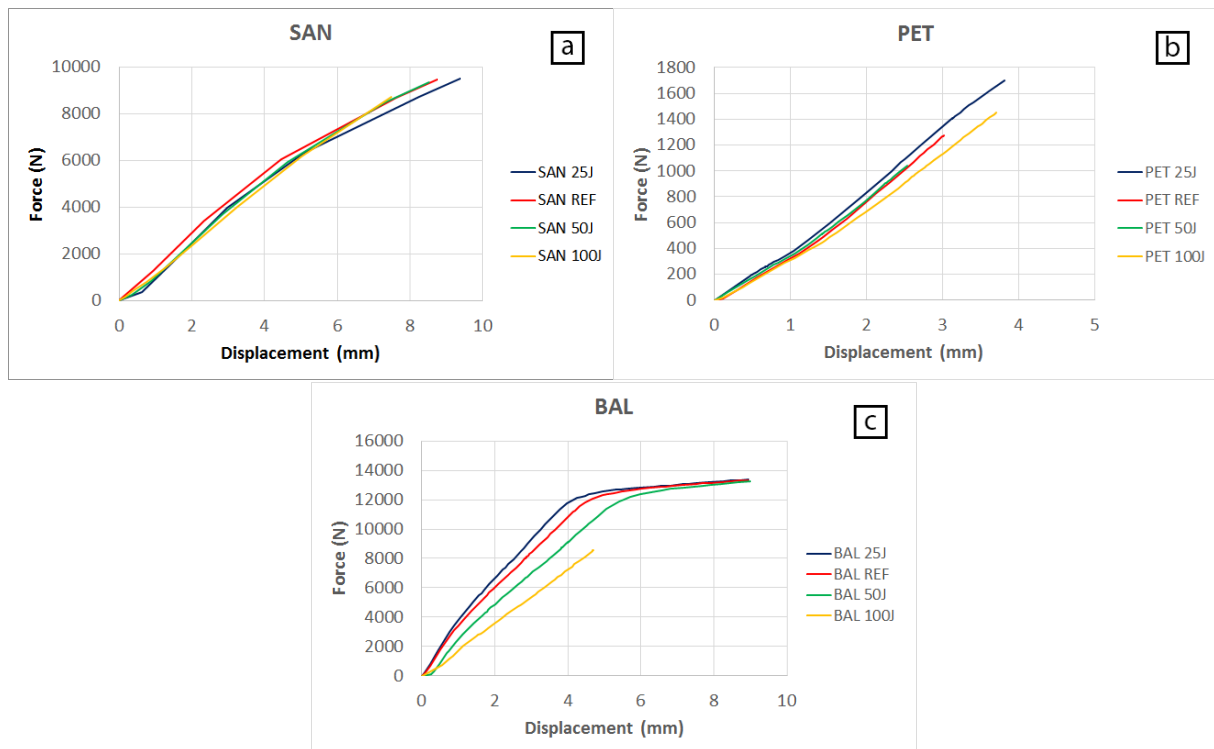


Figure 4.48: BAI force-displacement graphs of the different impact energies of a) the SAN foam core, b) the PET foam core and c) the Balsa core.

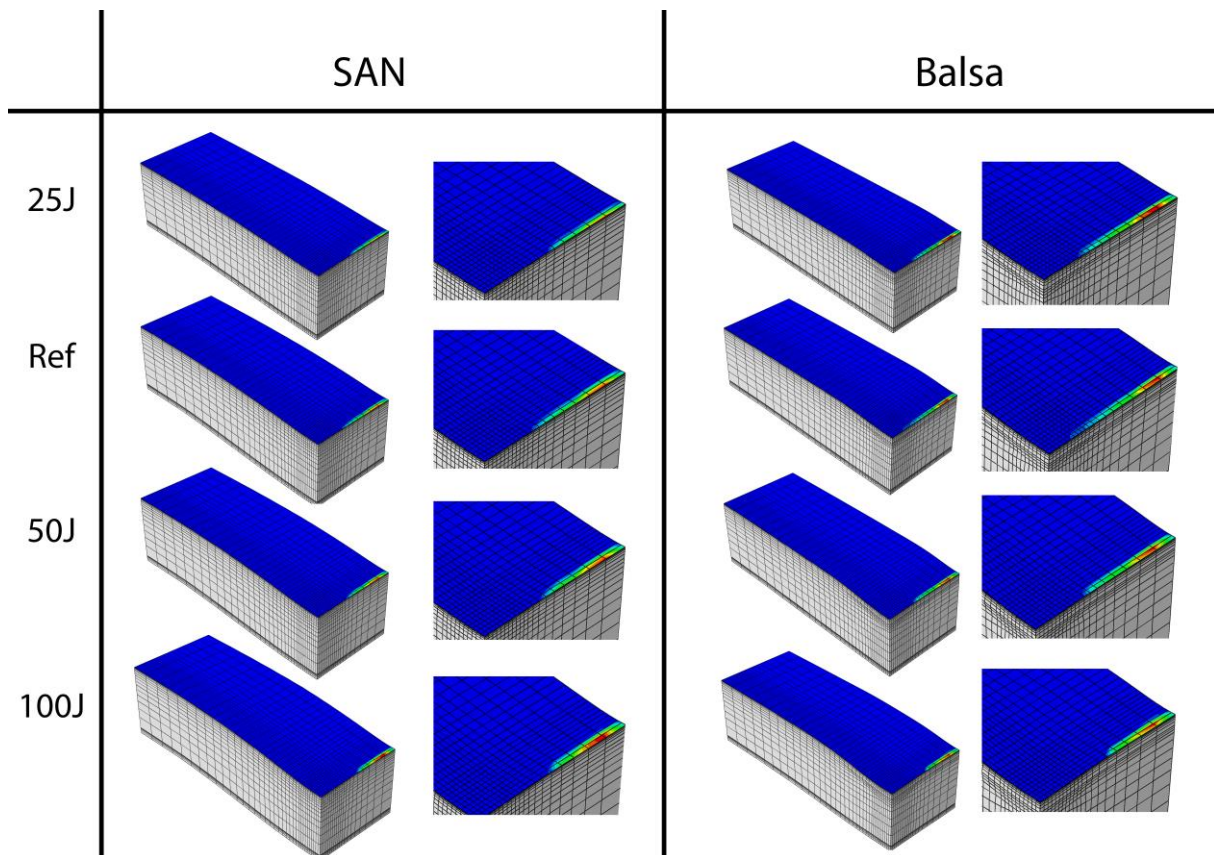


Figure 4.49: Comparison of contact normal forces of the SAN foam and Balsa panels at 4.0 mm displacement.

Investigating the BAI behaviour in Figure 4.50, it can be seen that the impact energy has no significant influence on the shear stress distribution in the SAN foam core, except for the height of the maximum

(shear) stress levels. Furthermore, the impact energy has little influence on the shear stress distribution in the PET foam core and has a significant influence on the shear stress distribution in the Balsa core.

As in the previous FEM results in sections 4.1.2 *FEM analysis*, 4.2.2 *FEM analysis* and 4.3.2 *FEM analysis* the maximum shear stresses of interest are in the middle of the simulated panel (in between the upper and bottom fixture as shown in Figure 4.9 and Figure 4.10. These maximum shear stresses are summarized in Table 4.11. It can be seen that for the PET foam and the SAN foam the impact energy has a significant influence on the shear stresses and for the Balsa wood it has little to no influence.

Table 4.11: Maximum shear stresses in the different impact energies.

	SAN	PET	BAL
25J	1.02 MPa	0.37 MPa	1.74 MPa
REF	0.93 MPa	0.36 MPa	1.69 MPa
50J	0.85 MPa	0.34 MPa	1.61 MPa
100J	0.75 MPa	0.32 MPa	1.74 MPa

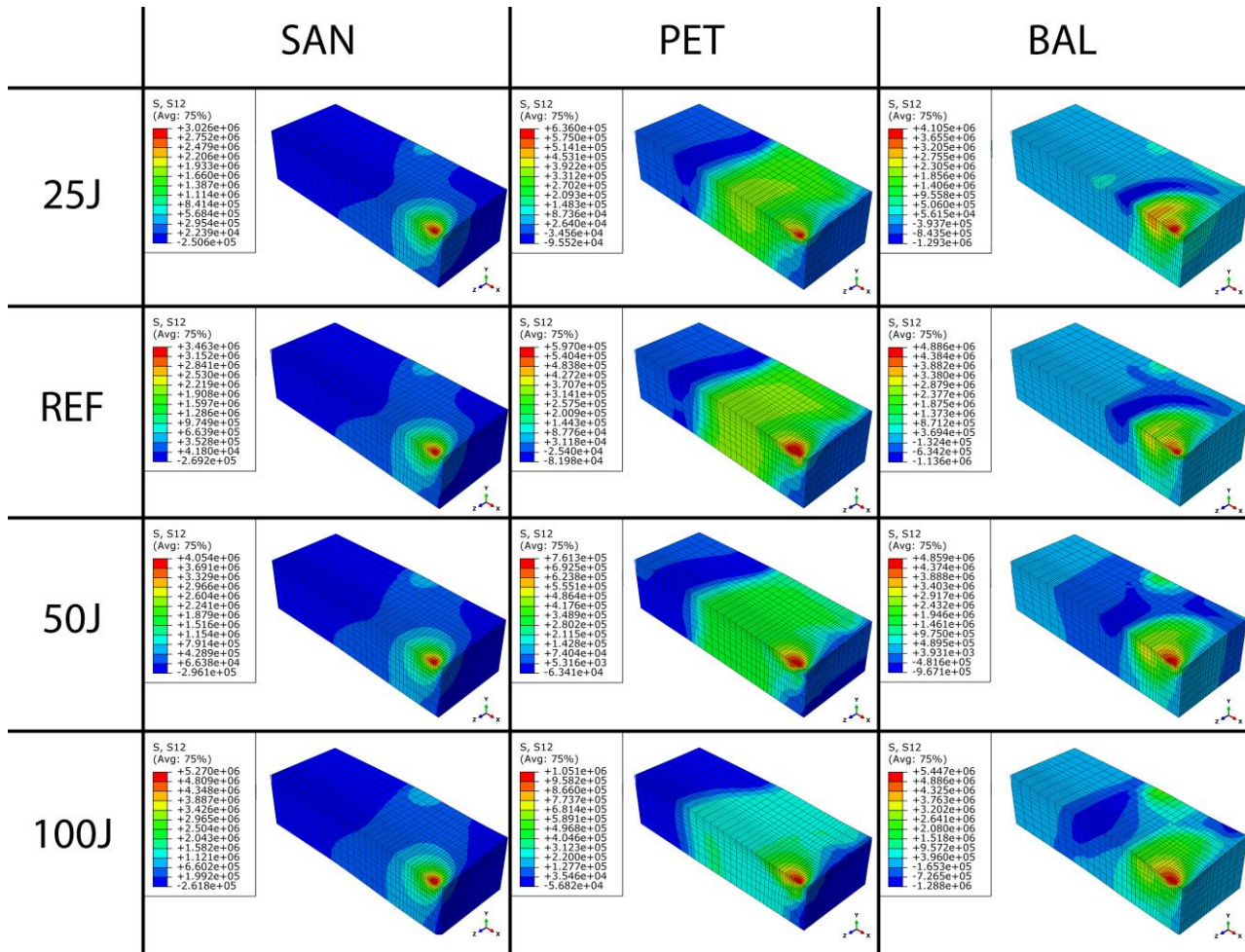


Figure 4.50: The shear stresses (S_{12}) in BAI of the different cores with the different impact energies.

5. Conclusions & Future recommendations

5.1 Conclusions

In this thesis the mechanical behaviour of composite sandwich panels is investigated in bending, impact and bending after impact. The residual mechanical performance of sandwich composites with SAN foam, PET foam and Balsa core with (quadrax) glass/epoxy facesheets are investigated for the first time in literature. Experimental analysis as well as a Finite Element Method analysis are used as the methodology in order to answer the research questions in section 1.3 *Research goal and objectives*. Despite of the lack of literature investigation about the extraction of the reaction force in impact simulations, it is succeeded to extract this information and use this in this investigation. The develop

ed FEM models are found to agree well with the experimental findings based on the assumptions taken in the numerical models. The damage zones in the core and facesheets are examined under optical microscopy.

The experimental analysis and the Finite Elements Method analysis show that the Balsa core has the highest stiffness as well as the highest impact reaction force, which is expected because of its high properties. The downside of this material is that there is a lot of variety in the results since the balsa core is a natural product with non-isotropic properties. By contrast, the SAN foam and the PET foam show consistent results, since these are isotropic polymer foams. In the experimental bending analysis, the main failure mechanism is a sudden failure of core shearing, with occasionally a skin-core debonding simultaneously.

The experimental impact analysis shows that the balsa cored specimens have a skin-core debonding at the backside of the panel. The FEM analysis shows that this can be explained by the high shear stresses in the core due to this impact. Furthermore, the experimental analysis shows that the PET cored specimens have the least damage to the surface compared to the SAN cored specimens and the Balsa cored specimens.

The experimental impact specimens are affected by the impact and have a certain impact-affected zone. The impact zones are studied in a microscopic analysis in order to determine the exact affected zones. These impact-affected zones are compared with the plastic deformed zone (PEEQ) of the FEM analysis. The simulations without damage criteria of the skins give better approximation than the simulations with damage criteria.

It is shown that an impact has a significant influence on the residual bending stiffness of composite sandwich panels, the rate of influence is dependent on the core material. Therefore, the first research objective is answered. The SAN foam core is affected the most from an impact; it loses 46.1% in terms of bending stiffness. PET loses 25.7% bending stiffness and Balsa loses about 19.1% bending stiffness. It is also shown that Balsa is affected the most in terms of shear stress distribution in the core; the shear stresses in the Balsa core are reduced with 27.7%. The SAN foam core is affected with a decrease of 10.9% and the impact has almost no influence on the PET foam core, in which the shear stresses only decrease with 0.4, which answers research objective three. In the experimental Bending-after-Impact analysis the specimens of the SAN foam and the PET foam frequently show miniature cracks prior to the main failure mechanism of (as in the Bending only case) sudden core shearing, which answers research objective two.

It is also investigated what the influence is of the impact energy on the mechanical behaviour of the composite sandwich by a Finite Elements Method analysis. In this study it is shown that the higher the impact energy, the lower the bending stiffness for the PET foam core and the Balsa core. The impact energy has no influence on the SAN foam core in the FEM analysis. It is also shown that the impact

energy has a significant influence on the shear stress distribution of the Balsa core. The SAN and the PET foam cores seemed to suffer less for higher impact energies in terms of shear stress distribution. With this last part, research objective four is answered.

5.2 Recommendations

In this thesis it is shown that the models with damage criteria of the skin are insufficient in order to predict the correct impact behaviour and thus also the bending-after-impact behaviour. Therefore, it is wise to study how these damage criteria can be implemented a working FEM model and working simulations in order to predict the correct bending behaviour, impact behaviour and bending after impact behaviour.

As already mentioned in the conclusions, the literature shows lack of information about retrieving force information from an explicit impact model. It is also of importance that the way this information is retrieved in this thesis gets validated in order to ensure reliable results.

In the experimental analysis, it appeared that the material properties were not the properties provided by the datasheets. It is wise to determine these properties by practical tests in order to be able to describe the material properties and to predict the behaviour in bending, impact and bending after impact.

6. References

- Alemi-Ardakani, M. M. (2014). On complexities of impact simulation on fibre reinforced polymer composites: A simplified modeling framework. *The scientific world journal*.
- Arbaoui, J. S. (2014). Effect of core thickness and intermediate layers on mechanical properties of polypropylene honeycomb multi-layer sandwich structures. *Metallurgy and Materials Vol. 59*, 11-16.
- ASTM-C393/C393M. (2012). Standard test method fo core shear properties of sandwich constructions by beam flexure. *ASTM International*.
- Barbero, E. C. (2013). Determination of Material Parameters for Abaqus Progressive Damage Analysis of E-Glass Epoxy Laminates. *Composites Part B*, 211-220.
- Campbell, F. (2010). *Structural composite materials*. Ohio: ASM International.
- Can, W. H.-r.-k. (2010). Experimental investigation of interfacial fracture behaviour in foam core sandwich beams with visco-elastic adhesive interface. *Composite Structures 92*, 1085-1091.
- Castilho, T. S. (2014). Impact Resistance of Marine Sandwich Composites. In T. S. C. Guedes Soares, *Maritime Technology and Engineering* (pp. 607-617). Lisbon: CRC Press.
- Castro, O. S. (2010). Cork agglomerates as an ideal core material in lightweight structures. *Materials and Design 31*, 425-432.
- Chawla, K. K. (1998). *Composite Materials: Science and Engineering second edition*. New York: Springer Science and Business Media.
- Daniel, I. (2009). Influence of core properties on the failure of composite sandwich beams. *Journal of Mechanics of Materials and Structures Vol. 4*, 1271-1286.
- Daniel, I. G.-A. (2002). Failure Modes of Composite Sandwich Beams. *International Journal of Damage Mechanics 11*, 309-334.
- Falk, L. (1994). Foam core sandwich panels with interface disbonds. *Composite Structures 28*, 481-490.
- Flores-Johnson, E. L. (2011). Experimental study of the indentation of sandwich panels with carbon fibre-reinforced polymer face sheets and polymeric foam core. *Composites: Part B 42*, 1212-1219.
- Gkaidatzis, R. (2014). *Bio-based FRP structures: A pedestrian bridge in Schiphol Logistics Park*. Delft: Architecture, Urbanism and Building Sciences.
- Gupta, N. (2002). Response of Syntactic Foam Core Sandwich Structured Composites to Three-Point Bending. *Sandwich Structures and Materials Vol. 4*, 249-272.
- Hassan, M. C. (2012). The influence of core properties on the perforation resistance of sandwich structures – An experimental study. *Composites: Part B 43*, 3231-3238.
- Kabir, M. E. (2006). Tensile and fracture behaviour of polymer foams. *Materials Science and Engineering A 429*, 225-235.
- Kanny, K. M. (2002). Dynamic mechanical analyses and flexural fatigue of PVC foams. *Composite Structures 58*, 175-183.

- Kim, J. L. (1999). Evaluation of durability and strength of stitched foam-cored sandwich structures. *Composite Structures* 47, 543-550.
- McQuigg, T. K. (2012). *Compression After Impact on Honeycomb Core Sandwich Panels with Thin Facesheets, Part 1: Experiments*. Blacksburg: Virginia Polytechnic Institute and State University.
- Özdemir, O. (2012). *Core Material Effect on Impact Behaviour of Glass Fibre Sandwich Composites*. Izmir: School of Natural and Applied Sciences of Dokuz Eylül University.
- Panduranga, R. S. (2007). *Energy absorption performance of eco-core - a syntactic foam*. Greensboro: North Carolina A&T State University.
- Pramanik, B. M. (2012). Energy Absorption of Nano-Reinforced and Sandwich Composites in Ballistic and Low-Velocity Punch-Shear. *Open Journal of Composite Materials*, 87-96.
- RapraTechnology. (2007). *Blowing agents and foaming processes*. Frankfurt, Germany: Smithers Rapra Ltd.
- Sakly, A. L. (2016). Experimental and modelling study of low velocity impacts on composite sandwich structures for railway applications. *Engineering Failure Analysis* 68, 22-31.
- Shipsha, A. B. (2000). On Mode I Fatigue Crack Growth in Foam Core Materials for Sandwich Structures. *Sandwich Structures and Materials* 2, 103-116.
- Shipsha, A. Z. (2005). Compression-after-Impact Strength of Sandwich Panels with Core Crushing Damage. *Springer*, 149-164.
- Simulia. (2016). Abaqus Analysis 2016 User's guide.
- Steeves, C. F. (2004). Collapse mechanisms of sandwich beams with composite faces and a foam core, loaded in three-point bending. Part I: analytical models and minimum weight design. *International Journal of Mechanical Sciences* 46, 561-583.
- Steeves, C. F. (2004). Material selection in sandwich beam construction. *Scripta Materialia* 50, 1335-1339.
- Thomas D. McQuigg, R. K. (2012). *Compression After Impact on Honeycomb Core Sandwich Panels with Thin Facesheets, Part 1: Experiments*. Blacksburg: Virginia Polytechnic Institute and State University.
- Vinson, J. R. (2001). Sandwich structures. *Applied Mechanical Reviews*, 201-213.
- Vries, D. d. (2009). *Characterization of polymeric foams*. Eindhoven: Eindhoven University of Technology.
- Vural, M. R. (2003). Microstructural aspects and modeling of failure in naturally occurring porous composites. *Mechanics of Materials*.
- Vuure, A. v. (2000). Mechanical properties of composite panels based on woven sandwich fabric preforms. *Composites: Part A* 31, 671-680.
- Wachenfelt, H. v. (2013). Measurement of kick loads from horses on stable fittings and building elements. *Biosystems Engineering* 116, 487-496.

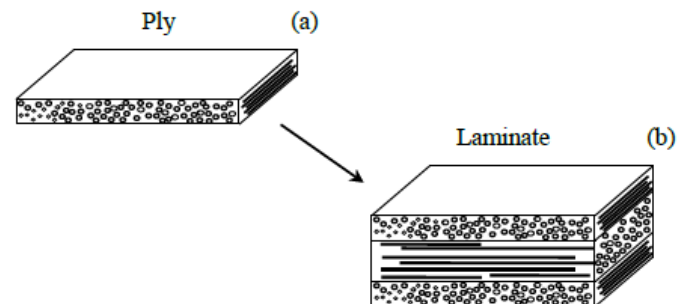
- Wang, J. W. (2013). Experimental and numerical study on the low-velocity impact behaviour of foam-core sandwich panels. *Composite Structures* 96, 298-311.
- Xanthos, M. D. (2001). Properties and Applications of Sandwich Panels Based on PET Foams. *Reinforced Plastic and Composites* 20, 786-793.

Appendix A: Composites background information

A composite material can be described as a combination of two or more constituents. Generally, the characteristics of the components are combined to obtain certain properties, which can't be acquired with the individual constituents.

In this report it will be restricted to continuous fibre reinforced plastics. The fibres are used for their high strength and stiffness, whilst the matrix (resin) is used to protect the fibres, binds them together and transfers the load between the fibres. The combinations of fibres and matrices are nearly unlimited. Every composite is attuned to a certain application.

The stacking of multiple layers (plies) is called a laminate, on which is focused in this report. The fibres in the ply of Figure 0.1 are aligned unidirectional (all in one way). Stacking layers in different orientations can customize the properties of the laminate. The laminate in Figure 0.1 are stacked in a $[0/90/0]$ orientation which means that the fibres are oriented in respectively the length, the width and again the length direction. In this way tensile forces in these directions can be adapted well by the fibres. (Composites handout 2014) The same way a quasi-isotropic layup can be made, which means the laminate is equal in every direction. A quasi-isotropic layup is a layup with fibres in the $[0/+45/-45/90]$ direction. In this way forces in every direction are distributed evenly. Quadrax is a laminate with a quasi-isotropic layup stitched together to keep the fibres in place.



A.1 Fibres

Fibres are an important constituent in fibre reinforced polymers, as they are good at absorbing the load when a force loads the laminate. Different fibres have different characteristics and stand out in different situations. While lots of fibres are available, there is only focused on several interesting fibres which properties can be found in Table 0.1.

Material		E-glass fibre	Basalt fibre	Carbon fibre	Aramid fibre
Product name		Glass E grade fibre	Basaltfibre	Carbon HS fibre	DuPont Kevlar 29
Density	Kg/m ³	2550 - 2600	2500 - 2890	1800 - 1840	1430 - 1450
Young's Modulus	GPa	72 - 85	71 - 110	225 - 245	62 - 80
Compressive strength	MPa	4000 - 5000		4900 - 5000	200 - 300
Tensile strength	MPa	1950 - 2050	1430 - 4900	4500 - 4800	2900 - 3600
Flexural strength	MPa	3300 - 3450	1430 - 4900	4500 - 4800	2500 - 3000
Shear modulus	GPa	30 - 36	31,3 - 40,7	100 - 110	1 - 1,3
Elongation at break	%	2,6 - 2,8	3,1 - 3,3	2 - 2,2	2,5 - 4,4
Price	%	100,00	102,46	1202,19	1333,33

Table 0.1 Different fibres and their properties

This table shows that E-glass and Basalt are in the same price range and that Carbon and Aramid have prices which are a decade higher. Therefore, can be concluded that these fibres are too expensive to use. The focus will be on E-glass fibre since it is a widely used fibre.

A.2 Matrices

As mentioned above, a composite structure contains a matrix for two reasons: protection of the fibre and transfer of the load to the fibres. Although the matrix is of very little importance in absorbing the forces in the fibre directions, the matrix plays an important role in absorbing the in-plane shear forces (very important for torsion) and interlaminar shear forces (very important for bending) in the laminate. Therefore, it is necessary to select a proper matrix.

In general, there can be distinguished three types of polymers (Composites handout 2014):

1. *Thermosets*: strong bonding by crosslinking between molecules. Up to a certain temperature not affected, but above the temperature the molecule breaks down. Formation of thermosets usually requires heat.
2. *Thermoplastics*: weak secondary bonding forces between the molecules. Soften when heated.
3. *Elastomers*: rubber-like material due to linking of a small number of valency bonds. More elastic properties than a simple thermoplastic.

For this project it is necessary that the bonding is strong and that the material does not deform when heat is applied. The best choice seems to be a thermoset resin as the matrix in the alternative panel, also because thermoplastic polymers can't be processed in vacuum infusion. There are several thermoset resins available, which can be seen in Table 0.2.

Table 0.2 An overview of different resins and their properties

Material		Epoxy	Vinyl ester	Polyester
Density	Kg/m ³	1150 – 1250	1150 – 1250	1150 – 1250
Young's Modulus	GPa	3,5	2,4 – 4,6	3,0 – 3,5
Tensile strength	MPa	60 – 80	45 – 85	50 – 80
Elongation at break	%	3,0 – 5,0	1,2 – 4,5	5,0
Curing shrinkage	%	< 2,0	6,0 – 8,0	5,0 – 7,0
Price	%	100	11,8	18,6

This table shows that Epoxy is the most expensive resin, but in terms of performance is better than the other two. Another important property is the curing shrinkage, which is least in an epoxy resin.

A.3 Production techniques

In order to produce qualitatively proper composite products, an appropriate production technique needs to be selected if. In general, there are two types of techniques in order to produce composite products; open mould and closed mould. An overview is provided in Figure 0.2

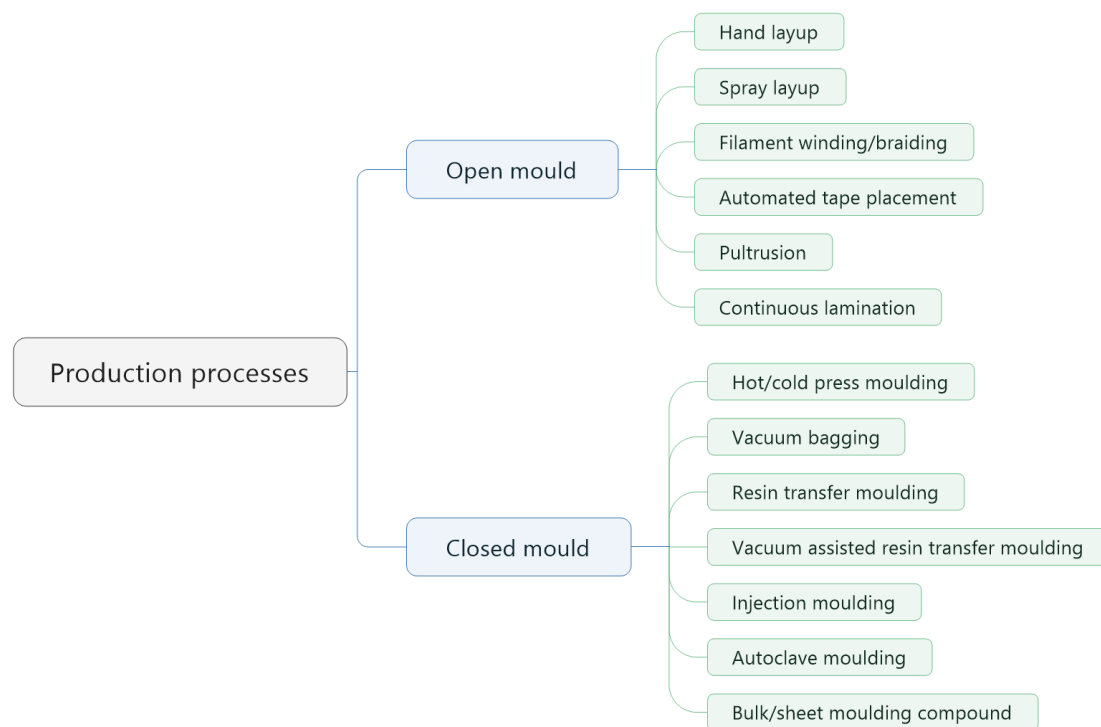


Figure 0.2: Overview of the different composite production techniques.

A.3.1 Open mould processes

A.3.1.1 Hand layup

Hand layup, also called wet layup, is one of the oldest and most frequently used techniques for making composite products. This process may be the simplest and cheapest way to produce a composite part and is suitable for large parts or parts with curvy shapes. Hand layup is more suitable for small batches, for large batches it is too labour-intensive. The hand layup technique is depicted in Figure 0.3.

In the hand layup process only one mould is used. For moulds which are used only several times, mostly metal sheet or wooden moulds are used. For complex moulds, foams like polyurethane foam can be used to shape a mould, but it often can only be used once as the foam is damaged during the first demould. If a mould should be used over 100 reuses, glass-reinforced polymer moulds are more suitable. For the ease of demoulding, the surface of the mould often is coated with release agent before the process.

The first step in the process is placing the first layer of fibres in the mould. After proper positioning the fibres, the resin is mixed and poured on top of the fibres. The resin can be spread with a brush or roller. Then pressure is build up during rolling over the laminate to remove air bubbles in the resin. This process is repeated each layer until the desired thickness of the laminate is reached.

Generally, this process is only appropriate for thermoset resins, since the viscosity needs to low in order to be able to impregnate the fibres by hand. Thermoplastic resins mostly have a high viscosity at operating temperature, so it become hard to impregnate the fibres.

Beneficial of this process is that it is relatively cheap since equipment and tooling costs are low and only one mould is required, which mostly is a simple shape and can be made of cheap materials. The disadvantage of this process is that it relatively labour-intensive, while the quality of the product is

relatively low. Another disadvantage is that longer curing time is required since it is a manual lamination process. The process has also issues concerning the health and safety, since it is an open mould process with low viscosity resins which are potentially harmful (especially with styrene based resins). (Campbell, 2010)

Hand lay-up

- 1 Mould
- 2 Release agent
- 3 Gelcoat
- 4 Layer of fleece (surface layer)
- 5 Resin
- 6 Fibre reinforcement (textile)
- 7 Brush (resin application)
- 8 Deaerating roller

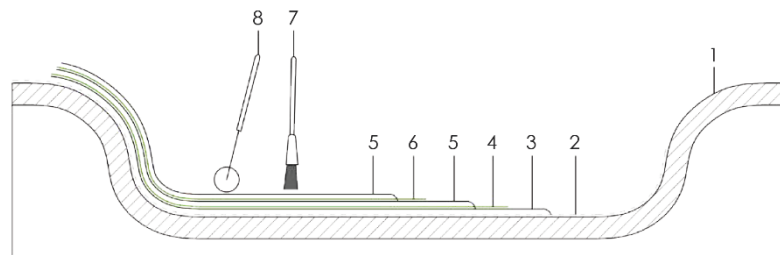


Figure 0.3: The hand lay-up technique, schematically depicted.

A.3.1.2 Spray layup

Spray layup, or spray-up, is a simple production process which is quite inexpensive and is suitable for large products with complex shapes. This process is based on spraying a mixture of resin with chopped fibres onto the mould. As with the hand layup process, spray layup also makes use of one single mould often made of wood or glass-fibre reinforced polymer in combination with a spray-gun and rollers. The spray layup technique is depicted in Figure 0.4.

The spray-gun is supplied with resin and a continuous roving which is chopped inside the spray-gun into short fibres. By using the rollers after the mixture is sprayed onto the mould, the air bubbles are pressed out to ensure a proper layer. For a multilayer panel, these steps are repeated with small breaks in between to (partly) cure the subjacent layer until the desired thickness is reached.

Like the hand layup process, this process is also only appropriate for thermoset resins, as the resin needs to be low viscous in order to be sprayable.

The advantage of this process is that it is less labour-intensive than hand layup and that it is suitable for a high surface-area to thickness ratio.

The (major) disadvantage is that the products consist of chopped fibres instead of continuous fibres, which comes at the expense of performance in terms of strength and stiffness. Another disadvantage is that the products produced by spray layup tend to be much heavier, due to the high resin-fibre ratio. The process has also, like hand layup, issues concerning the health and safety, since it is an open mould process with low viscosity resins which are potentially harmful (especially with styrene based resins). (Campbell, 2010)

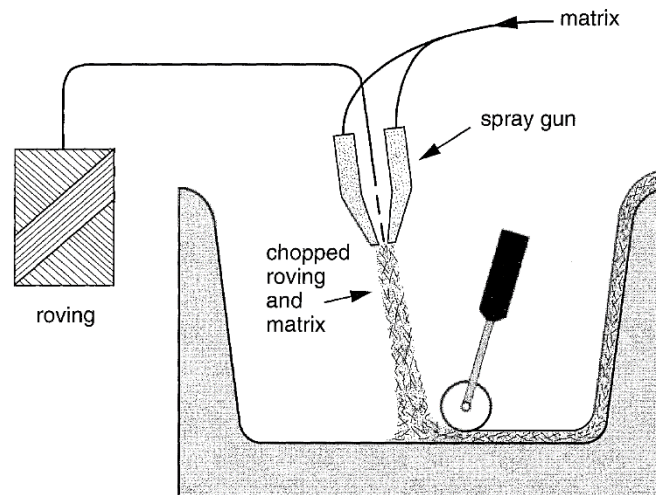


Figure 0.4: Spray layup technique, schematically depicted.

A.3.1.3 Filament winding/braiding

Filament winding, often also called wrapping, is a production process in which continuous rovings are wound (or braided in filament braiding) around a rotating mandrel. The rovings used in this process can be prepreps (pre-impregnated fibres) or dry fibres which get impregnated during/after the process. When the impregnation of the fibres is done 'in-line', the fibres pass through a bath of resin (often epoxy or polyester) after which they are wound around the mandrel shown in Figure 0.5.

The mandrel is, depending on the geometry and the batch size of the product, made of aluminium, steel or plaster and has a non-complex conical, round or cylindrical shape. The shape of the mandrel cannot be complex for the sake of the removal of the mandrel out of the product after curing. Although the mandrel has limitations in terms of shape, the size can be very large.

Due to the fact that the machine used in filament winding is able to vary the resin content, density, winding angle, winding tension in separate layers, thickness and direction of strength of the composite, this process can produce high quality products. Because of the high fibre-resin ratio, the products are well-quality products. The process uses continuous fibres and preferred directions, which also improves the performance.

The initial costs of this process are relatively high, since the purchase of a winding machine and a mandrel are expensive. The material costs for one single products are rather low, which means that the costs are normal if the batch size is high. (Campbell, 2010)

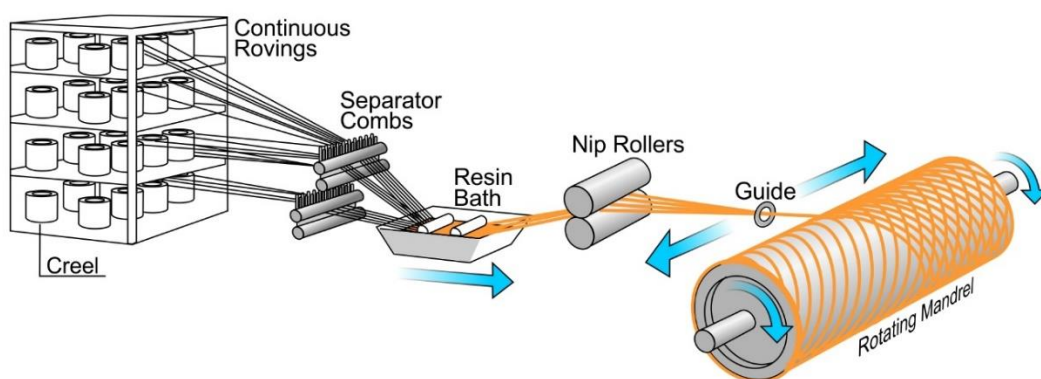


Figure 0.5: Filament winding production technique.

A.3.1.4 Automated tape placement

Automated tape placement, or automated tow placement, is an open mould process which doesn't require an autoclave for curing the laminate, shown in Figure 0.6. This process is based on the placement of layers of preimpregnated fibres (prepregs) in the form of tape. This tape is made of unidirectional fibres, impregnated with a resin, which usually is a partly cured epoxy resin. In order to avoid complete curing, the prepreg fibres are stored in cool conditions.

In this process, the prepreg tape is deposited by the tape-laying head of the machine and carried over the surface by an NC multi-axis machine. Due to the heat which is put into the placed tape, the tape starts to consolidate and forms a strong fibre reinforced surface.

The quality of products produced by ATP is excellent, because it is a highly accurate process and the repeatability is good. The roller exerts pressure in a uniform way during the layup of the laminate which ensures less air bubbles in the laminate and a compact laminate and therefore a high quality product. The fibres direction can easily be adjusted by the tape-laying head which enables multiple fibre orientations inside a product. This process allows a wide variation in size, fibre orientation and size.

The cost for this process are high, since the initial costs of the machinery are very high and the production rates are low because it is a slow process. However, when comparing it to other process which have high labour-intensity, it can save up to 86% of labour costs. It is an inefficient process for small, complex products with low requirements. It is not possible to produce hollow cylindrical or highly curved parts (curvature radii smaller than the radius of the laying head). This process is rather suitable for large scale production of simple to medium-complex parts with very high requirements. Like other open mould processes, it can be harmful since toxic gasses are released during curing of the laminate. (Campbell, 2010)

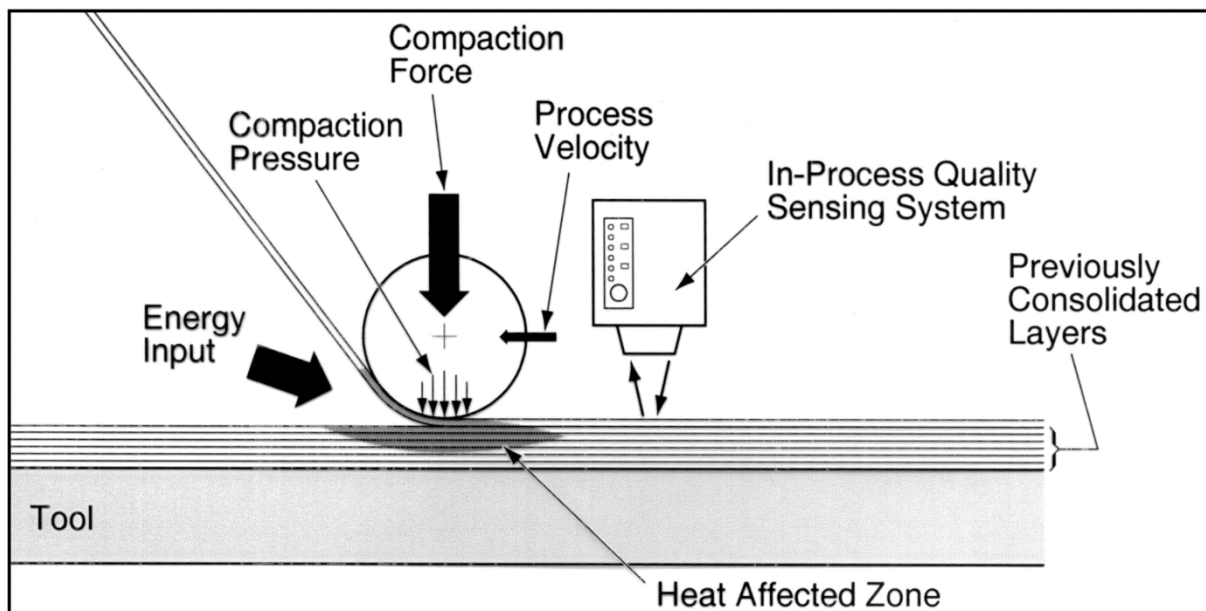


Figure 0.6: Automated tape placement production technique.

A.3.1.5 Pultrusion

Pultrusion is a production process which is continuous and is widely used for producing consistent cross-sectional composite profiles. The dry fibres pass through a bath of resin after which it is formed in a forming die as depicted in Figure 0.7. Hereafter the impregnated and formed fibres pass through an oven (which starts right before the forming dies) in which the profile is cured into a rigid composite

profile. Then the profiles are cut by a special cutting device to obtain profiles of desired lengths. The profiles pultruded in this process have constant thin walls. Common extrusion profiles are tubes, hollow rectangles, channels, I-beams and rods. This process also allows the production of profiles with a core material inside (wood, wire, foam).

The most common materials in this process are thermosetting matrices (polyester, epoxy) and glass fibres (and sometimes also carbon or aramid fibres) with a fibre volume fraction of 60-75%. (Knippers, Cremers, Gabler & Lienhard, 2011).

The operation speed in this process is highly depended on the thickness, the viscosity and the curing of the resin. The orientation of the fibres is of great importance for the mechanical properties of the profiles. Often, unidirectional fibres are put in the length direction of the profile, which ensures good properties in that direction, but poor properties in the transverse directions.

The labour-intensity of this product is low, since it is a highly automated process. The initial costs are rather high, since the machine is relatively expensive. Therefore, the batch size needs to be high (over 1000 production meters) to be feasible. (Campbell, 2010)

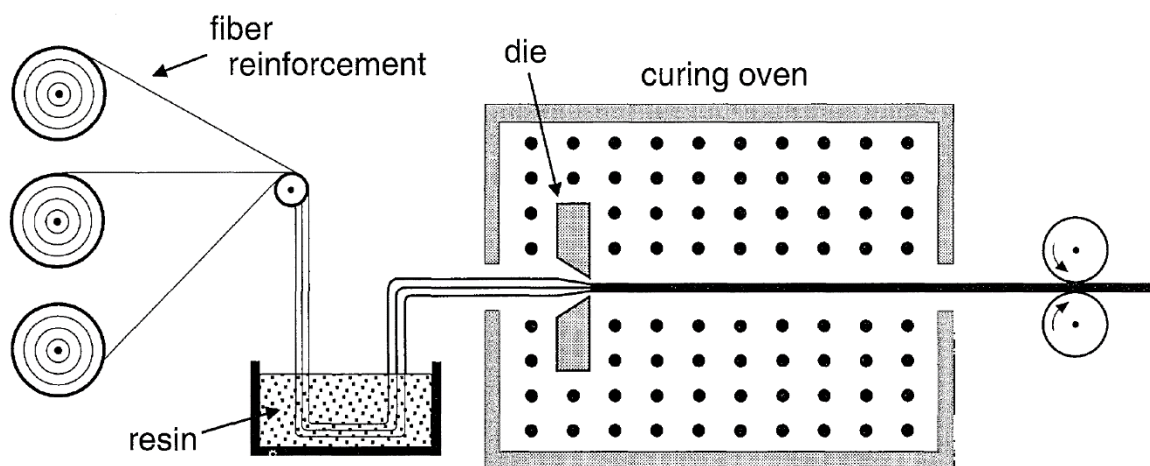


Figure 0.7: Pultrusion production technique.

A.3.1.6 Continuous lamination

Continuous lamination is a process which doesn't make use of single fibre rovings, but fibre mats of fabrics instead. The fibres are, like in pultrusion, pulled through a bath of (a thermosetting) resin and then pulled through an oven in order to cure. Then the continuous plate is cut into separate plates of desired lengths. This process is limited to single sheets with limited dimensions. (Campbell, 2010)

A.3.2 Closed mould processes

A.3.2.1 Hot/cold press moulding

Cold press moulding is a moulding process which is done under low pressure ($< 0,5$ MPa) without heating the moulds. The exothermic reaction ensures the polymerization of the resin and is also sufficient for keeping the moulds at a certain temperature around 70°C in a continuous process. The moulds need to be coated with a release coating. The fibres and the matrix, mostly a prepreg, are put in the mould and then pressed together. The time to consolidate the product is dependent on the resin and the temperature. This production process is efficient with medium quantities (4-12 products/hour)

and less expensive than hot press moulding, because of the inexpensive tools and lightweight hydraulic press. The productivity is however lower than hot press moulding. (Campbell, 2010)

Hot press moulding is a moulding process which is done with pressure varying between 0,5 to 15 MPa with, as the name already suggests, heated moulds controlled by hydraulic presses. As with cold press moulding, the mould needs to be coated with a release coating. The polymerization time depends on the resin type and the thickness of the laminate. The moulds are opened, the fibres and matrix (mostly prepregs) are put in and the mould closes with accurate speed control. After polymerization the moulds are opened again and the products are consolidated. The production process is efficient for high production volumes (15-30 products/hour) of small to medium size with good mechanical properties. The costs for hot press moulding are high (Campbell, 2010). This process is depicted in Figure 0.8.

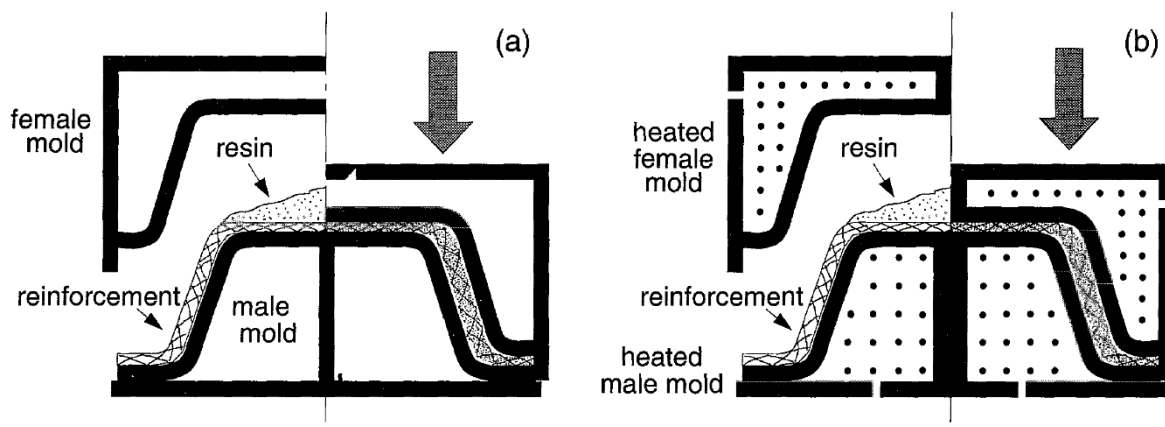


Figure 0.8: Hot/cold press moulding production process.

A.3.2.2 Vacuum bagging

Vacuum bagging, or pressure bagging, basically is done with prepregs or is often an addition to the hand layup process or the spray layup process, which are described above in sections A.3.1.1 and A.3.1.2. The addition is that pressure is applied in order to 'press' the resin into the laminate and therefore improve the consolidation as shown in Figure 0.9.

The laminate, fibres impregnated with the resin, is placed in the mould and then sealed with an airtight bag. The difference between pressure bagging and vacuum bagging is the first technique makes use of pressure which presses upon the laminate while the latter makes use of a vacuum inside the bag which gives a pressure on the laminate. With these techniques large products can be produced.

Both techniques require only one mould, so the initial price is low. However, these techniques require operators with special training which makes it a bit more expensive. Overall it is a reasonably priced process. (Campbell, 2010)

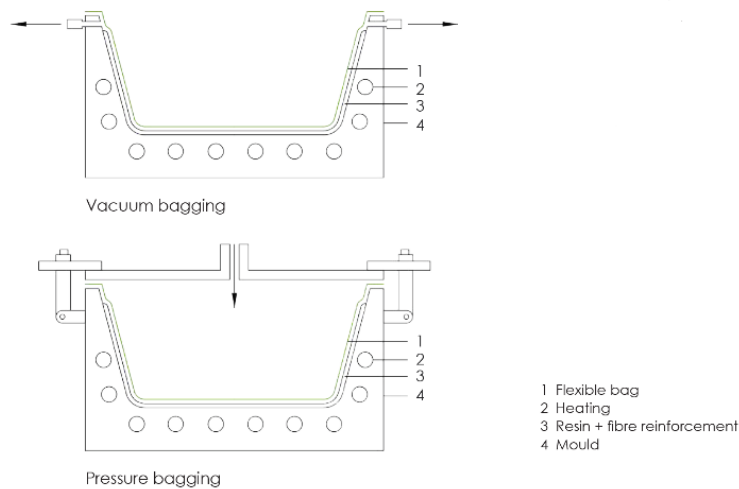


Figure 0.9: Vacuum bagging production technique.

A.3.2.3 Resin transfer moulding

Resin transfer moulding (RTM) is a technique in which the dry fibres are mixed with the resin inside a closed mould. This process makes use of two moulds which have a cavity in the shape of the product and is usually made of steel or GRP. This process is suitable for a wide range of products from complex, high performance products to simple, low performance products and from large to small in size.

The dry laminate is placed in the first mould in form of dry fibre mats together with release film and breather. The second mould is pressed on the first and under low pressure a low viscous resin (polyester, vinyl ester or epoxy) is injected into the cavity between the two moulds. When the matrix is fully impregnated by the resin, the resin cures at curing temperature. Because of the closed mould, toxic gasses like styrene cannot become harmful as they are reduced exposed to the operator. Beside the health of the operator, the closed mould is also beneficial in the surface quality of the product. Since both sides of the product are in contact with a mould, both sides have a smooth surface. This production process is depicted in Figure 0.10.

The initial costs for this process are high, since the purchase of such a machine are high and the relative costs per product are low. Therefore, the process is only efficient for a big batch size. (Gkaidatzis, 2014)

MAIN STEPS OF RTM PROCESS

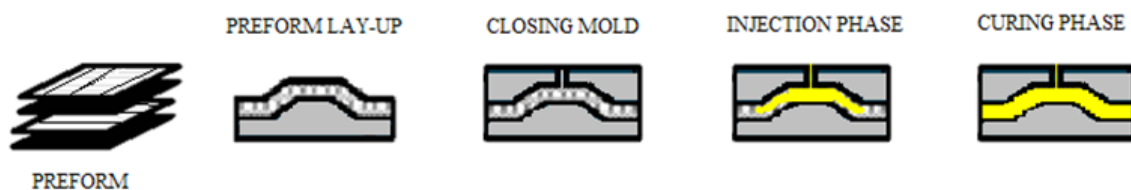


Figure 0.10: RTM process, schematically depicted.

A.3.2.4 Vacuum assisted resin transfer moulding

A production process similar to Resin Transfer Moulding is Vacuum Assisted Resin Transfer Moulding (VARTM), or sometimes also called Vacuum Assisted Resin Injection (VARI) or Vacuum Infusion is shown in Figure 0.11. The closed mould process is similar to RTM, the only difference is that the top

mould is replaced by a vacuum bag (as with the vacuum bagging technique). The pressure under which the resin is injected is not created by an injection system, but by the vacuum instead.

As with RTM a dry laminate is placed in the bottom mould in form of dry fabrics/fibre mats together with the release film and breather. Then the mould is sealed with a vacuum bag until it is airtight. The resin is distributed over the dry laminate and cured on the curing temperature.

This process is suitable for small batch sizes for its low initial costs. However, for this process, the operator needs special training to ensure a proper product. The quality of the products produced by this process is very good. Due to the use of only one mould, the surface finish is only good on one side of the product. (Gkaidatzis, 2014)

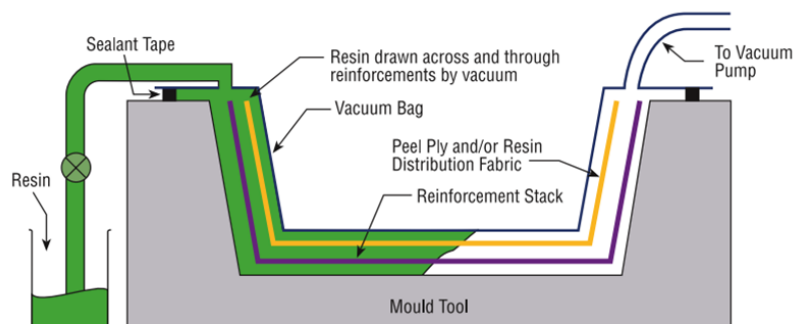


Figure 0.11: VARTM production process.

A.3.2.5 Injection moulding

Injection moulding is a process which is mostly used with non-continuous (chopped) fibres and a thermoplastic matrix. The process makes use of high pressure for the injection moulding of the thermoplastic matrix, which is also possible for thermoset resins. The matrix is fluidized and extruded by a screw (the Archimedes screw) and then injected into the heated mould under high pressure (Figure 0.12). Due to the heat of the mould, polymerization starts to occur and the product starts to consolidate.

The products produced with this technique are usually called reinforced plastics instead of composites. The Young's modulus and the strength are 2-4 times higher than the Young's modulus and strength of the resin itself.

This production process is suitable for (very) large batch sizes of small to medium products. Due to the high initial costs of the moulds and machines, the costs of this process is rather high and therefore only efficient with large batch sizes. (Gkaidatzis, 2014)

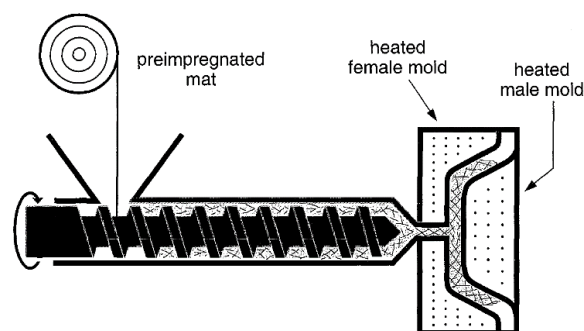


Figure 0.12: Injection moulding process.

A.3.2.6 Autoclave moulding

Autoclave moulding is a production technique which is similar to vacuum bagging, but it differs in that the autoclave is used for curing the composite. The autoclave is a machine, which basically is a large pressurized oven, shown in Figure 0.13. The autoclave uses high pressure and high temperatures together with a vacuum in between the mould and the vacuum bag. The machine can go up to 400 °C in temperature and up to 0,7 MPa in pressure.

As with vacuum bagging, the layup is done in the mould, impregnated with a resin and covered with release film, breather and a vacuum bag. Then the mould is placed in the autoclave, which usually reaches 0,55 MPa, and heated to a certain resin dependent temperature. The vacuum and the pressure ensure small ratios of air bubbles and voids. Due to the external pressure, an evenly distributed pressure can be achieved which is better than vacuum bagging only. This leads to a better performance of the thermoset composite products. Therefore, this process is used for the production of very high performance products.

Due to the high initial costs of the machine, this process is a relatively high cost process. It is also very time consuming and labour intensive due to the long curing time of composites. Because of the high costs of this process, it is only used for specialized products which require high performance. (Gkaidatzis, 2014)

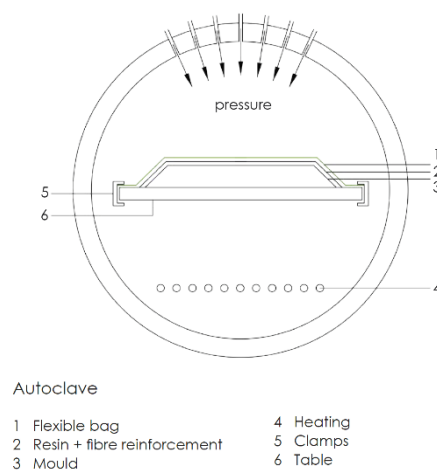


Figure 0.13: Autoclave moulding process.

A.3.2.7 Bulk/sheet moulding compound

Bulk Moulding Compound (BMC) is a production method which makes use of premixed materials and a compression mould. The mould is heated and the compound is compressed with pressures varying between 0,5 MPa to 15 MPa.

The compound is placed in the cavity of the mould and pressed into the desired shape. The mould temperature depends on the matrix but is mostly in the range of 140 °C to 160 °C. The resins used in this process are occasionally thermoplastic like PP or PA6, but usually thermoset resins such as polyester, vinyl ester or epoxy. The fibres used in this process usually are short chopped fibres of glass or carbon in random orientation. Due to the short, randomly distributed fibres, the products produced with this process have low mechanical performance.

Sheet Moulding Compound (SMC) is a production process similar to BMC, with the difference that the mixed compound, resin mixed with chopped fibres, is inserted in form of a sheet. The pre-cut sheet is

placed in the mould, which presses the sheet with a pressure between 3 MPa and 7 MPa and a mould temperature between 130 °C and 160 °C in order to cure the product. (Gkaidatzis, 2014) The production processes are schematically depicted in Figure 0.14.

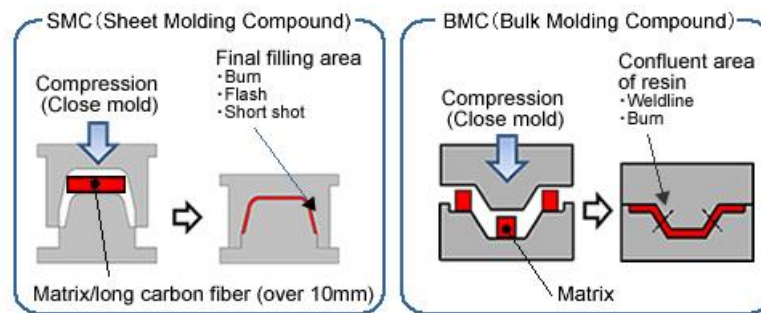
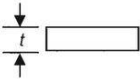
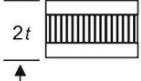
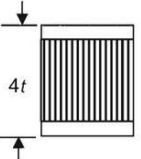


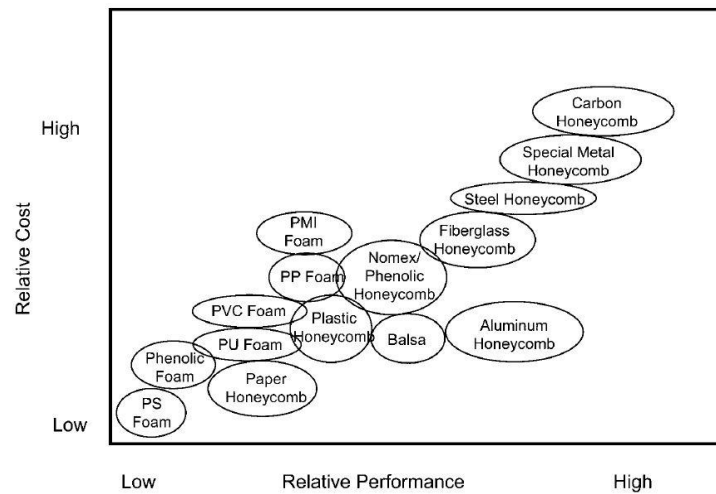
Figure 0.14: SMC and BMC production processes.

A.4 Sandwich constructions

Sandwich structures are used extensively in aerospace, automotive and commercial industries, as sandwich constructions are extremely light in weight and at the same time very strong and stiff, which means a very high strength-to-weight ratio. Sandwich constructions basically consist of two facings with a core in between. The facings of the sandwich panel, also called skins, are made of fibre reinforced polymer and have the ability to carry the bending loads on the panel while the core, usually made of a honeycomb construction or a wood or foam type, carries the shearing loads and maintains the distance between the two face sheets. Typically, sandwich constructions have thin skins with a thicker core. The idea of a sandwich construction is basically the idea of an I-beam. Beneficial of sandwich constructions, notably honeycomb sandwich constructions, is that they are extremely structural sufficient, explicitly in stiffness-critical applications. In Figure 0.15, it can be seen that the stiffness extremely increases with an increasing thickness, while the weight only increases a bit. Obviously this extreme relation doesn't account for all types of cores, but with the appropriate choice of materials for skins and core, constructions with high ratios of stiffness-to-weight can be achieved. Usually sandwich constructions are used for their insulation, structural or energy absorption properties. In Figure 0.16 overall relative performance is plotted against price. (Campbell, 2010)

In order to bond the faces together with the skin, several bonding methods can be used. It is possible to adhesively bond the two skins on the core (gluing); the skins and the core are produced and prepared separately and bonded together afterwards. A different option is in-situ bonding, like in pultrusion; the skins are impregnated and, with a core in between, pressed together in a die to form a solid sandwich panel. Another way to ensure the bonding between skins and core is by placing the dry laminates, with the core in between, in a mould and run resin through it by RTM or vacuum infusion. In this way the skins and the core bond together very well.

	Solid Material	Sandwich Construction	Thicker Sandwich
			
Stiffness	1.0	7.0	37.0
Flexural Strength	1.0	3.5	9.2
Weight	1.0	1.03	1.06



A.5 Cores

As mentioned in the previous chapter, the core of a sandwich construction is of main importance to absorb the shear stresses and maintain the distance between the two skins. Many different cores are available for commercial use; some common used examples are (Figure 0.17):

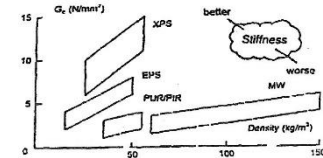
- Balsa
- Cork
- Synthetic polymer foams
- Honeycombs
- Fibre reinforced foams

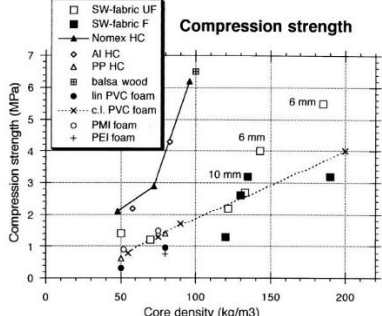
The different core materials have all different characteristics and therefore different advantages. Most honeycomb constructions are very light and very strong, but are not convenient in a continuous or closed mould process. Polymer foams are usually very light and have many different sorts and therefore many diverse properties. Balsa and cork are natural products and therefore compostable after use.



Appendix B: Literature table

Literature	Subject	Conclusions	Values
<i>Impact resistance of marine sandwich composites</i> T. Castilho, L.S. Sutherland & C. Guedes Soares	Comparing different cores at impact and bending.	Cork is better than PVC and balsa at absorbing impact energy, but has a low first peak load. PVC has higher peak load than cork, but balsa has the highest peak load.	First peak occurs at 8103 N for PVC, at 5398 N for Cork NL10, at 7654 N for Cork NL20 and at 8688 N for Balsa.
<i>The influence of core properties on the perforation resistance of sandwich structures – An experimental study.</i> M.Z. Hassan, W.J. Cantwell	Impact tests on sandwich panels of E-glass with epoxy matrix with a core of; Linear PVC Foam versus Cross-linked PVC Foam versus PET Foam	Cross-linked PVC is the best solution for the core, it has the highest perforation force.	Cross-linked PVC has a first peak in force at 972 N, linear PVC has a first peak at 760 N and PET has a first peak at 751 N.
<i>On Mode I Fatigue Crack Growth in Foam Core Materials for Sandwich Constructions</i> A. Shipsha, M. Burman and D. Zenkert	Fracture toughness and stress intensity threshold for H100 (PVC) and WF51 (PMI) sandwich panels.	PVC has a higher fracture toughness and stress intensity threshold than PMI.	The fracture toughness of PVC was 0.220 MPa $\sqrt{\text{m}}$ and the fracture toughness of PMI was 0.072 MPa $\sqrt{\text{m}}$
<i>Experimental and numerical study on the low-velocity impact behaviour of foam-core sandwich panels</i> J. Wang, A.M. Waas, H. Wang	Impact tests on sandwich panels of carbon-epoxy with a core of 10 mm or 25 mm PUR foam.	'The absorbed energy/impact energy ratio and contact duration decrease with the face-sheet thickness, while the peak load increases.' 'The impact response and damage state are independent of the foam core thickness.'	The differences in first peak between 10 mm and 25 mm foam are respectively 3.91-3.84, 5.63-6.03 and 6.27-6.72.
<i>Evaluation of durability and strength of stitched foam-cored sandwich structures</i> Jae Hoon Kim, Young Shin Lee, Byoung Jun Park, Duck Hoi Kim	Difference between a stitched and a non-stitched foam in a sandwich panel of E-glass-epoxy-PU composite sandwich panel made by hot-pressing.	'The bending strength of the stitched specimen is improved by 50% compared with the non-stitched specimen, and the stiffened specimen is over 10 times stronger than the non-stitched.' 'After fatigue loading of 10^6 cycles, the bending strengths of all specimens decrease compared with those in the static test. The reduction of bending strength of foam-cored sandwich specimens is caused by the stiffness degradation of foam due to the aging of polyurethane foam during fatigue cycles.'	The bending peak force of non-stitched foam is 1 kN while the stitched foam has a bending peak force of 1.5 kN.
<i>Core Material Effect on Impact Behaviour of Glass Fibre Sandwich Composites</i> O. Özdemir	Impact tests in 0 mm, 5 mm, 10 mm and 15 mm PET and PVC sandwich panels.	The shear strength and compressive strength value of core materials play a significant role on impact behaviour of specimens especially having small core thickness in the same densities. But, in the thicker core thickness, impact behaviour of specimens is little affected from those values. 5 mm core thickness is most suitable for the highest impact force.	5 mm core thickness is the optimal thickness concerning impact peak load. PET core has a first peak around 4 kN, Cross-linked PVC core has a first peak load around 4 kN and the Linear PVC core has a first peak load slightly below 4 kN.

Literature	Subject	Conclusions
<i>Energy Absorption of Nano-Reinforced and Sandwich Composites in Ballistic and Low-Velocity Punch-Shear.</i> Brahmananda Pramanik, P. Raju Mantena	Impact and ballistic tests on sandwich panels; Vinylester with e-glass/Tycor, e-glass/PVC, e-glass/Balsa, e-glass/Eco Core	Eco Core performed best in Energy absorption but was poor in ballistic tests. Tycor core absorbed most energy during ballistic tests. Low velocity punch shear tests show a 10% improvement in impact energy absorption when 2.5 wt. pct. Graphite platelets are added to the vinylester.
<i>Sandwich structures.</i> Jack R Vinson	Sandwich constructions	 Fig 3. Shear stiffness of typical core materials as a function of density
<i>The influence of core properties on the perforation resistance of sandwich structures – An experimental study.</i> M.Z. Hassan, W.J. Cantwell	Impact tests on sandwich panels of E-glass with epoxy matrix with a core of; Linear PVC Foam versus Crosslinked PVC Foam versus PET Foam	Crosslinked PVC is the best solution for the core, it has the highest perforation force.
<i>Properties and Applications of Sandwich Panels Based on PET Foams.</i> M. Xanthos, R. Davalikar, V. Tan, S.K. Dey and U. Yilmazer	Three point bending of sandwich panels of 25mm thickness of foam cores (PET, PVC, PIC, PS) versus commercial available wood panel cores (plywood, flakeboard, oriented strand, fibre board, particle board)	'Sandwich laminates from high-density PET foams (virgin and post-consumer) have bending properties close to those of wood panels, superior water resistance and good thermal stability. Lower density sandwich laminates are competitive to alternate rigid foam products in terms of their specific modulus and strength.'
<i>Foam core sandwich panels with interface disbands</i> L. Falk	Fracture toughness of (Divinycell) PVC foam versus (Rohacell) PMI foam.	The fracture toughness of PVC was higher than the fracture toughness of PMI foam.
<i>Compression-after-Impact Strength of Sandwich Panels with Core Crushing Damage</i> A. Shipsha and D. Zenkert	Compression strength of a glass-vinylester-Rohacell (PMI) sandwich panel after impact damage.	'Experiments showed that the impact damage reduces the compressive strength of the panels, albeit this reduction was not so significant.'
<i>On Mode I Fatigue Crack Growth in Foam Core Materials for Sandwich Constructions</i> A. Shipsha, M. Burman and D. Zenkert	Fracture toughness and stress intensity threshold for H100 (PVC) and WF51 (PMI) sandwich panels.	PVC has a higher fracture toughness and stress intensity threshold than PMI.
<i>Experimental investigation of interfacial fracture behaviour in foam core sandwich beams with visco-elastic adhesive interface</i> Wang Can, Chen Hao-ran, Lei Zhen-kun	Interfacial toughness of a sandwich panel of E-glass-Polyester-PMI, enhanced (with an interfacial layer: chopped glass-fibre mat) and unenhanced.	'The interfacial enhancement method using chopped glass fibre mats for sandwich beams is efficient. Robust interfacial load capacity and improved toughness have been obtained by the method, which means that the enhanced structure is more damage tolerant.' Up to a 100% increment of toughness at a cost of up to 6% weight increment.
<i>Experimental study of the indentation of sandwich panels with carbon fibre-reinforced polymer face sheets and polymeric foam core</i> E.A. Flores-Johnson, Q.M. Li	Indentation of different densities of PMI foam sandwich constructions	'The indentation resistance of the sandwich is mainly contributed from the indentation resistance of the core material.'
<i>Experimental and numerical study on the low-velocity impact behaviour of foam-core sandwich panels</i> J. Wang, A.M. Waas, H. Wang	Impact tests on sandwich panels of carbon-epoxy with a core of 10mm or 25mm PUR foam.	'The absorbed energy/impact energy ratio and contact duration decrease with the face-sheet thickness, while the peak load increases.' 'The impact response and damage state are independent of the foam core thickness.'
<i>Evaluation of durability and strength of stitched foam-cored sandwich structures</i> Jae Hoon Kim, Young Shin Lee, Byoung Jun Park, Duck Hoi Kim	Difference between a stitched and a non-stitched foam in a sandwich panel of E-glass-epoxy-PU composite sandwich panel made by hotpressing.	'The bending strength of the stitched specimen is improved by 50% compared with the non-stitched specimen, and the stiffened specimen is over 10 times stronger than the non-stitched.' 'After fatigue loading of 10 ⁶ cycles, the bending strengths of all specimens decrease compared with those in the static test. The reduction of bending strength of foam-cored sandwich specimens is caused by the stiffness degradation of foam due to the aging of polyurethane foam during fatigue cycles.'

<p><i>Failure Modes of Composite Sandwich Beams</i> I.M. Daniel, E.E. Gdoutos, K.A. Wang, J.L. Abot</p>	<p>Failure modes of sandwich composite beams with a PVC foam.</p>	<p>Compressive face sheet failure is likely under pure bending conditions or when the shear load is low enough and the core stiff and strong enough to avoid core failure. A maximum stress failure criterion for the composite face material is sufficient to predict this type of failure. Face sheet debonding is not very common in sandwich beams with foam cores, unless there are initial fabrication defects. It is more likely under impact loading. Indentation failure is a serious problem whenever there is any load concentration on foam-core sandwich panels. It results from local (multiaxial) compressive failure of the core under the load and is followed by local face sheet bending to failure of the face sheet.</p>
<p><i>Dynamic mechanical analyses and flexural fatigue of PVC foams</i> Krishnan Kanny, Hassan Mahfuz, Leif A. Carlsson, Tonnia Thomas, Shaik Jeelani</p> <p><i>Flexural fatigue characteristics of sandwich structures at different loading frequencies</i> K. Kanny and H. Mahfuz</p>	<p>Comparison between sandwich panels with different PVC foam densities (closed cell, lightly crosslinked); 75, 130, 260 and 300 kg/m³, 12 mm thick.</p>	<p>The higher the density of the foam, the higher the strength and the stiffness of the sandwich panel, however an inverse relationship is observed when the relative fatigue strength increases. Cracks mostly occur first in the tension side of the beam.</p>
<p><i>Mechanical properties of composite panels based on woven sandwich-fabric preforms</i> A.W. van Vuure, J.A. Ivens, I. Verpoest</p>	<p>The investigation of a 3D stitched sandwich panel. Comparison with different types of cores.</p>	 <p>Compression strength</p> <p>Core density (kg/m³)</p> <p>6 mm</p> <p>10 mm</p>
<p><i>Tensile and fracture behaviour of polymer foams</i> Md. E. Kabir, M.C. Saha, S. Jeelani</p>	<p>Comparison of PUR vs PVC foam as a sandwich core.</p>	<p>(Crosslinked) PVC is better than PUR. The tensile and quasi-static fracture behaviours are found to be fairly linear up to the failure load. Both the tensile strength and the modulus are found to be strongly dependent on the foam density. The fracture toughness is also found to be strongly dependent on the foam density as well as the microstructure.</p>
<p><i>Material selection in sandwich beam construction</i> Craig A. Steeves, Norman A. Fleck</p>	<p>Failure modes of sandwich beams.</p>	<p>Four failure modes which regularly arise in sandwich beams in three-point bending are core shear, face yield or microbuckling, ductile indentation, and elastic indentation.</p>
<p><i>Impact resistance of marine sandwich composites</i> T. Castilho, L.S. Sutherland & C. Guedes Soares</p>	<p>Comparing different cores at impact and bending.</p>	<p>Cork is better at absorbing impact energy. Balsa has higher stiffness.</p>

Appendix C: Materials

Resin

The resin used in the current panel is an epoxy resin of Airstone:

- Airstone 780E/785H

This type makes use of 780E resin of Airstone with the 785H hardener mixed at a ration 100:31 (resin:hardener). After mixing both components a chemical reaction occurs which ensures crosslinking in the mixture (Figure 0.1). After hardening the resin has a density of 1102 kg/m³. The current panel, with six layers of quadraxial fibres and 25.4 mm balsa in between, contains about 4.0 – 4.5 kg/m² of epoxy resin.

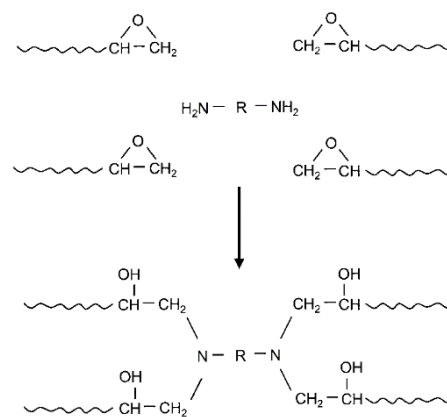


Figure 0.1: The chemical reaction in epoxy resin during curing.

Core materials

SAN foam core

For the third core use is made of (Figure 0.2):

- Gurit Corecell M80 closed cell SAN foam.

SAN (Styrene acrylonitrile) foam is a tough, closed cell polymer foam made of SAN material. Before impregnation the foam has a density of 85 kg/m³. The foam panel used in the experiments has a thickness of 25.4 mm which results in 1.65 kg/m² before impregnation.



Figure 0.2: Panels of SAN foam, used as a core material in composite sandwich panels.

PET foam core

For the second core use is made of (Figure 0.3):

- Airex T90.60 closed cell PET foam.

PET (Polyethylene terephthalate) foam is a thermoplastic, closed cell, recyclable polymer foam made of PET material. Before impregnation the foam has a density of 65 kg/m^3 . The foam panel used in the experiments has a thickness of 25.4 mm which results in 1.65 kg/m^2 before impregnation.

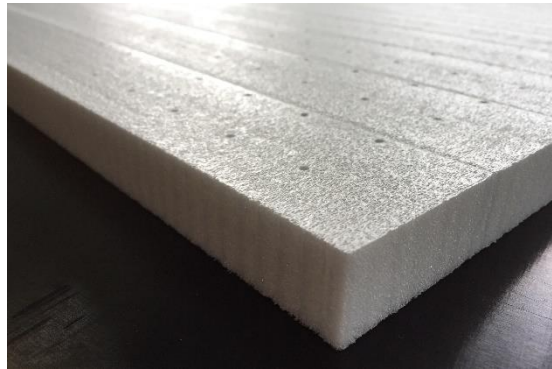


Figure 0.3: A panel of PET foam, used as a core in composite sandwich panels.

Balsa wood core

As the first core material use is made of (Figure 0.4):

- Baltek Sb.100 end grain balsa.

This core is an end grain balsa core which means the grains in the balsa core are in vertical direction. This type of balsa has, before impregnation, a density of 155 kg/m^3 . The currently used balsa has a thickness of 25.4 mm which results in 3.75 kg/m^2 before infusion of the resin.

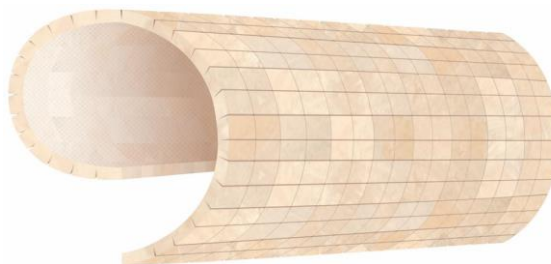


Figure 0.4: A mat of balsa wood, used as a core in composite sandwich panels

Production process

The current panel is produced by vacuum infusion as can be seen in Figure 0.5. The laminate is build up on top of the mould. First the laminate layup, as described above, is placed onto the mould. Thereafter, peel ply is placed on top of the laminate, which is peeled off after infusion in order to ensure an evenly distributed rough surface finish. On top of that a release film is placed in order to be able to easily remove the top layer, which is the (green) mesh. The mesh ensures the equal distribution

of the resin during the infusion. Then the runner, which makes it possible for the resin to be distributed over the complete width of the panel, is placed on top and the breather, which distributes the vacuum inside the bag and ensures the resin to flow towards the pump, is placed around the laminate. A vacuum hose is placed on the breather and a hose for the resin supply are positioned and then the complete package is sealed with a vacuum bag.

After leaving the laminate on vacuum for an hour, the resin is infused under a temperature of 40 °C. When the entire laminate is saturated with resin, the laminate gets reduced and heated up to 80 °C. The mould is heated up to 80 °C for 8 hours to ensure proper curing of the laminate.



Figure 0.5: The vacuum infusion process; in the picture it can be seen that the laminate is under vacuum and ready for the infusion of the resin.

Appendix D: Datasheets

SAN foam:

MECHANICAL PERFORMANCE

Type	Test Method	Units	M60		M80		M100		M130		M200	
Short Edge Marking	-	-	Yellow	Green	Yellow	Blue	Yellow	Black	Yellow	Pale Brown	Yellow	Brown
Nominal Sheet Size	-	mm	1285 x 2605		1220 x 2440		1130 x 2275		1015 x 2045		915 x 1830	
		inches	50.5 x 102.5		48 x 96		44.5 x 89.5		40 x 80.5		36 x 72	
Nominal Density		kg/m ³	65		85		107.5		140		200	
		lb/ft ³	4.1		5.3		6.7		8.7		12.5	
Density Range		kg/m ³	61-69		81-89		100-115		130-150		185-215	
		lb/ft ³	3.8-4.3		5.1-5.6		6.2-7.2		8.1-9.4		11.5-13.4	
Compressive Strength	ASTM D1621	MPa	0.55		1.02		1.55		2.31		4.40	
		psi	80		148		225		336		638	
Compressive Modulus	ASTM D1621 – 1973	MPa	45		71		107		170		317	
		psi	6480		10340		15570		24670		45977	
	ASTM D1621 - 2004	MPa	31		52		76		111		210	
		psi	4530		7610		11080		16100		30458	
Shear Strength	ASTM C273	MPa	0.68		1.09		1.45		1.98		2.95	
		psi	98		158		211		287		428	
Shear Modulus	ASTM C273	MPa	20		29		41		59		98	
		psi	2900		4240		5920		8600		14214	
Shear Elongation at break	ASTM C273	%	53%		58%		52%		43%		20%	
Tensile strength	ASTM D1623	MPa	0.81		1.62		2.11		2.85		4.29	
		psi	118		234		306		414		622	
Tensile modulus	ASTM D1623	MPa	44		72		109		176		334	
		psi	6440		10420		15880		25510		48443	
Thermal Conductivity	ASTM C518	W/mK	0.03		0.04		0.04		0.04		0.04	
HDT	DIN 53424	°C	110		110		110		110		110	
		°F	230		230		230		230		230	

PET foam:

MECHANICAL PROPERTIES							
Typical properties for AIREX® T90		Unit (metric)	Value ¹⁾	T90.60	T90.100	T90.150	T90.210
Density	ISO 845	kg/m ³	Average <i>Typ. range</i>	65 60 - 70	110 105 - 115	145 140 - 150	210 200 - 220
Compressive strength perpendicular to the plane	ISO 844	N/mm ²	Average <i>Minimum</i>	0.80 0.7	1.4 1.2	2.2 2.0	3.5 3.2
Compressive modulus perpendicular to the plane	ISO 844	N/mm ²	Average <i>Minimum</i>	50 35	85 75	115 100	170 145
Tensile strength perpendicular to the plane	ASTM C297	N/mm ²	Average <i>Minimum</i>	1.5 1.2	2.2 1.6	2.7 2.2	3.0 2.4
Tensile modulus perpendicular to the plane	ASTM C297	N/mm ²	Average <i>Minimum</i>	85 70	120 90	170 140	225 180
Shear strength	ISO 1922	N/mm ²	Average <i>Minimum</i>	0.46 0.4	0.8 0.7	1.2 1.1	1.85 1.5
Shear modulus	ISO 1922	N/mm ²	Average <i>Minimum</i>	12 10.5	20 18	30 26	50 44
Shear elongation at break	ISO 1922	%	Average <i>Minimum</i>	25 15	10 5	8 4	5 3
Thermal conductivity at 10°C	EN 12667	W/m.K	Average	0.037	0.035	0.038	0.045
Standard sheet	Width ²⁾	mm ± 5		610	610	610	610
	Length ²⁾	mm ± 5		1220	1005	1220	1220
	Thickness	mm ± 0.5		5 to 100	5 to 100	5 to 100	5 to 100

Balsa:

Group - Shell Balsa 155kg/m ³	155Kg/m ³ Grid score sheet 25.4mm X 50.8mm						
	6.35mm	12.7mm	19.1mm	25.4mm	38.1mm		
Slit width	0.6	0.6	0.6	0.6	0.6	[mm]	Calculated
Sandwich areal density	2.35	3.76	5.15	6.56	7.78	[kg/m ²]	Calculated
Sandwich volumetric density	370	296	271	258	245	[kg/m ³]	Calculated
Core resin consumption	1.40	1.86	2.31	2.77	3.03	[kg/m ²]	Calculated
E_x			142			[MPa]	SB46-R-01-00020R04
E_y			142			[MPa]	SB46-R-01-00020R04
E_{zt}			118			[MPa]	Value Lowest in the group average
E_{zc}			385			[MPa]	Value Lowest in the group average
G_{xy}			18			[MPa]	SB46-R-01-00020R04
G_{xz} / G_{yz}			326			[MPa]	Value Lowest in the group average
ν_{xy}			0.45			[-]	SB46-R-01-00020R04
ν_{xz} / ν_{yz}			0.014			[-]	SB46-R-01-00020R04
σ_{zt}			6.5			[MPa]	Value Lowest in the group average
ϵ_{zt}			56200			[µm/m]	Value Lowest in the group average
σ_{zc}			-7.9			[MPa]	Value Lowest in the group average
ϵ_{zc}			-55833			[µm/m]	Value Lowest in the group average
τ_{xz}			2.5			[MPa]	Value Lowest in the group average
γ_{xz}			8000			[µm/m]	Value Lowest in the group average

Appendix E: Microscopic analysis

E.1 Introduction

A composite material is a material that consists of two or more constituent materials with entirely different properties. When combining these materials, a completely different material remains, with totally different properties than the individual constituents. It is frequently used in the aircraft industry and it is rising in the car industry. When composites are mentioned, often Fibre Reinforced Polymers (or FRP's) are meant, as also in this report. An FRP is a polymer which is reinforced with a fibre, like glass fibre or carbon fibre. The reason that it is commonly used is because it has several benefits with regard to the weight, strength and price.

When used in practical products like floors or sidewalls, the material can suffer some impacts during its lifespan. Necessary is that the materials do not lose too much stiffness in order to remain their function. The damage can be either visible (penetration, perforation) or invisible (delamination, debonding), but in both cases the material loses (part of) its stiffness. Important is that the loss of stiffness doesn't affect the primary function of the part and that the part is able to maintain this function.

This study is done in order to investigate the behaviour of the sandwich composite after impact, and especially the behaviour of the core and the bonding with the skins. In this study, use is made of glass/epoxy skins with three different cores; SAN foam, PET foam and Balsa wood. These sandwich panels are then impacted in an impact test and investigated under a microscope.

E.1.1 Previous work

Several studies investigated the impact behaviour in microscopic detail. Some of them are described in this section.

R. Mohammed et al. (2008) investigated low velocity impact on foam cored sandwich composites. In impact situation, R. Mohammed et al. distinguishes four failure modes; Matrix failure, Delamination, Fibre failure and Penetration which are applicable for heterogeneous and anisotropic fibre reinforced plastic (FRP) laminates. For sandwich constructions three different classifications can be distinguished; facesheet damage, core-facesheet interface damage and core damage.

Bhuiyan et al. (2009) investigated the low velocity impact response of sandwich composite structures with a nanophased foam core and biaxial braided facesheets. By doing a weight drop impact test, the sandwich construction with biaxial carbon fibre fabrics and a core of polyurethane was impacted with different impact energies. After the impact the specimens were investigated under a SEM

microscope in order to determine the zone which was affected by the impact.

J. Wang et al. (2012) investigated the low velocity impact behaviour of foam core sandwich panels. Composite sandwich panels made of plain weave carbon fibre fabrics and a polyurethane foam are used and impacted with a drop weight impact machine. After impact the damaged specimens are inspected with a Micro-CT scan in order to detect the damaged area. Thereafter, the damaged areas are investigated through microscopic images of these damaged spots. In these microscopic images the damaged fibres and the crushed core are shown.

Lin et al. (2006) studied the mechanical behaviour nanoparticle filled composites at low velocity impacts. The composite panels are impacted with a 1.5 kg tip at 2-9 m/s impact speed. Different mixtures of resin with nanoparticles were investigated and the results were investigated in a SEM microscope in order to determine the difference.

Russo et al. (2014) investigated the impact damage in composite laminates based on

waste polyolefins. Film-stacked composite laminate plates were subjected to a falling weight impact test. A SEM microscope is then

E.2 Failure of composite sandwich panels

Composite sandwich constructions have advantages in stiffness and weight over normal composite panels. However, there are more possibilities of failure, because there are more elements which can fail. According Craig A. Steeves, (2004), composite sandwich structures, during three-point bending, have four main failure mechanisms (Figure 0.1);

- Core shearing
- Microbuckling
- Indentation
- Face wrinkling

The first one, *core shearing*, is a failure of the core due to the large shear stresses in the core of sandwich construction. Since the core has worse properties than the facesheets, the core is the vulnerable point in the construction.

The second failure mechanism is *Microbuckling*. Microbuckling is also called face yielding, which occurs when the axial stresses in the facesheet exceed the limits and therefore fails. These failure types are predicted and expressed in lots of expressions, such as Tsai-Wu, Tsai-Hill, maximum stress criterion or Hashin damage criterion. The last one, *Hashin damage criterion*, is widely used in

used in order to investigate the impacted areas.

modelling software packages, because of its distinction between 4 kinds of failure; fibre compressive, fibre tension, matrix compressive and matrix tension. In this way it can be seen how and where the facesheet fails.

The third failure mechanism is *indentation*. This failure type is also called elastic indentation, in which the facesheet deforms elastically and the core yields plastically.

The last failure mechanism is *face wrinkling*, where there's a short wavelength elastic buckling of the top facesheet which is resisted by the elastic core underneath, causing the facesheet to wrinkle (Craig A. Steeves, 2004).

The failure criteria mentioned are failure criteria of sandwich constructions. Since the skin is made of a composite laminate, there is also need for failure criteria of composite laminates. In impact loading on a laminate, the most common failure mechanisms are (Mohammed, 2008);

- **Matrix cracking:** cracking of the matrix can occur parallel to the fibres due to tension, shear and/or compression.
- **Delamination:** delamination can occur due to interlaminar shear stresses.

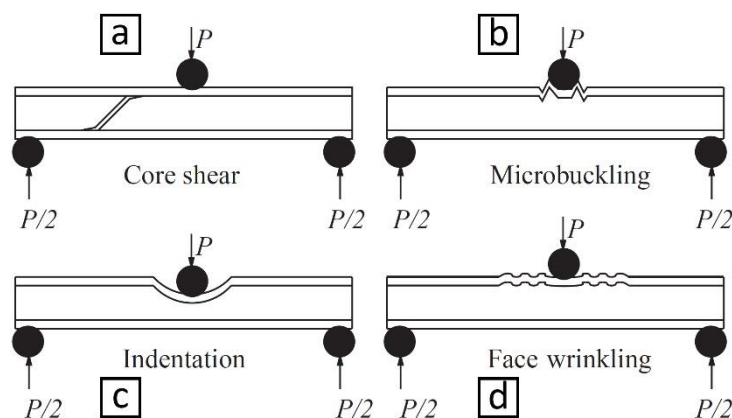


Figure 0.1: Different failure mechanisms of composite sandwich constructions. (Craig A. Steeves, 2004)

- **Fibre cracking/buckling:** fibre break-age can occur due to tension and fibre buckling can occur due to compression.
- **Penetration:** penetration occurs when the indenter completely penetrates the laminate.

E.3 Methodology

In order to be able to understand the behaviour of composite sandwich materials during impact and bending after impact, certain practical tests are done.

E.3.1 Materials

The used materials are discussed separately and the properties of all materials are summarized in Table 0.1.

E.3.1.1 Glass fibre

Use is made of a certain glass fibre fabric:

- Saertex S32EQ260-00820-01270-450000 Quadraxial-glass-fabric 822 g/m² with PES tricot-warp stitching and with [0/-45/90/+45] layup

This type of fabric is quadraxial which means it has four different fibre directions inside one single ply. In Figure 0.3, it can be seen how these plies are build up. The single fibre orientations are stitched together with a PES tricot-warp stitching. One single layer including the stitches have a weight of 822 grams per square meter.

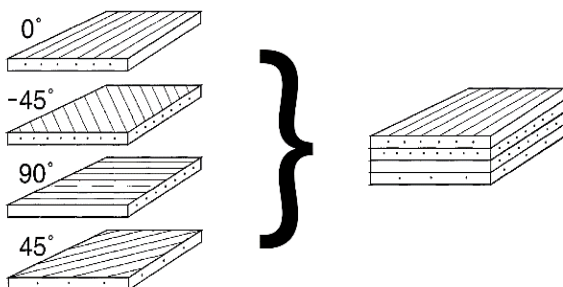


Figure 0.3: The layup of the quadrax glass fibre mat, made up of 4 single UD plies..

E.3.1.2 Epoxy resin

The resin used in the current panel is an epoxy resin of Airstone:

- Airstone 780E/785H

This type makes use of 780E resin of Airstone with the 785H hardener mixed at a ratio 100:31 (resin:hardener). After mixing both components a chemical reaction occurs which ensures crosslinking in the mixture (Figure 0.2). After hardening the resin has a density of 1102 kg/m³. The current panel, with six layers of quadraxial fibres and 25.4 mm balsa in between, contains about 4.0 – 4.5 kg/m² of epoxy resin.

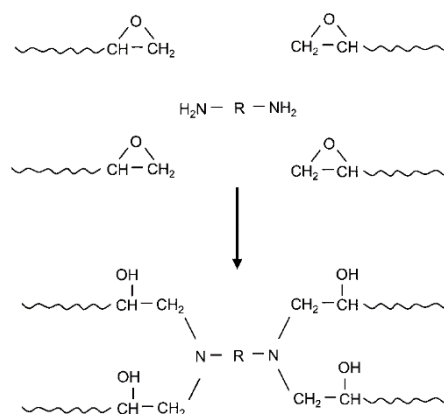


Figure 0.2: The chemical reaction in epoxy resin during curing.

E.3.1.3 Cores

Balsa core

As the first core material use is made of (Figure 0.4):

- Baltek Sb.100 end grain balsa.

This core is an end grain balsa core which means the grains in the balsa core are in vertical direction. This type of balsa has, before impregnation, a density of 150 kg/m³. The currently used balsa has a thickness of 25.4 mm which results in 3.75 kg/m² before infusion of the resin.

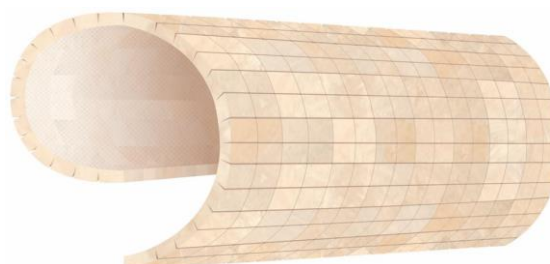


Figure 0.4: A mat of balsa wood, used as a core in composite sandwich panels

PET foam core

For the second core use is made of (Figure 0.6):

- Airex T90.60 closed cell PET foam.

This core is a thermoplastic, closed cell, recyclable polymer foam made of PET material. Before impregnation the foam has a density of 65 kg/m^3 . The foam panel used in the experiments has a thickness of 25.4 mm which results in 1.65 kg/m^2 before impregnation.

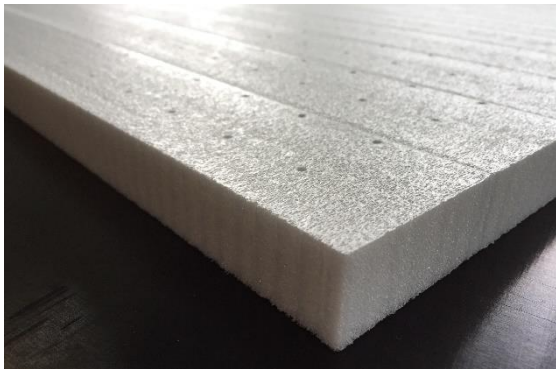


Figure 0.6: A panel of PET foam, used as a core in composite sandwich panels.

SAN foam core

For the third core use is made of (Figure 0.7):

- Gurit Corecell M closed cell SAN foam.

This core is a tough, closed cell polymer foam made of SAN material. Before impregnation the foam has a density of 65 kg/m^3 .



Figure 0.7: Panels of SAN foam, used as a core material in composite sandwich panels.

The foam panel used in the experiments has a thickness of 25.4 mm which results in 1.65 kg/m^2 before impregnation.

E.3.1.4 Layup

The panels are build up in the mould with first three layers of quadraxial fibres. The core is placed on top of that and then again three layers of quadraxial fibres are placed on top of the core. The quadraxial fibres are orientated with the 0° layer faced towards the core,

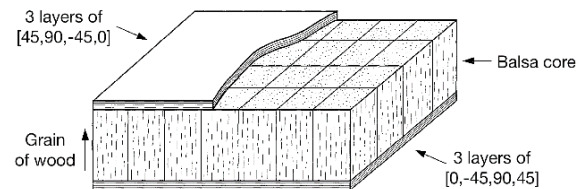


Figure 0.5: The layup of the composite sandwich panel; 3 layers of quadrax (with the 0° faced towards the core), than the core and op top again three layers of quadrax (with the 0° faced towards the core) symmetric with the core.

symmetric around the core. In Figure 0.5 an example is shown of the balsa panel layup.

E.3.1.5 Production process

The current panel is produced by vacuum infusion as can be seen in Figure 0.8. The laminate is build up on top of the mould. First the laminate layup, as described above, is placed onto the mould. Thereafter, peel ply is placed on top of the laminate, which is peeled off after infusion in order to ensure an evenly distributed rough surface finish. On top of that a release film is placed in order to be able to easily remove the top layer, which is the (green) mesh. The mesh ensures the equal

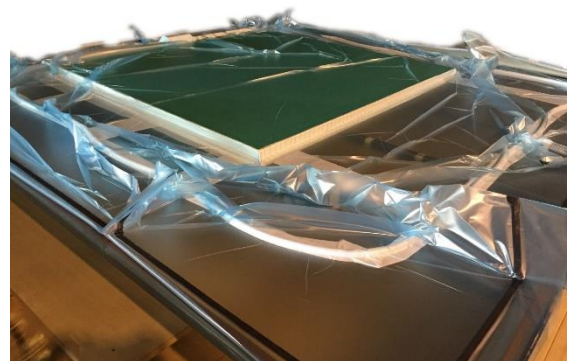


Figure 0.8: The vacuum infusion process; in the picture it can be seen that the laminate is under vacuum and ready for the infusion of the resin.

distribution of the resin during the infusion. Then the runner, which makes it possible for

the resin to be distributed over the complete width of the panel, is placed on top and the breather, which distributes the vacuum inside the bag and ensures the resin to flow towards the pump, is placed around the laminate. A vacuum hose is placed on the breather and a hose for the resin supply are positioned and then the complete package is sealed with a vacuum bag.

After leaving the laminate on vacuum for an hour, the resin is infused under a temperature of 40 °C. When the entire laminate is saturated with resin, the laminate gets reduced and heated up to 80 °C. The mould is heated up to 80 °C for 8 hours to ensure proper curing of the laminate.

Table 0.1: Properties of the used materials.

	Units	Glass facesheet	Model 1; SAN core	Model 2; PET core	Model 3; Balsa core
Density	Kg/m ³	1,500	85	65	155
Young's Modulus E ₁	MPa	20,696	85	25	300
Young's Modulus E ₂	MPa	20,696	85	25	300
Young's Modulus E ₃	MPa	12,578	85	25	300
Poisson ratio ν_{12}		0.285	0	0	0.45
Poisson ratio ν_{13}		0.285	0	0	0.014
Poisson ratio ν_{23}		0.375	0	0	0.014
Shear Modulus G ₁₂	MPa	4,860	29	12	18
Shear Modulus G ₁₃	MPa	6,360	29	12	326
Shear Modulus G ₂₃	MPa	4,860	29	12	326
Longitudinal Tensile Strength σ_{1t}	MPa	272	1.6	1.5	6.5
Longitudinal Compressive Strength σ_{1c}	MPa	340	1.4	0.6	5.5
Transverse Tensile Strength σ_{2t}	MPa	207	1.6	1.5	6.5
Transverse Compressive Strength σ_{2c}	MPa	308	1.4	0.6	5.5
Longitudinal Shear Strength τ_{12}	MPa	100	1.1	0.5	2.5
Transverse Shear Strength τ_{13}	MPa	100	1.1	0.5	2.5

E.3.2 Impact testing setup

The specimens are cut into pieces of 150 mm x 100 mm with a thickness of 30.2 mm as shown in Figure 0.10. The specimens are subjected to an impact force of 3.4 m/s with a weight of 5.895 kg, from a height of 60 cm, resulting in 34.7J impact energy. The test is performed according testing standard *ASTM D7136/D7136M* (ASTM-C393/C393M, 2012) on a *Dynatup 8250* falling weight impact machine. The specimens are impacted with a hemispherical tup of 16 mm diameter. The loading cell used in this test is a *Kistler 901 1A SN1530440*, capable of processing a 15 kN force. The impact-tup is attached to an extension beam, in order to enable the impact on the panel on the sub-plateau of the machine. The extension beam is attached to the added weight (4.95 kg). The complete setup (extension beam, bolts, tup, added weight), weights 5.895 kg. The specimens are clamped with four clamps to prevent the specimens from moving. After the impact has occurred two pneumatic support units move up, in order to prevent a second impact of the impact tup after bouncing. The complete setup is shown in Figure 0.9.

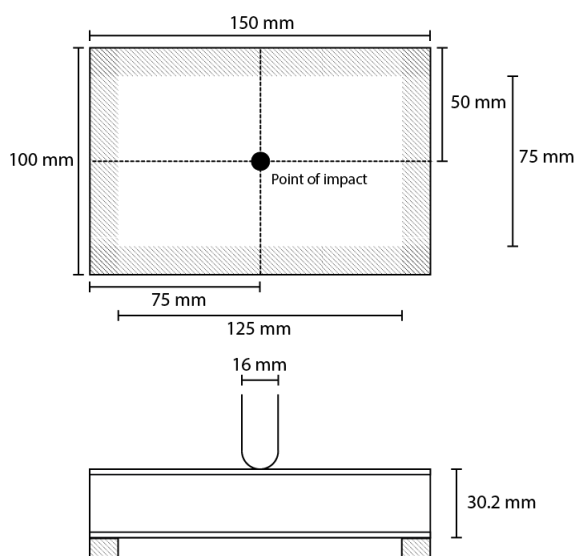


Figure 0.10: The dimensions of the impact test panels according the *ASTM D7136/D7136M* standard.

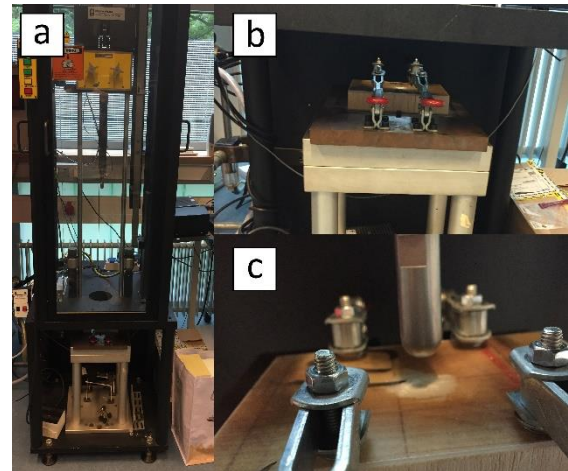


Figure 0.9: Complete impact setup according testing standard *ASTM D7136/D136M*. In a) the complete machine, in b) the fixture and in c) the impact tip.

E.3.3 Microscopic analysis

In order to investigate the damage behaviour of the impact specimens, an optical microscope is used. The optical microscope which is used is the *VHX 5000*, with a magnification lens of 100-1000 times magnification (VH Z100). The complete setup is shown in Figure 0.11.

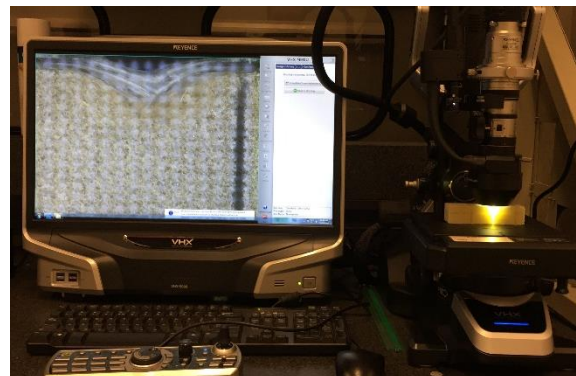


Figure 0.11: Optical microscope *VHX 5000*.

E.4. Results

Examining the panels after the impact tests, it can be seen that all panels have visible damage (Figure 0.1). The PET foam core sandwich panel have the least visible damage and the Balsa panel the most. This can be explained by the lower elastic modulus of the PET foam. The foam absorbs the energy by deforming instead of breaking like the balsa wood which can be seen in the graphs of the tests. The PET sandwich panels have much more deformation than the Balsa specimens and the SAN specimens.

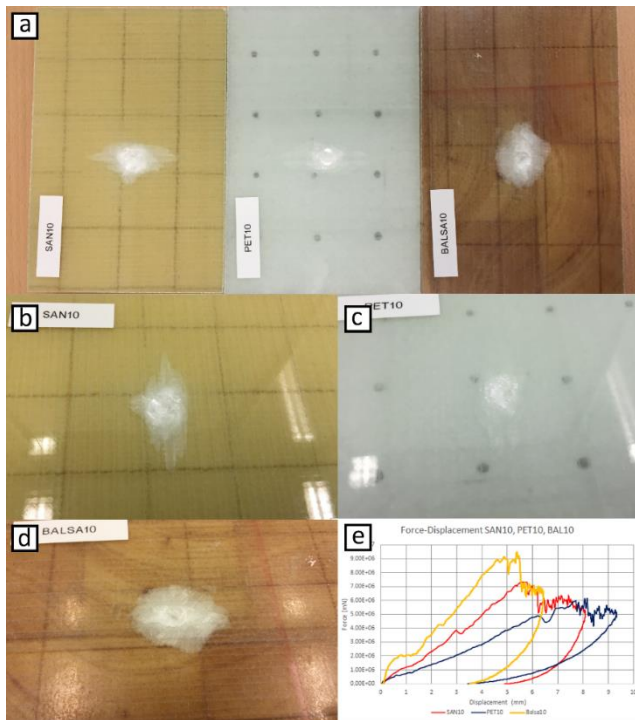


Figure 0.1: Visible damage of the different cored panels; a) all panels, b) the SAN10 panel, c) the Balsa10 panel, d) the PET10 panel and e) the corresponding force-displacement graph.

Examining the bottom of the impact panels, it can be seen that the Balsa panels have some sort of failure (probably debonding/delamination) underneath. It seems that the core and the skin start debonding, probably due to the out-of-plane shearing behaviour of Balsa. The bottom of the panels is shown in Figure 0.3, in which can clearly be seen that the Balsa panel has debonded in a circle around the impact area.

In order to investigate this behaviour and the impact-affected zone, the panels are cut in half (in the middle of the impact point) and then examined through the optical microscope described in section 3.3, which is able to magnify up to 1000 times. The debonding in between the core and the bottom skin in the BAL9 panel is clear and is depicted in Figure 0.2-c. In the specimens with the other core materials, the SAN and PET cored specimens, it can be seen that there is no debonding in between the bottom skin and the core (Figure 0.2-a and Figure 0.2-b).

When investigating this phenomena under the microscope in Figure 0.3-a, it can be seen that

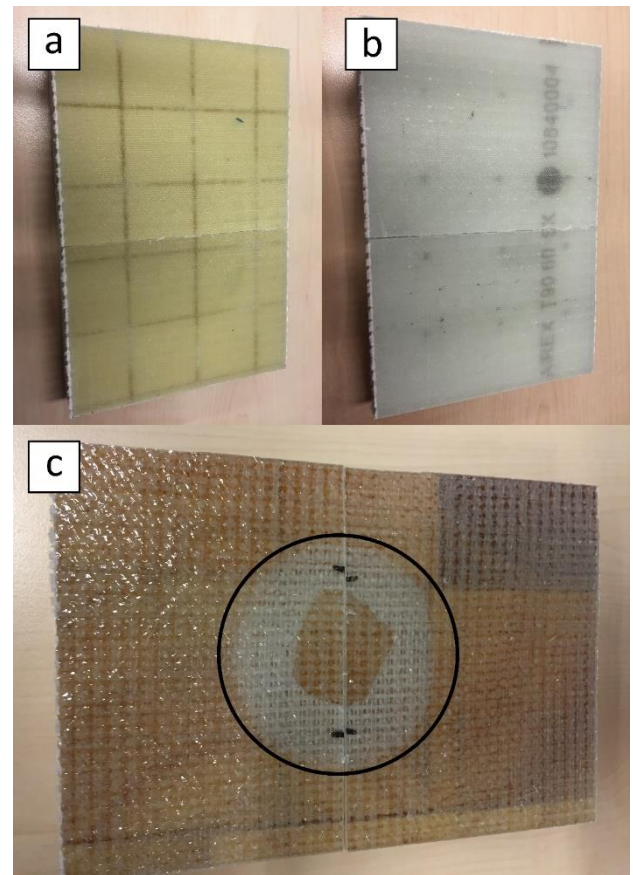


Figure 0.2: The bottom of the impact panels; a) SAN10, b) PET10 and c) Bal9

the Balsa panel really has indications of skin-core debonding. When comparing this to the PET foam and SAN foam cores in Figure 0.3-b and Figure 0.3-c, it can be seen that these panels do not have debonding between the bottom skin and the core.

From the microscopic analysis, not only the bottom failure between skin and core can be investigated, but also the impact-affected zone and the upper skin failure are analysed.

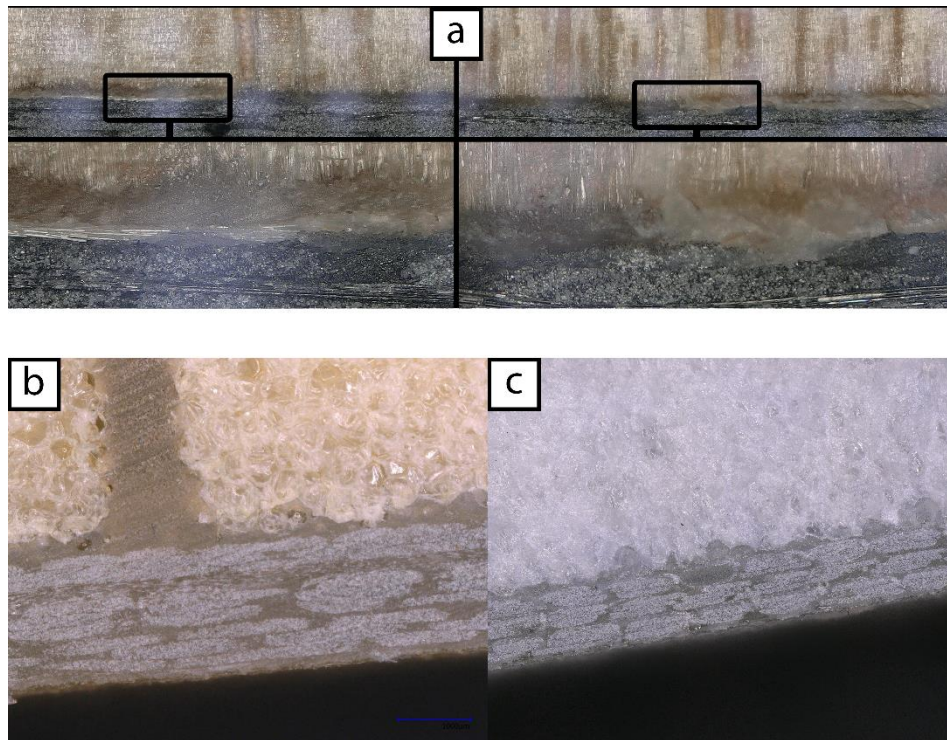


Figure 0.3: a) Bottom skin-core delamination of the Balsa (BAL9) specimen, b) bottom of the SAN (SAN9) specimen and c) the bottom of the PET (PET9) specimen.

In Figure 0.4-a the failure of the upper skin of the SAN9 specimen is depicted. It can be seen that there is a clear sign of fibre breakage (Figure 0.4-b) and also clear signs of matrix cracking (Figure 0.4-c). In the damaged zone of the PET9 specimen in Figure 0.5-a also the fibre breakage is shown (Figure 0.5-c), but not as clear as in the SAN foam specimen.

Figure 0.5-b also shows that the upper skin of the PET9 is damaged by the matrix cracking. When investigating the impacted zone of the

BAL9 specimen in Figure 0.6, also the fibre breakage is clearly depicted in Figure 0.6-b. The matrix cracking is also shown in Figure 0.6-c.

In Figure 0.4-a, Figure 0.5-a and Figure 0.6-a it can also be seen that the specimens have (a large amount of) debonding of the upper skin and the core, especially the PET9 specimen. This can be explained by the large amount of displacement of the core, which causes shear stresses between the core and the upper skin.

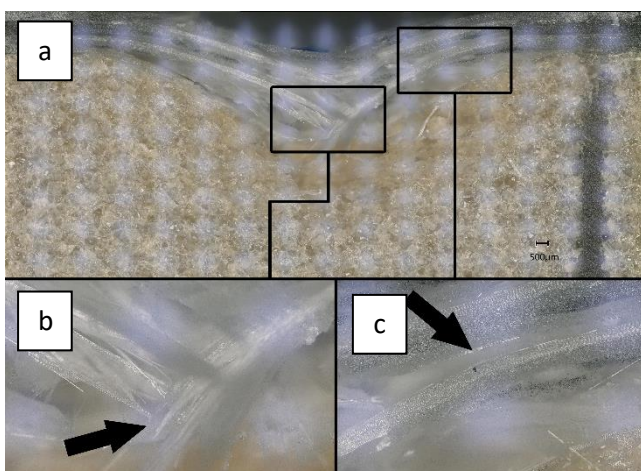


Figure 0.4: Skin failure of the SAN9 specimen.

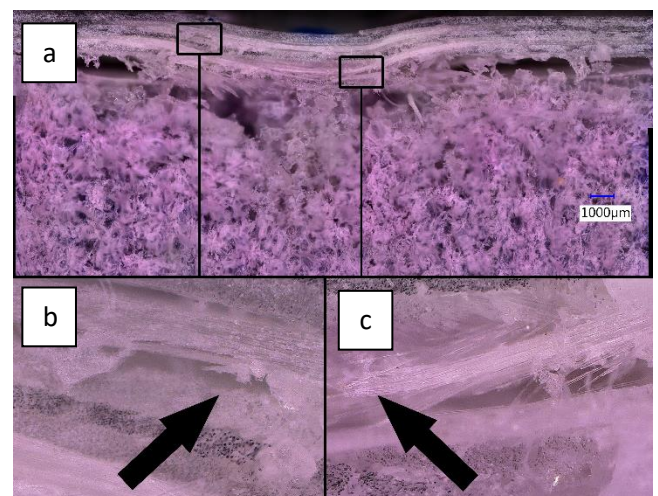


Figure 0.5: Skin failure of the PET9 specimen.

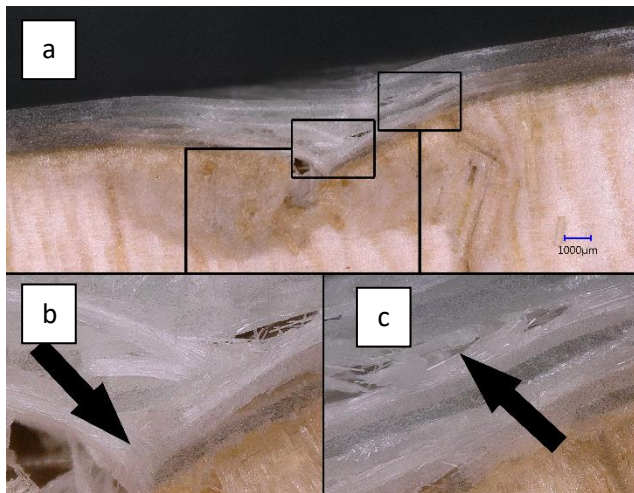


Figure 0.6: Skin failure in the BAL9 specimen.

After investigating the failure behaviour of the skins, the impact-affected zone is analysed.

As depicted in Figure 0.7, there is a difference between the non-affected cells (Figure 0.7-c) and the affected cells (Figure 0.7-b) of the SAN foam. In this way, the impact affected zone can be determined as shown in Figure 0.10-a.

This difference of affected and non-affected cells is even more clear in the PET foam in Figure 0.8. The impact has damaged the cells of the PET foam and by distinguishing the damaged cells from the undamaged cells, the impact-affected zone can be identified as depicted in Figure 0.10-b.

In the impacted zone of the balsa panel in Figure 0.9-a, the difference between the

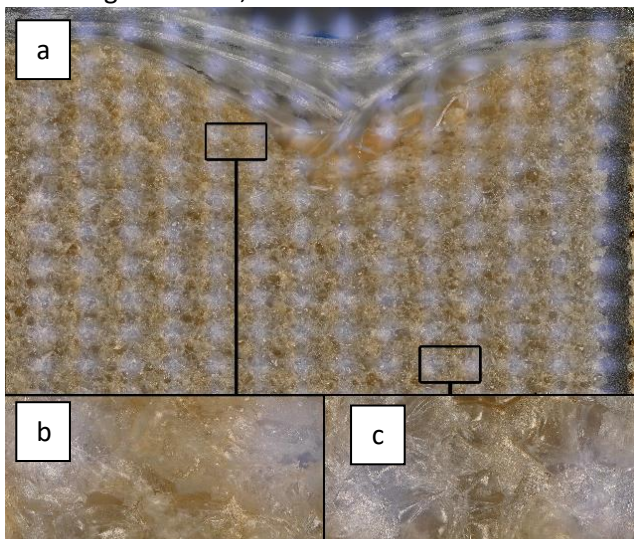


Figure 0.7: Comparing damaged with undamaged cells of the SAN foam after impact.

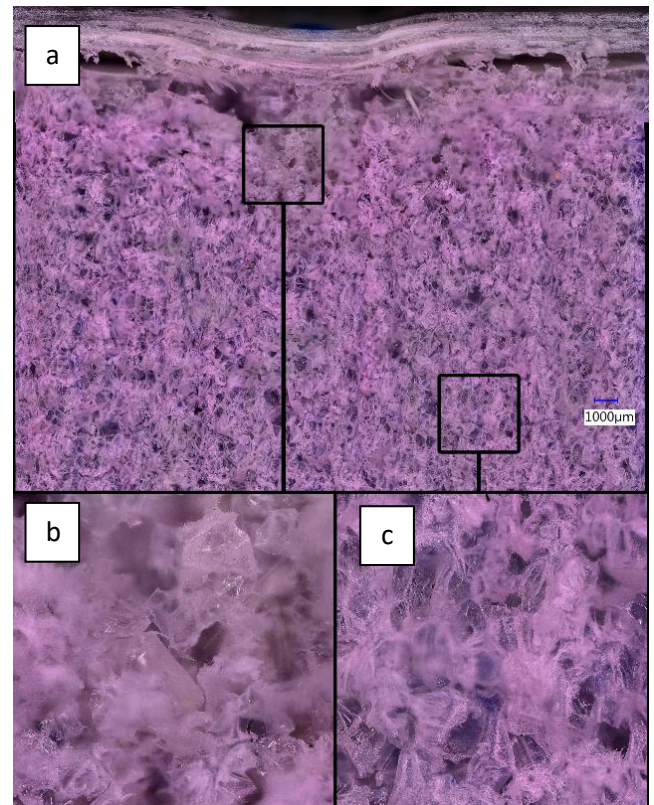


Figure 0.8: Comparing damaged cells (b) with undamaged cells (c) of the PET foam after impact.

damaged cells (Figure 0.9-c) and the undamaged cells (Figure 0.9-b) can be clearly seen. This can be translated to an impact-affected zone of the Balsa core in Figure 0.10-c.

Comparing these impact-affected zones, it can be seen that the PET foam has the widest zone affected from the impact. This can be caused

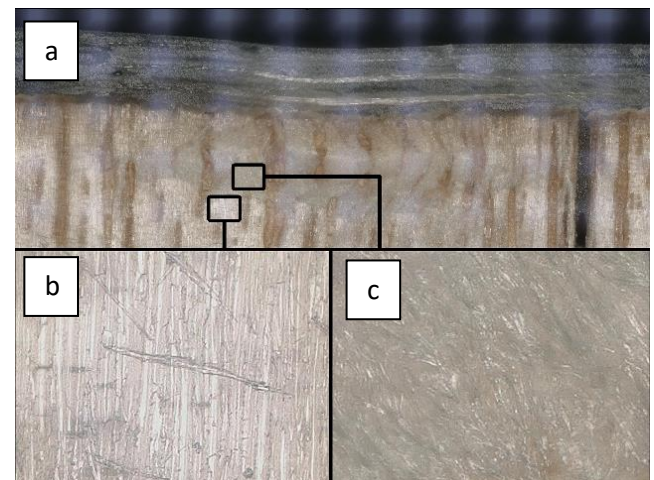


Figure 0.9: Comparing damaged with undamaged cells of the Balsa wood after impact.

by its low value for the E-modulus and plasticity behaviour. Furthermore, it can be seen that the Balsa core is affected the least from the impact.

This may be caused by its high values for E-modulus and shear modulus. The SAN foam has a deep penetration of the affected zone, but not as wide spread as the PET foam. This is caused by the better properties of the SAN foam in comparison with the PET foam.

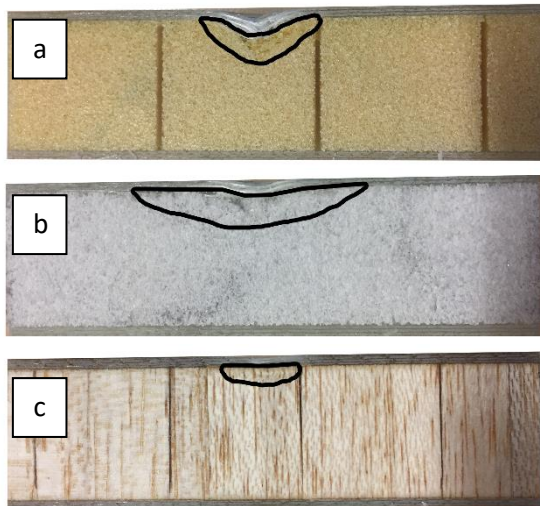


Figure 0.10: Impact-affected zones of the SAN foam (a), PET foam (b) and Balsa (c) cored specimens.

These results align with the findings of Bhuiyan et al. (2009), in which the PUR foam contains damaged cells which can clearly be distinguished from the non-damaged cells. The results also show the same skin failure as discussed in this research.

Ramakrishnan et al. (2012) investigated the impact behaviour on composite sandwich panels, in which also a clear debonded area at the bottom of the panel is shown.

E.5 Conclusions and future recommendations

In this report, the internal failure mechanisms of three different cored composite sandwich panels after impact are studied in microscopic detail. It was shown that the three different core materials respond differently in impact loading. All three panels show the same failure mechanisms in the skin, i.e. fibre failure and matrix cracking.

It is shown that the Balsa wood has skin-core debonding at the bottom skin-core interface due to the impact, which was not ascertained in the PET foam cored specimen and the SAN foam cored specimen. The skin-core debonding can be explained by the high properties of the Balsa wood, which thence transfers the impact energy through the core to the bottom skin, causing the balsa and the skin to debond.

Furthermore, microscopic analysis is used in order to determine the impact-affected zone. It was shown that the PET foam has the widest affected zone and that Balsa has the smallest affected zone. This can be devoted to the relatively low material properties of the PET and the relatively high properties of the Balsa.

E.6 References

- Ahmed, A. W. (2015). The Low-Velocity Impact Damage Resistance Of The Ccomposite Structures - A Review. *Rev. Adv. Mater. Sci.* 40, 127-145.
- ASTM-C393/C393M. (2012). Standard test method fo core shear properties of sandwich constructions by beam flexure. *ASTM International*.
- Craig A. Steeves, N. A. (2004). Material selection in sandwich beam construction. *Scripta Materialia* 50, 1335-1339.
- J. Wang, A. W. (2012). Experimental Study on the Low-velocity Impact Behaviour of Foam-core Sandwich Panels. *Structures, Structural Dynamics and Materials Conference*. Honolulu, Hawaii: American Institute of Aeronautics and Astronautics.
- Lin, J. C. (2006). Mechanical behaviour of various nanoparticle filled composites at low-velocity impact. *Composite Structures* 74, 30-36.
- Md.A. Bhuiyan, M. H. (2009). Low-velocity impact response of sandwich composites with nanophased foam

core and biaxial (+/-45) braided face sheets. *Composites: Part B*, 561-571.

R. Mohmmmed, A. A. (2008). Low Velocity Impact Properties of Foam Sandwich Composites: A Brief Review. *International Journal of Engineering Science and Innovative Technology*, 579-591.

Ramakrishnan, K. S. (2012). A comparative study of the impact properties of sandwich materials with different cores. *EPJ Web of Conferences* 26, 01031 p1 - 01031 p6.

Russo, P. S. (2014). Low velocity impact damage in composite laminates based on waste polyolefins. *Procedia Engineering* 88, 165-172.

Appendix F: Stress table

Without Chawla

BO-SAN									BAI-SAN						
		1	2	3	4	5	6	Avg	1	2	3	4	5	6	Avg
σ	ASTM	36.32	32.67	35.37	38.62	37.28	32.64	35.48	11.92	23.66	20.62	19.42	20.8	18.27	19.12
	CHA	15.94	14.34	15.53	16.95	16.36	14.33	15.58	5.23	10.38	9.05	8.53	9.13	8.02	8.39
	ARB	36.32	32.67	35.37	38.62	37.28	32.64	35.48	11.92	23.66	20.62	19.42	20.8	18.27	19.12
	Avg	36.32	32.67	35.37	38.62	37.28	32.64	35.48	11.92	23.66	20.62	19.42	20.8	18.27	19.12
τ	ASTM	1.16	1.05	1.13	1.24	1.19	1.04	1.14	0.38	0.76	0.66	0.62	0.67	0.58	0.61
	CHA	1.61	1.44	1.56	1.71	1.65	1.44	1.57	0.53	1.05	0.91	0.86	0.92	0.81	0.84
	ARB	1.16	1.05	1.13	1.24	1.19	1.04	1.14	0.38	0.76	0.66	0.62	0.67	0.58	0.61
	Avg	1.16	1.05	1.13	1.24	1.19	1.04	1.14	0.38	0.76	0.66	0.62	0.67	0.58	0.61
BO-PET									BAI-PET						
		1	2	3	4	5	6	Avg	1	2	3	4	5	6	Avg
σ	ASTM	18.05	16.95	18.38	21.12	19.71	19.3	18.91	13.94	15.44	13.18	12.87	13.91	14.43	13.96
	CHA	7.92	7.44	8.07	9.27	8.65	8.47	8.3	6.12	6.78	5.79	5.65	6.11	6.33	6.13
	ARB	18.05	16.95	18.38	21.12	19.71	19.3	18.91	13.94	15.44	13.18	12.87	13.91	14.43	13.96
	Avg	18.05	16.95	18.38	21.12	19.71	19.3	18.91	13.94	15.44	13.18	12.87	13.91	14.43	13.96
τ	ASTM	0.58	0.54	0.59	0.68	0.63	0.62	0.61	0.45	0.49	0.42	0.41	0.45	0.46	0.45
	CHA	0.8	0.75	0.81	0.93	0.87	0.85	0.84	0.62	0.68	0.58	0.57	0.61	0.64	0.62
	ARB	0.58	0.54	0.59	0.68	0.63	0.62	0.61	0.45	0.49	0.42	0.41	0.45	0.46	0.45
	Avg	0.58	0.54	0.59	0.68	0.63	0.62	0.61	0.45	0.49	0.42	0.41	0.45	0.46	0.45
BO-BAL									BAI-BAL						
		1	2	3	4	5	6	Avg	1	2	3	4	5	6	Avg
σ	ASTM	78.72	75.54	106.24	63.53	84.85	77.33	81.03	82.61	62.9	53.59	47.95	62.17	66.07	62.55
	CHA	34.55	33.16	46.63	27.88	37.24	33.94	35.57	36.26	27.61	23.52	21.05	27.29	29	27.46
	ARB	78.72	75.54	106.24	63.53	84.85	77.33	81.03	82.61	62.9	53.59	47.95	62.17	66.07	62.55
	Avg	78.72	75.54	106.24	63.53	84.85	77.33	81.03	82.61	62.9	53.59	47.95	62.17	66.07	62.55
τ	ASTM	2.52	2.42	3.4	2.03	2.72	2.47	2.59	2.64	2.01	1.71	1.53	1.99	2.11	2
	CHA	3.48	3.34	4.69	2.81	3.75	3.42	3.58	3.65	2.78	2.37	2.12	2.75	2.92	2.76
	ARB	2.52	2.42	3.4	2.03	2.72	2.47	2.59	2.64	2.01	1.71	1.53	1.99	2.11	2
	Avg	2.52	2.42	3.4	2.03	2.72	2.47	2.59	2.64	2.01	1.71	1.53	1.99	2.11	2